Title

The roles of cytochrome P450 3A and P-glycoprotein in the absorption, metabolism and elimination of a novel cysteine protease inhibitor

Author

Zhang, Yuanchao,

Publication Date

1998

Peer reviewed|Thesis/dissertation

THE ROLES OF CYTOCHROME P450 3A AND P-GLYCOPROTEIN IN THE ABSORPTION, METABOLISM AND ELIMINATION OF A NOVEL CYSTEINE PROTEASE INHIBITOR

by

Yuanchao (Derek) Zhang
B.S. Chemistry, Fudan University, Shanghai, M.S. Chemistry, University of Rochester, New York

DISSERTATION

Submitted in partial satisfaction of the requirements for the degree of

DOCTOR OF PHILOSOPHY

in

PHARMACEUTICAL CHEMISTRY

in the

GRADUATE DIVISION

of the

UNIVERSITY OF CALIFORNIA

San Francisco

. . . . . .

Date **University Librarian**

Degree Conferred: . . . . . .

Acknowledgments

I would like to convey my sincerest thanks to my research advisor, Dr. Leslie Z. Benet, for his great mentorship. During my graduate life at UCSF, especially in Dr. Benet's research group, I had the unique opportunity to receive excellent education in drug metabolism, drug transport and pharmacokinetics, as well as a broad basic understanding in diverse disciplines, such as cellular and molecular biology, computational and combinatorial chemistry, macromolecule structure determination (X-ray crystallography, NMR and Mass Spectrometry), and clinical sciences which helped me to shape my career goal, to be a research scientist in the pharmaceutical industry and to contribute to the development of more effective and safer pharmaceuticals for human health.

I would also like to thank Drs. Alma L. Burlingame and James H. McKerrow, committee members of this thesis, for their timely and critical reading of this dissertation. Heartfelt thanks to my orals committee, Drs. Kathleen M. Giacomini (chair), Almira M. Correia, Paul R. Ortiz de Montellano, Martin D. Shetlar and Robert S. Warren, for their time and advice. Thanks also to Drs. Emil T. Lin, Deanna L. Kroetz, Jeffrey A. Silverman, Antony F. McDonagh, Robert A. Upton and Christopher Cullander for fruitful discussions, advice and useful help.

Special thanks to numerous members (past and present) of the Benet group and the Department for their friendship and help: Chi-Yuan Wu,

Dr. Vincent J. Wacher, Dr. Takashi Izumi, Dr. Guo Xisheng, Dr. Yunsheng Hsieh, Dr. Hiroyuki Sasabe, Dr. Leonid Voronov, Dr. Mark Grillo, Dr. Jenny Zheng, Dr. Tetsuya Aiba, Dr. Hsiu-Ling Hsiao, Dr. Graham Jang, Dr. Rae Yuan, Dr. Marci Schaner, Dr. Laurent Salphati, Dong Yan Yang, Yong-Chang Qiu, Lolin Ip, Milagros Hann, Natalya Guterman, Shi-Fang Wang, Karen Baner, Albert Chang, Lingling Guan, Shawn Flanagan, Dolly Parasrampuria, Dr. Laviero Mancinelli, Dr. Ignacio Segarra, Dr. Uwe Christians, Dr. Leslie Floren, Dr. Andrea Soldner, and Dr. Natalie Serkova. Special thanks also go to the incomparable Vivian Tucker and Ms. Gloria Johnson.

Heartfelt thanks also go to my family members, 八伯伯，爸爸，媽媽，暉暉, for their love, encouragement, and unyielding support across the Pacific Ocean from China.

Last but not the least, I would like to thank Lei Zhang, my wonderful fiancee, for her love, support, encouragement and friendship.

Abstract

The Roles of Cytochrome P450 3A and P-glycoprotein in the Absorption, Metabolism and Elimination of A Novel Cysteine Protease Inhibitor

Yuanchao Zhang

Morpholine-Urea-Phenylalanine-Homophenylanaline-Vinylsulfone-Phenyl (Mu-Phe-Hph-VSPh, K02, aka K11002), a newly developed peptidomimetic, acts as a potent cysteine protease inhibitor of cruzain, cathepsins B, K, L and S. Here I investigated the disposition features of K02 by characterizing the drug's interaction with cytochrome P450 3A (CYP3A), a major intestinal and hepatic CYP in drug oxidative biotransformation, and P-glycoprotein (P-gp), an ATP-dependent drug efflux pump expressed on the apical side of many epithelial cells in various organs. The observed overlaps between substrate specificity and tissue distribution for CYP3A and P-gp suggest that CYP3A and P-gp may play complementary roles in drug absorption, distribution, metabolism and elimination by biotranformation and countertransport. Especially in the villi of small intestines, CYP3A and P-gp act synergistically as a barrier to oral drug availability. For the present work, I tested this hypothesis by investigating the interaction of K02 with CYP3A and P-gp using both *in vitro* systems and *in vivo* pharmacokinetic studies in male Sprague-Dawley rats. K02 is demonstrated to be a substrate for CYP3A and CYP3A is the principle CYP for K02 oxidation in human liver, rat liver and intestinal microsomes. K02 is also demonstrated to be a substrate for P-gp by transport studies of ^{14}C-K02, utilizing MDR1-MDCK and

Caco-2 cell monolayers in the Transwell system. Pharmacokinetic studies of K02 in male Sprague-Dawley rats demonstrated that K02 oral bioavailability increased markedly (10-fold) with a concomitant oral dose of ketoconazole (20 mg/kg), a potent CYP3A inhibitor and a moderate P-gp inhibitor. These results strengthen our working hypothesis that CYP3A and P-gp play complementary roles in peptidomimetic disposition and that poor oral peptidomimetic bioavailability caused by the intestinal CYP3A/P-gp barrier can be improved by approaches such as co-administration of CYP3A and/or P-gp inhibitors.

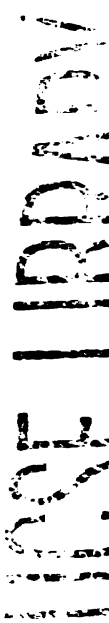

Table of Contents

Chapter 1 Cysteine Protease Inhibitors, Cytochrome P450 3A and P-glycoprotein

List of Tables

List of Figures

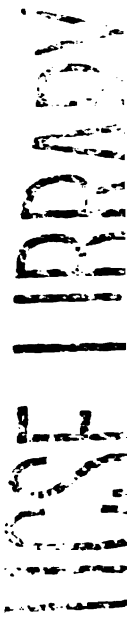

Chapter 1 Cysteine Protease Inhibitors, Cytochrome P450 3A and P-glycoprotein

1.1 Cysteine Protease Inhibitors as New Therapeutic Agents in Treatment of Cancer and Parasitic Diseases

Proteases are responsible for facilitating a broad spectrum of physiological functions, including cell growth, differentiation and death (apoptosis), cell nutrition, intra- and extra-cellular protein turnover, cell migration and invasion, and fertilization and implantation(Clawson, 1996; DeClerk and Imren, 1994). Elevated levels of active proteases have been observed in many disease states, for example thrombotic disorders, hypertension, osteoarthritis, chronic degenerative diseases and cancer(Das and Mukhopadhyay, 1994). Restoring the natural balance of protease activities by inhibiting the overexpressed proteases in various disease states provides unique opportunities for drug development. Therefore, proteases have become new targets for the development of specific inhibitors as potential therapeutic agents(Hugli, 1996). Successful examples include captopril, the first drug developed to target angiotensin converting enzyme (metallo protease) in the treatment of hypertension and recently, HIV protease inhibitors in the treatment of AIDS. The HIV protease inhibitors target viral aspartyl protease(Chrusciel and Romines, 1997).

Cysteine proteases, such as cathepsins B, K and L, have been implicated in progressive cartilage and bone degradation associated with arthritis, and cathepsin S has been found to be highly expressed in osteoclastoma tissue(Palmer *et al.,* 1995). Cathepsins B and L also have been linked to

metastasis and invasion of cancer cells, e.g., bladder, breast, colon, gastric and prostate carcinomas and glioblastomas(Calkins and Sloane, 1995; Elliott and Sloane, 1996). A key event necessary to allow the invasion of tumor cells into normal tissues is the degradation of extracellular matrix. Both cathepsins B and L have been shown to be active against extracellular matrix proteins at physiological pH. It is known that expression of cathepsin B is elevated approximately ten-fold in tumor cells. There are endogenous inhibitors of cysteine proteases (cystatins). Cystatins are downregulated in some tumor cells, thus making the proteolytic effect of cathepsin B even greater(Sloane *et al.*, 1990). Several synthetic cathepsin B inhibitors effectively block cancer cell (glialblastoma) invasion *in vitro* (Rasnick, 1996). Knowledge of X-ray crystal structures of cathepthins B and L and their substrate selectivities may enable the structural based rational design of novel cysteine protease inhibitors as potential antineoplastic drugs(Podobnik *et al.*, 1997; Turk *et al.*, 1995).

Accumulated evidence suggests that parasite cysteine proteases play important roles in host-parasite interactions and pathogenesis(Robertson *et al.*, 1996). Cruzain, a key cysteine protease (cathepsin L like cysteine protease) present in *Trypanosoma cruzi*, is the major proteolytic activity in the life cycle of the parasite. *Trypanosoma cruzi*, a protozoan parasite, is the etiologic agent of American trypanosomiasis or Chagas' disease(McKerrow *et al.*, 1995). *Trypanosoma cruzi* is transmitted to humans, as an infectious trypomastigote form, from the bite of a blood-sucking insect. The trypomastigote enters the host bloodstream and ultimately invades a cardiac muscle cell, where it transforms

into the intracellular amastigote. Amastigotes replicate within cells, transform back to trypomastigotes, and rupture the cell, releasing the infectious form back into the bloodstream or to other cells, thereby amplifying the infection. Several synthetic cysteine protease inhibitors, e.g., peptidyl fluoromethyl ketones, block the replication and differentiation of *Trypanosoma cruzi* in parasite infected mammalian cells *in vitro*(Harth *et al.*, 1993). With the availability of a high-resolution X-ray crystal structure of cruzain, structural-based approaches have been undertaken for discovery and modification of new antiparasitic lead compounds(McGrath *et al.*, 1995).

1.2 Morpholine-Urea-Phenylanaline-Homophenylanaline-Vinylsulfone-Phenyl (K02), a Novel Cysteine Protease Inhibitor

Morpholine-Urea-Phenylanaline-Homophenylanaline-Vinylsulfone-Phenyl (K02) (Figure 1.2.1) is a member of the class of vinylsulfone peptidomimetic cysteine protease inhibitors(Palmer *et al.*, 1995).

K02 is an irreversible cysteine protease inhibitor which inhibits cathepsin B (K_i = 11 μM), cathepsin K (K_i = 30 μM), cathepsin L (K_i = 1.0 μM), cathepsin S (K_i = 0.01 μM) and cruzain (K_i = 0.36 μM). K02 is unreactive toward serine proteases, metalloproteases, aspartyl protease and circulating thiols such as

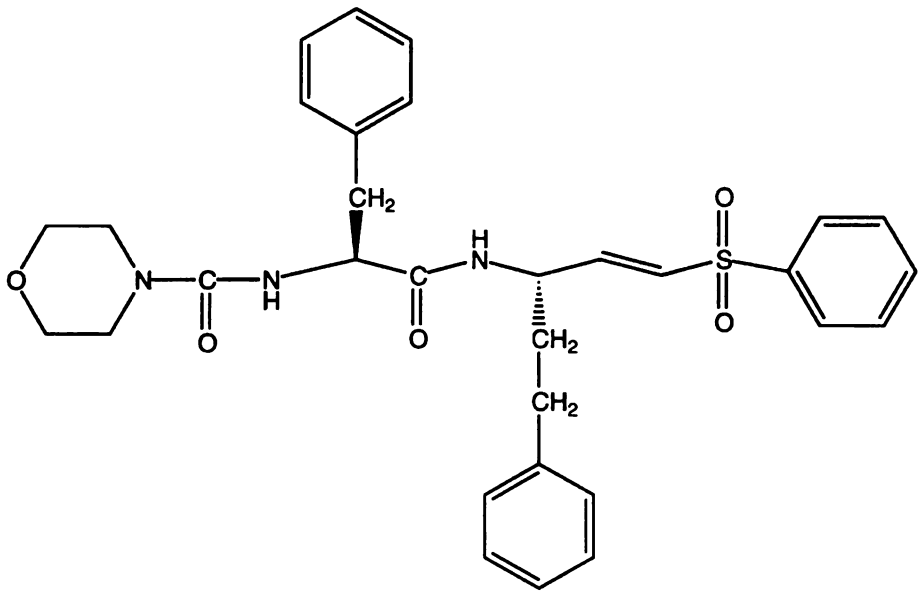

Figure 1.2.1 Chemical Structure of K02

glutathione. K02 binds to the catalytic site of cysteine proteases where it serves as a Michael acceptor. The vinylsulfone moiety of the K02 molecule forms a thioether with proteases via nucleophilic Michael attack by the cysteine residue at the catalytic site. In *Trypanosoma cruzi* infected IEC-6 cells, the IC_{50} of K02 inhibition of parasite survival is 5 μM. In a *Trypanosoma cruzi* infected mouse model, i.p. administration of K02 at a dose of 100 mg/kg/day can cure the infection. Thus, K02 is a promising lead compound for antiparasitic and antineoplastic drug development. Figure 1.2.2 shows the mechanism of action of K02.

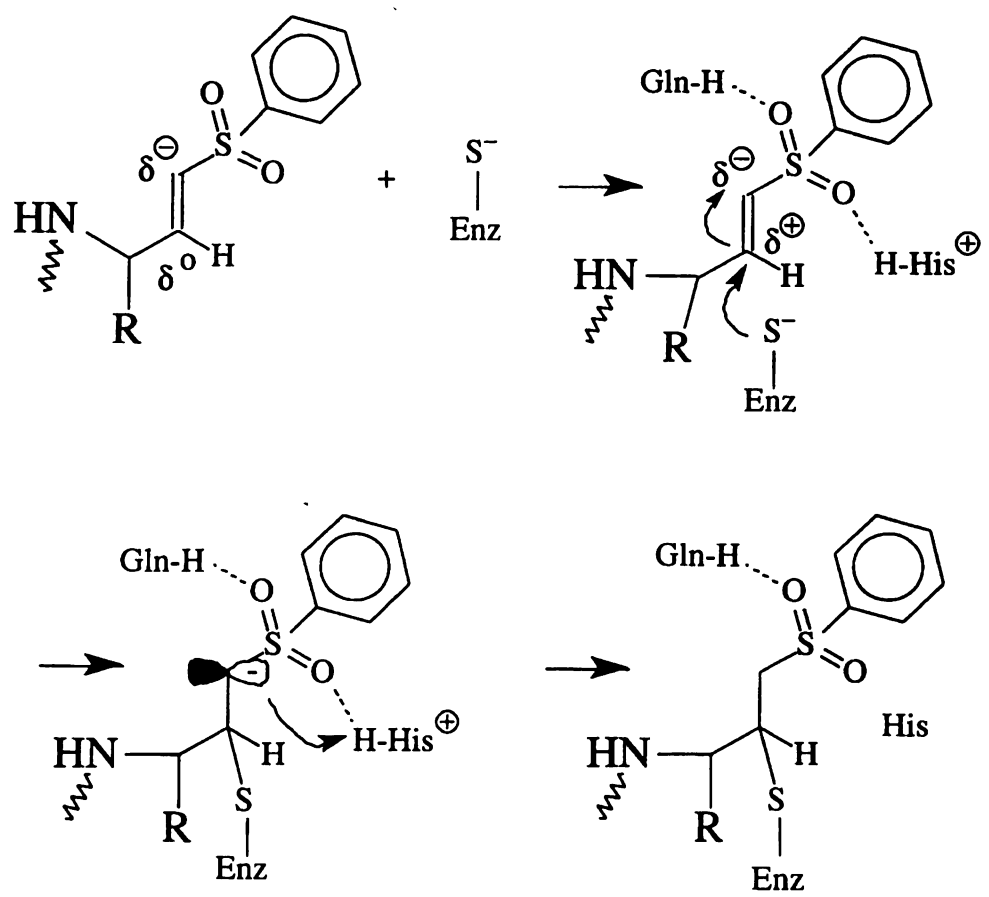

Figure 1.2.2 Mechanism of γ-amino vinylsulfone inactivation of cysteine proteases. Adapted from Palmer *et al.* (1995).

K02 may serve as a good model for studies of drug metabolism, drug transport and pharmacokinetics of other cysteine protease inhibitors with potential as therapeutic agents.

1.3 Cytochrome P450 3A (CYP3A), a Major Cytochrome P450 (CYP) in Drug Metabolism

Cytochromes P450 (CYPs) localized in the smooth endoplasmic reticulum of numerous tissues are heme-containing membrane proteins which belong to a superfamily of mixed function oxidase (MFO). At the last official count, the CYP superfamily was comprised of 481 genes found in 85 eukaryotes (both animal and plants) and 20 prokaryotes (many CYPs in prokaryotes are soluble and cytosolic proteins). Of 74 gene families so far described, 14 families exist in all mammals examined to date. These 14 families comprise 26 mammalian subfamilies, of which 20 and 15 have been mapped in the human genome and the mouse genome, respectively(Nelson *et al.*, 1996). The CYP superfamily is the major enzyme family responsible for oxidative biotransformation of a variety of endogenous substrates, e.g., steroids, fatty acids, prostaglandins, and bile acids) and xenobiotics including drugs, carcinogens, environmental pollutants, and many other synthetic chemicals(Wrighton *et al.*, 1996). The oxidative biotransformations catalyzed by CYPs are generally classified into the following categories: hydroxylation (aromatic and aliphatic side chains), dealkylation (N-, O-, and S-dealkylation), N-oxidation, sulfoxidation, N-hydroxylation, deamination, dehalogenation, and desulfuration(Guengerich, 1991). In addition, CYPs can catalyze a number of reductive reactions(Riley *et al.*, 1993; Spracklin *et al.*, 1996). The metabolites formed from the majority of substrates by the CYPs are

more hydrophilic than the parent compounds and are thus more readily excreted from the body.

The CYP superfamily has the predominant role in xenobiotic phase I metabolism. Only three CYP gene families (i.e., CYP1, CYP2, and CYP3) are currently identified to be responsible for the majority of drug metabolism in human and rat(Wrighton, 1996). The relative contribution of the major human CYPs in the drug metabolism in human is illustrated in Figure 1.3.1 (Benet *et al.*, 1996a). The major CYPs in human liver and intestine are listed in Table 1.3.1.

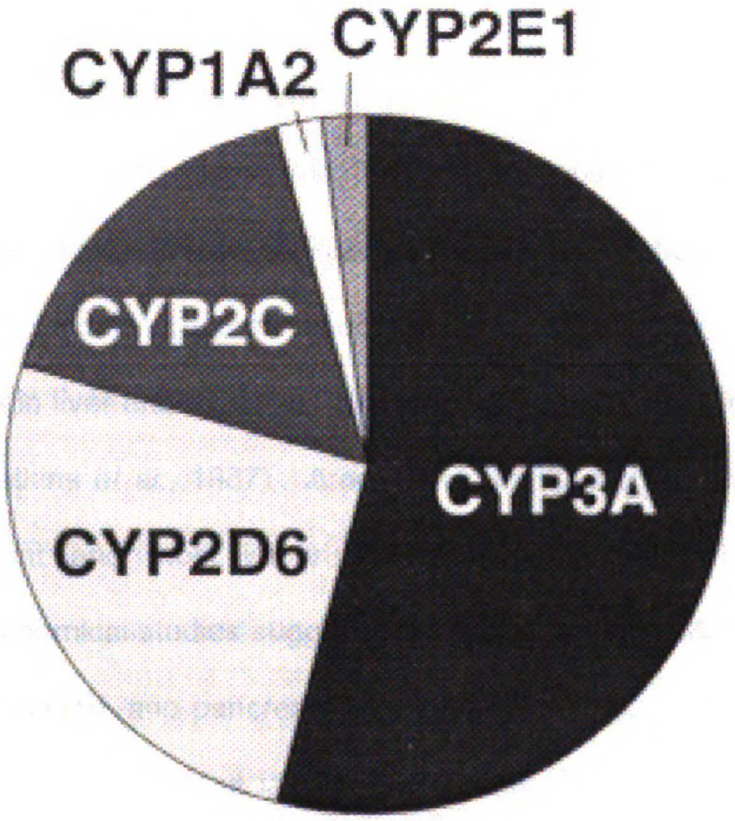

Figure 1.3.1 The proportion of drugs metabolized by the major CYPs in human(Benet *et al.*, 1996a).

Table 1.3.1 Major liver and intestinal CYPs in human(de Waziers *et al.*, 1990)

Liver (% of total liver CYPs)	Intestine (% of respective liver levels)
CYP3A (30%)	CYP3A4 (80-100%) and CYP3A5 (?)
CYP2C (20%)	CYP2C (5-10%)
CYP1A2 (13%)	CYP1A2 (?)
CYP2E1 (7%)	CYP2E1 (trace)
CYP2D6 (2%)	CYP2D6 (20%)

CYP3A is the primary CYP subfamily responsible for CYP-mediated phase I metabolism of greater than 50% of drugs administered to humans(Benet *et al.*, 1996a). CYP3A is primarily located in hepatocytes and the biliary epithelial cells of the liver and the villous columnar epithelial of the jejunum(Murray *et al.*, 1988). CYP3A is also reported to be expressed in other organs, such as kidney (Haehner *et al.*, 1996). CYP3A comprises 30% and 70% of total CYPs in liver and intestine, respectively(Kolars *et al.*, 1992b; Shimada *et al.*, 1994; Watkins *et al.*, 1987). Among the CYP3A subfamily, CYP3A4 is the most abundant and most important enzyme in human drug metabolism. Immunohistochemical studies suggests that the major CYP3A protein present in liver, jejunum, colon, and pancreas is CYP3A4. CYP3A5 is expressed in about 25-30% of human livers, but is more commonly expressed in small intestine, stomach and has recently been found to be ubiquitously expressed in kidney(Haehner *et al.*, 1996). Immunoblots suggest that levels of CYP3A4 in small intestine are approximately 80-100% of CYP3A4 levels in the liver(de

Waziers, 1990). Microsomal preparations of human jejunal enterocytes have demonstrated that CYP3A4 protein concentrations and enzyme activities are equal to or greater than those of liver microsomes(Watkins *et al.*, 1987).

Recently, CYP3A has been found to be expressed or overexpressed (compared to normal tissues) in a number of neoplasms such as breast and colon tumors, esophagus squamous carcinoma and some soft tissue sarcomas (leiomyosarcoma, fibrosarcoma and malignant fibrous histiocytoma) (Murray *et al.*, 1994; Murray *et al.*, 1995a and b). These facts suggest that CYP3A may contribute to resistance of neoplasms to chemotherapeutic agents.

CYPs are also found to be expressed in some parasites, e.g., *Trypanosoma cruzi*, *Trypanosoma brucei, Leishmania donovani* and Crithidia *fasciculata*(Berger and Fairlamb, 1993). The carbon monoxide difference spectra of microsomal fractions, and their ethoxycoumarin deethylase and ethoxyresorufin deethylase activities are consistent with the presence of CYPs in these organisms. Systematic genetic and biochemical studies of CYPs present in parasites are needed to elucidate the physiological functions of parasitic CYPs and their interactions with antiparasitic drugs.

CYP3A enzymes can be induced by a number of structurally unrelated compounds, namely steroids (including synthetic glucocorticoids and anti-glucocorticoids), phenobarbital-type inducers, macrolide antibiotics, and antifungal compounds(Williams *et al.*, 1997). For examples, both intestinal and hepatic CYP3A4 can be induced by dexamethasone and rifampin.

CYP3A4 has a very broad substrate specificity. It is known that CYP3A4 catalyzes the metabolism of a large, growing number of structurally diverse and clinically important drugs, covering a wide therapeutic range, for example, antiarrhythmics, antifungals, calcium-channel blockers, cancer chemotherapeutic agents (e.g., etoposide, paclitaxel, vinblastine and vincristine), homones, immunosuppressants (cyclosporine, tacrolimus and rapamycin), and HIV protease inhibitors (e.g., saquinavir, indinavir, ritonavir and nelfinavir) (Chiba *et al.*, 1997; Fitzsimmons and Collins, 1997; Kumar *et al.*, 1996; Li *et al.*, 1995; Perry and Benfield, 1997). Based on molecular modeling, a predictive model for CYP2D6 substrates was postulated - there should be a 5 or 7 Angstrom distance between the oxidation site and the basic nitrogen atom(Koymans *et al.*, 1992). In contrast to substrates for CYP2D6, CYP3A4 substrates are much more structurally diverse(Smith and Jones, 1992). The most common characteristic of CYP3A4 substrates is hydrophobicity. Recently, a model of the active site of CYP3A4 was built on the basis of sequence homology with CYP_{cam}, a bacterial soluble CYP in *Pseudomonas Putida*(Ferenczy and Morris, 1989). The structure of CYP_{cam} is the first of four known bacterial CYP structures solved by X-ray crystallography. By docking known CYP3A4 substrates into the binding pocket, molecular dynamic analysis reveals that the major feature of CYP3A4 substrate binding is a hydrophobic interaction. Another unique characteristic of the CYP3A enzymes is their ability to be activated by certain compounds such as 7,8-benzoflavone, which is itself a CYP3A4 substrate. 7,8-Benzoflavone can activate CYP3A4-catalyzed phenanthrene metabolism. Detailed kinetic studies

suggest that CYP3A4 can simultaneously bind two substrates (7,8-benzoflavone and phenanthrene) in the CYP3A active site(Shou *et al.*, 1994).

Recently, intestinal phase I metabolism and active efflux drug transport systems, such as P-glycoprotein, have been recognized as important determinants of oral drug bioavailability(Benet *et al.*, 1996b). The contribution of intestinal CYP3A-mediated drug metabolism to poor oral drug bioavailability has been shown to be clinically important for many drugs, such as midazolam, cyclosporine and tacrolimus(Floren *et al.*, 1997; Hebert *et al.*, 1992; Thummel *et al.*, 1996; Wu *et al.*, 1995).

1.4 P-glycoprotein (P-gp), an ATP-Dependent Efflux Transporter for Xenobiotics

P-glycoprotein (P-gp) is a plasma membrane glycoprotein of about 170 KDa that belongs to the superfamily of ATP-binding cassette (ABC) transporters(Higgins, 1992). P-gp was discovered by Juliano and Ling (1976) in multidrug resistance (MDR) cancer cells after several reported observations that mammalian cancer cells, selected for resistance to a single cytotoxic agent, displayed cross-resistance to a broad spectrum of structurally and functionally unrelated compounds. P-gp functions as an energy-dependent drug efflux pump that lowers intracellular drug concentrations. Studies using reconstituted purified P-gp systems revealed that transport of one substrate molecule by P-gp required

on average hydrolysis of two ATP molecules(Ambudkar *et al.*, 1997). Expressed in tumor cells, P-gp causes the MDR phenotype by the active extrusion of a wide range of cancer chemotherapeutic drugs(Patel and Rothenberg, 1994).

In human, there are two MDR genes, MDR1 and MDR2. MDR1 encodes a drug transporting P-gp which confers drug resistance, whereas MDR2 encodes a P-gp that is specific for phosphatidylcholine translocation in cells(Gottesman and Pastan, 1993). In rodents, there are three mdr genes; mdr1a (mdr1) and mdr1b (mdr3) conferring multidrug resistance, whereas mdr2 is responsible for cell phospholipids transport (Table 1.4.1)(Gottesman and Pastan, 1993).

Table 1.4.1 Multiplicity and nomenclature of some mammalian P-gp genes

Organism	Drug transporters	Phospholipid transporters
Humans	MDR1	MDR2
Mice	mdr1a, mdr1b	mdr2
Rats	mdr1a, mdr1b	mdr2
Hamsters	pgp1, pgp2	pgp3

In addition to being expressed in tumor cells, P-gp is present in normal tissues (see Table 1.4.2). P-gp (MDR1) is expressed at a high level on the apical surfaces of epithelial cells in the liver (bile canaliculi), kidney (proximal tubule), pancreas (pancreatic ductule cell), small intestine and colon (columnar mucosal cell), and adrenal gland(Cordon-Cardo *et al.*, 1990; Thiebaut *et al.*,

1987). P-gp is also expressed in the capillary endothelium of the brain and testes which suggest that P-gp is likely to limit entry of certain molecules into specific anatomic compartments(Schinkel *et al.*, 1994). The tissue distribution of P-gp (MDR1) leads to a reasonable expectation that P-gp plays a role in defense against xenotoxins, namely excreting cytotoxic agents into bile, the gastrointestinal tract, urine as well as participating in blood brain barrier function.

Like multidrug resistance in cancer chemotherapy, drug resistance has emerged as a devasting impediment to the treatment of parasitic disease(Cowman and Foote, 1990). Members of the P-glycoprotein genefamily have been identified in *Plasmodia, Leishmania,* and *Entamoeba*(Ullman, 1995). The expression of these P-gp-like transporters has been implicated, although the exact mechanism(s) of drug resistance remains obscure. In *Plasmodium falciparum*, the most dangerous form of malaria, there are two MDR genes, pfmdr1, and pfmdr2; pfmdr1 confers drug resistance. Several drugs exhibiting resistance associated with pfmdr1 overexpression have been confirmed, e.g., mefloquine(Cowman *et al.*, 1994). Recently, a P-gp-related tcpgp2 gene was cloned in *Trypanosoma cruzi*(Dallagiovanna *et al.*, 1996). The relevance of this protein in drug resistance of *Trypanosoma cruzi* is under intensive study.

Table 1.4.2 Relative levels of MDR genes in human, mouse and rat tissues

	Human		Mouse			Rat		
	MDR1	MDR2	mdr1a	mdr1b	mdr2	mdr1a	mdr1b	mdr2
Liver	+++	++++	+	+	++	++	++	+++
Small Intestine	++++	-	+++	-	-	+++	+	-
Colon	++	-	ND	ND	ND	ND	ND	ND
Kidney	+++	+	+	++	-	++	+	-
Lung	++	-	++	+	+	++	++++	++
Spleen	++	+	+	+	++	+	+	++
Uterus (pregnant)	ND	ND	ND	+ (++++)	-	ND	ND	ND
Brain	+	-	++	+	ND	++	-	+
Heart	ND	+	++	++	++	+	-	+
Skeletal muscle	+	+	+	+	++	-	-	+

The number of + symbols indicate relative expression level. The - symbol indicates not found, and ND, not determined. Adapted from Silverman and Schrenk (1997).

MDR has become a synonym of P-gp overexpression in tumor cells in response to drug exposure, at least at the molecular level. P-gp can be up-regulated by a wide range of structurally unrelated compounds, many of which are P-gp substrates or inhibitors(Schuetz *et al.*, 1996; Silverman and Thorgeirsson, 1995).

P-gp has a broad substrate specificity covering a large number of structurally diverse compounds(Wacher *et al.*, 1995). It is not clear what determines the substrate specificity of P-gp. In general, P-gp substrates are hydrophobic and/or, organic cations at physiological pH.

A variety of genetic and biochemical approaches have been taken to understand the structure, function and mechanism of P-gp. Structurally, P-gp is a single polypeptide with two homologous halves connected by a short stretch of linker region(Gorski *et al.*, 1997) (see Figure 1.4.1). Each half consists of six transmembrane domains followed by a consensus ATP binding site (or called ATP-binding cassette, ABC). The transmembrane topology of P-gp was deduced from hydropathy analysis. The N- and C-termini, two ATP-binding sites and the linker region (connecting two ABCs) were experimentally confirmed to be located intracellularly, but the exact number of transmembrane domains within each ABC still remains putative.

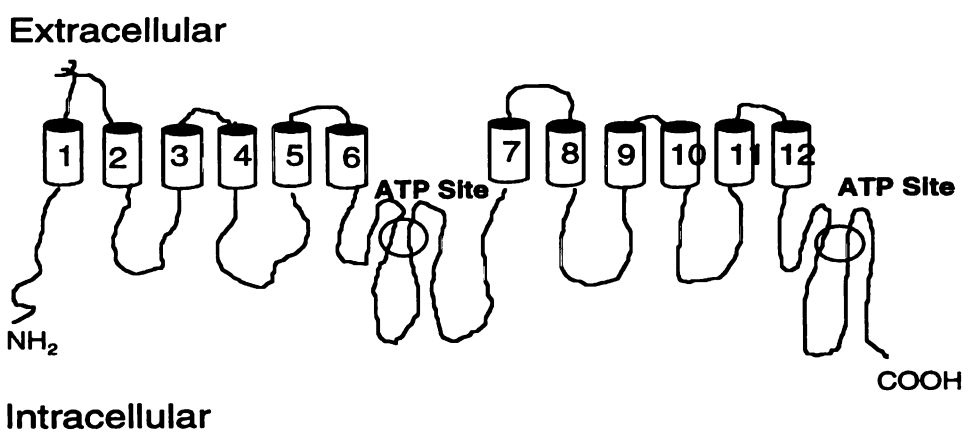

Figure 1.4.1 Two dimensional model of human MDR1 product P-glycoprotein (Gottesman and Pastan, 1993).

The substrate binding pockets of P-gp are under intensive study, using labeling and mutational analysis(Greenberger, 1993). There is general agreement that transmembrane segments 6 and 12 play a special role in drug binding. Amino acid substitutions at various transmembrane segments have been demonstrated to affect P-gp substrate specificity and/or transport activity, but it is not clear whether these alterations are due to the altered amino acid residues being directly involved in substrate binding or that the mutations change the global three-dimensional conformation of P-gp(Loo and Clarke, 1997; Taguchi *et al.*, 1997; Zhang *et al.*, 1995). Accumulating P-gp transport kinetic studies suggest the presence of at least two nonidentical substrate interaction sites in P-gp(Dey *et al.*, 1997; Shapiro and Ling, 1997).

Several transport models of P-gp have been proposed(Gottesman and Pastan, 1993). The classic model hypothesizes that P-gp can function as a pump which transports its substrates out of cell from the cytoplasm through a putative central pore formed by transmembrane domains. A modification of this classic model is the "vacuum cleaner" model by which P-gp can pump drugs from the membrane as well as from the cytoplasm to the central pore of P-gp. Recently, a 2.5 nm resolution hamster P-gp structure was determined by electron microscopy and image analysis(Rosenberg *et al.*, 1997). Despite the low resolution of this structure, a large central pore at the cytoplasmic face of the membrane as well as an additional opening on the side of the membrane can be identified from the image. Another proposed model is that P-gp acts as a drug flippase(Higgins and Gottesman, 1992). In this model, P-gp flips drugs from the

inner leaflet of the plasma membrane towards the out leaflet against a concentration gradient. This model has received considerable experimental support. However, how exactly P-gp transports drugs is still an enigma.

P-gp undergoes considerable post-translational modifications such as N-glycosylation (three sites on the first extracellular loop) and phosphorylation (many serines and threonines in the linker region) (Germann *et al.*, 1996; Schinkel *et al.*, 1993). The post-translation generally affects the regulatory function of the protein. However, removal of these N-glycosylation sites does not affect the substrate specificity of P-gp, but rather lowers the stability of P-gp in the membrane. Systematic replacement of serines and threonines in the linker region by alanine scanning has not altered P-gp transport activity.

Knockout mice with disruption of mdr1a or mdr1b, and double knockout mdr1a/1b (-/-) provide unique opportunities for the study of the physiological functions of P-gp(Schinkel *et al.*, 1995a). Studies on these knockout mice demonstrate that the absence of P-gp leads to a decreased elimination (increased accumulation) of P-gp substrates from (in) the body. The complete loss of P-gp from the blood-brain barrier has profound effects on drug distribution resulting in dramatically increased penetration of some drugs into the brain, e.g., vinblastine levels increased by two orders of magnitude compared with the control normal mice(Schumacher and Mollgard, 1997). The complete loss of P-gp from the gut supports the important role for intestinal P-gp in the excretion of drugs into the intestine and in limiting the uptake of drugs from the intestine. For

example, the oral bioavailability of paclitaxel is three-fold higher in mdr1a(-/-) mice compared with mdr1a(+/+) mice(Sparreboom *et al.*, 1997).

1.5 Overlapping Substrate Specificity and Tissue Distribution of CYP3A and P-gp

A strong overlap between substrate specificity and tissue distribution of P-gp and CYP3A has been recognized(Wacher *et al.*, 1995). Table 1.5.1 summarizes some examples of substrates and inhibitors of both CYP3A and P-gp.

The human CYP3A4 gene is located at chromosome locus 7q22.1, whereas MDR1 gene has been mapped to the same chromosome at 7q21.1. This adjacent gene localization suggests the possible coordination of gene expression of CYP3A4 and P-gp. Schuetz and co-workers (1996) demonstrated that some shared CYP3A4/P-gp substrates, such as reserpine, rifampicin, phenobarbital, and triactyloleandomycin, coordinatedly up-regulated CYP3A4 and P-gp expression in a human colon carcinoma cell line, LS180. However, the full picture of neither CYP3A nor P-gp gene regulation is clear at the present time.

Table 1.5.1 Substrates for and inhibitors of both CYP3A and P-gp(Wacher *et al.*, 1995)

CYP3A substrate	P-gp	CYP3A substrate or inhibitor (I)	P-gp
Antiarrhythmics		Flavonoids	
Amiodarone	I	Kaempferol(I)	E
Lidocaine	I	Quercerin (I)	E
Quinidine	I	Hormones	
Antifungals		Dexamethasone	S
Itraconazole	I	Hydrocortisone	S, I
Ketoconazole	I	Progesterone	I
Calcium-channel blockers		Testosterone	I
Diltiazem	S, I	Immunosuppressant	
Felodipine	I	Cyclosporine	S, I
Nicardipine	S, I	Tacrolimus (FK506)	S, I
Nitrendipine	I	Rapamycin	S
Nifedipine	I	HIV protease inhibitors	
Verapamil	S, I	Saquinavir	S
Chemotherapeutic agents		Indinavir	S
Etoposide	S	Ritonavir	S
Morpholino doxorubicin	S*	Nelfinavir	S
		Other	
Paclitaxel	S	RU486	I
Vinblastine	S	Erythromycin	I
Vincristine	S	Digitoxin	S**
Vindestine	S		

S, substrate; I, inhibitor; E, enhancer. * Doxorubicin is a P-gp substrate. ** Digoxin, a metabolite of digitoxin, is a P-gp substrate.

1.6 Working Hypothesis: Synergistic Actions of CYP3A and P-gp Play Complementary Roles in Drug Disposition

The above mentioned overlap between CYP3A and P-gp suggests that CYP3A and P-gp may play complementary roles in drug absorption, disposition, metabolism and elimination by biotransformation and counter-transport, especially in the villi of the small intestine. Our hypotheses are that CYP3A and P-gp act synergistically in the small intestine as a barrier to oral drug bioavailability and that the poor oral bioavailability caused by CYP3A and P-gp can be overcome by co-administration of CYP3A and/or P-gp inhibitors. Figure 1.6.1 illustrates our working hypotheses. Drug is absorbed by passive processes into the enterocyte where it may be metabolized by CYP3A and also subject to active countertransport by P-gp back into the gut lumen. The passive absorption and countertransport may continually cycle a drug between the enterocyte and the gut lumen, thus allowing the CYP3A to have repeated access to the drug molecule, or leading to non-absorption, due to the continual countertransport. The CYP3A-mediated metabolism and P-gp-mediated countertransport in the enterocyte limit the amount of intact drug which enters into the systemic circulation, thus decrease drug oral bioavailability (Figure 1.6.1a). We further hypothesize that this oral drug bioavailability barrier can be overcome by co-admistration of CYP3A and/or P-gp inhibitors (Figure 1.6.1b).

(a)

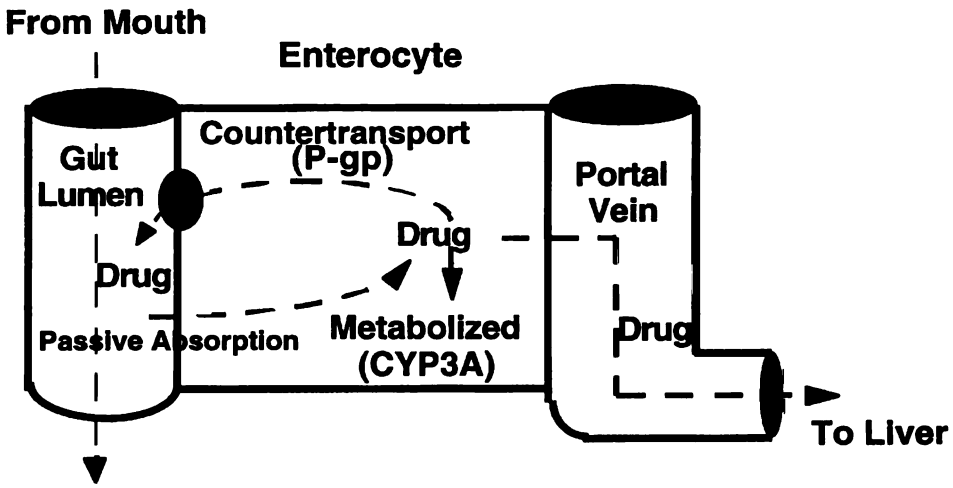

(b)

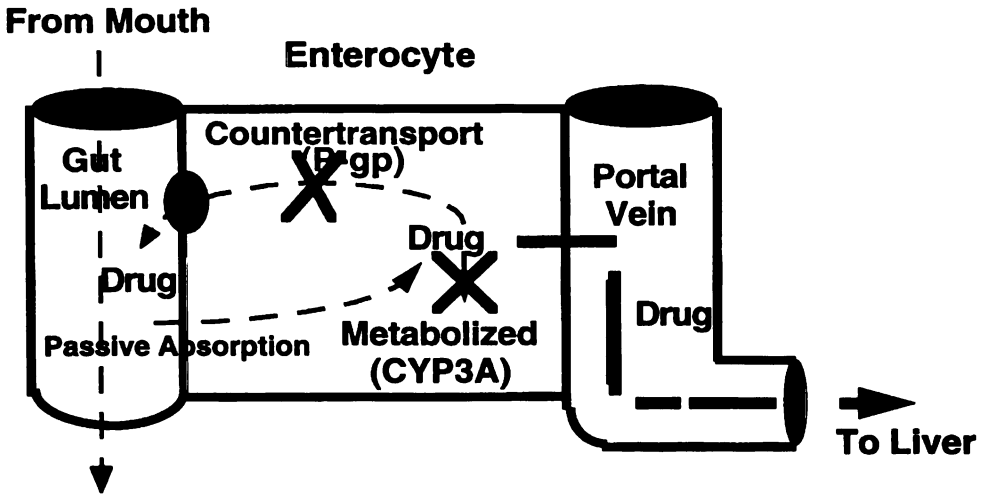

Figure 1.6.1 (a) Synergistic CYP3A/P-gp oral drug bioavailability barrier in the gut (b) enhancing drug uptake by inhibition of either CYP3A or P-gp.

1.7 Objectives

At present, there is very little data regarding the interactions of CYP3A4 and P-gp with peptidomimetics. K02 is the first example of therapeutically important peptidomimetics to be examined using both *in vitro* and *in vivo* approaches to assess the roles of CYP3A4 and P-gp in drug metabolism, counter-transport and pharmacokinetics. This study provides a vivid example of the impact of drug metabolism, drug transport and pharmacokinetics on modern drug development.

The overall goal of this study is to test the above mentioned hypotheses by studying K02, a novel peptidomimetic cysteine protease inhibitor.

The objectives are:

1. To determine if K02 is a substrate for CYP3A4 and to identify if CYP3A4 is the principle enzyme catalyzing K02 oxidation in human liver microsomal incubation systems.
2. To determine if K02 is a substrate for P-gp and to characterize the transport properties of K02 in MDR1-expressed epithelial cell monolayers.
3. To characterize the pharmacokinetics of K02 and to investigate the effects of CYP3A and/or P-gp inhibitors on K02 pharmacokinetics in male Sprague-Dawley (SD) rats.

Chapter 2 Biotransformation of K02, the Role of CYP3A in Catalyzing K02 Oxidation in Microsomal Incubation Systems

2.1 Introduction

As noted in Chapter 1, the human CYP3A subfamily of cytochrome P450 contains the most important CYP involved in drug metabolism of a growing list of medications. The human CYP3A subfamily is composed of 3 genes: CYP3A4, CYP3A5 and CYP3A7. CYP3A4, the major CYP expressed in the liver and small intestine, has been shown to be responsible for the metabolism of a large number of structurally diverse endogenous compounds and xenobiotics. CYP3A5 is polymorphically expressed in the liver of about 25% of adults, but ubiquitously expressed in kidney. CYP3A7 is present in the human fetal liver. In rat, CYP3A1 and CYP3A2 are two major members of the CYP3A subfamily. Because the CYP3A subfamily is involved in the metabolism of more than 50% of drugs metabolized by CYPs in human and CYP3A4 can be induced by many of its substrates, the potential for drug-drug interactions within these CYP3A drugs is of clinical importance. CYP3A4 also plays a significant role in intestinal drug metabolism and limits the oral bioavailability of drugs which are CYP3A substrates(Hebert *et al.*, 1992; Thummel *et al.*, 1996; Wu *et al.*, 1995).

We hypothesize that K02, a vinylsulfone peptidomimetic, is a CYP3A substrate and that CYP3A4 is the principle enzyme catalyzing the oxidation of K02 in human.

2.2 Materials and Methods

Chemicals and Biochemicals. Mu-Phe-Hph-VSPh (K02, aka K11002) was kindly supplied by Dr. James Palmer of Arris Pharmaceutical Corporation (South San Francisco, CA). Midazolam was a gift from Hoffmann-LaRoche (Nutley, NJ). Ketoconazole was purchased from USPC (Rockville, MD). 7,8-Benzoflavone, β-NADPH, quinidine and sulfaphenazole were obtained from Sigma Chemical Co. (St. Louis, MO). 4-Dimethylamino-4'-(imidazol-1-yl)chalcone was kindly provided by Dean George L. Kenyon, School of Pharmacy, UCSF. Other chemicals were of reagent grade and also purchased from Sigma. All solvents were of HPLC grade and obtained from Fisher Scientific (Santa Clara, CA). Biorad Protein Assay Kit with albumin protein standard was obtained from Biorad (Richmond, CA). The rabbit anti-human CYP3A polyclonal antibody and preimmune IgG were kindly provided by Dr. Steven A. Wrighton, Eli Lilly and Company (Indianapolis, IN). cDNA-expressed human CYP3A4 (M107r) was purchased from Gentest (Cambridge, MA). Male Sprague-Dawley (SD) rats were purchased from B&K Inc. (Fremont, CA).

Human Liver, Rat Liver and Intestinal Microsome Preparation. A human liver sample was obtained under a protocol approved by the Committee on Human Research, UCSF. An animal protocol for using male SD rat liver and intestine was approved by the Committee on Animal Research, UCSF. Microsomes were

prepared by differential centrifugation(Bornheim and Correia, 1989). The CYP content in microsomal suspensions was measured using the carbon monoxide difference spectrum (Omura and Sato, 1964), and protein concentration was determined by the method of Lowry *et al.* (1951).

Incubation Procedure for K02 Metabolism in Human Liver Microsomes and cDNA Expressed CYP3A4

General Incubation Procedure. K02 metabolism in human liver microsomes was found to be linear over 20-min incubations with microsomal protein concentration at 1-2 mg/ml. Incubation mixtures (final volumes of 0.5 ml) contained human liver microsomes (1.5 mg protein/ml) or microsomes prepared from a human B-lymphoblastoid cell line (engineered to stably express human CYP3A4 cDNA) (4 mg/ml) in 0.1 M phosphate buffer, and K02 (10 μM - 200 μM) in methanol (not greater than 1% v/v). After a 5-min preincubation at

37°C, the reaction was initiated by adding NADPH (1 mM) and incubated at 37°C for 10 min. The reaction was stopped by adding 0.5 ml of ice-cold precipitation reagent (62.5% methanol, 37.5% acetonotrile). The internal standard, 4-dimethylamino-4'-(imidazol-1-yl)chalcone in methanol, was added. The resultant mixture was vortex mixed and centrifuged at 13,400 g for 12min to precipitate protein. An aliquot of the supernatant (100 μl) was subjected to HPLC analysis.

Chemical Inhibition Study. The reversible inhibitors for CYPs used in this study, ketoconazole(CYP3A), 7,8-benzoflavone(CYP1A2), quinidine(CYP2D6), and

sulfaphenazole(CYP2C9), were added to the incubation mixture at the same time with K02 (50 μM). The incubation protocol was the same as that described above, see *General Incubation Procedure*.

Immunoinhibition Study A designated amount of polyclonal anti-CYP3A rabbit antibody or preimmune rabbit IgG was incubated with microsomes for 30 min at room temperature before the K02 incubation, as described above.

HPLC Assay for K02 and Metabolites. A Shimadzu LC-600 HPLC system and a Waters 710B WISP autosampler were used with a Shimadzu SPD-10A UV spectrophotometric detector operated at 220nm. A Dupont Zorbax SB-C18 column (MAC-MOD Analytical, Inc., Chadds Ford, PA), 3.0 x 250 mm was used with a precolumn 0.2 mm frit. The isocratic mobile phase of 10mM potassium phosphate, pH 6.0: methanol : acetonitrile (44:35:21; v:v:v) was delivered at 0.5ml/min. Under these conditions, K02 and the internal standard eluted at 29 and 35 min, respectively. All K02 metabolites eluted between 8 - 24 min. Chromatographic data were collected through a Hewlett Packard 3392A integrator.

Inhibition of Midazolam Oxidation by K02 in Human Liver Microsomes. The incubation procedure of midazolam in the presence or absence of K02 in human liver microsomes was the same as described above. The HPLC analysis of

midazolam, 4-hydroxymidazolam and 1'-hydroxymidazolam, was carried out following the method of Wrighton and Ring (1994).

Mass Spectrometric Analysis. Mass and tandem mass spectra of K02 and its metabolites were acquired using a PE SCIEX API III triple quadrupole mass spectrometer (Perkin-Elmer/ABI, Foster City, CA) equipped with a heated Nebulizer inlet (Thornhili, Ontario, Canada). Positive ionization was achieved by APCI (atmospheric pressure chemical ionization). Scans were acquired over the ranges of m/z 200 - 700 for MS and m/z 50 - 600 for MS/MS. Collisional activations were accomplished for MS/MS using 90% argon and 10% nitrogen as the collision gas at an energy of 25 ev.

2.3 Results

2.3.1 Metabolism of K02 in Human Liver Microsomes

Figure 2.3.1.1a illustrates a typical HPLC chromatograph of the metabolite profile for K02 in a human liver microsomal incubation. Three major metabolites, M12, M19 and M20 (numbered with reference to retention times) were chosen for further study to identify the major CYPs involved in the biotransformation. The formation of all metabolites were NADPH dependent, and the formation of these three metabolites appeared to follow single Michaelis-Menten type

kinetics. The corresponding K_m and V_{max} values are summarized in Table 2.3.1.1.

Table 2.3.1.1 Kinetic parameters of primary metabolites, M12, M19 and M20 of K02, in incubations of human liver microsomes and cDNA-expressed CYP3A4.

	K_m (μM)	V_{max} (nmol/min/mg protein)	Incubation system
M12	37.6 ± 3.4	1.51 ± 0.01	HLM
M12	10.9 ± 2.9	0.53 ± 0.04	CYP3A4
M19	52.4 ± 3.5	0.30 ± 0.02	HLM
M19	18.0 ± 3.2	0.45 ± 0.03	CYP3A4
M20	33.3 ± 8.4	1.19 ± 0.06	HLM
M20	31.2 ± 0.1	0.65 ± 0.01	CYP3A4

HLM, human liver microsomes; CYP3A4, cDNA-expressed CYP3A4

Determination of Metabolite Structure by Tandem Mass Spectrometry. M12, M19 and M20 were determined to be single hydroxylated products of the parent compound K02 by LC/MS. Analysis of tandem mass spectra of these three major primary metabolites revealed the possible hydroxylation sites. The deduced structures of M12, M19 and M20 and the corresponding MS/MS spectra are illustrated in Figure 2.3.1.2b-d, together with that for K02 (Figure 2.3.1.2a). Other K02 metabolites shown in Figure 2.3.2.1a were determined to be isomers of M12, M19 and M20 in terms of the corresponding hydroxylation regions.

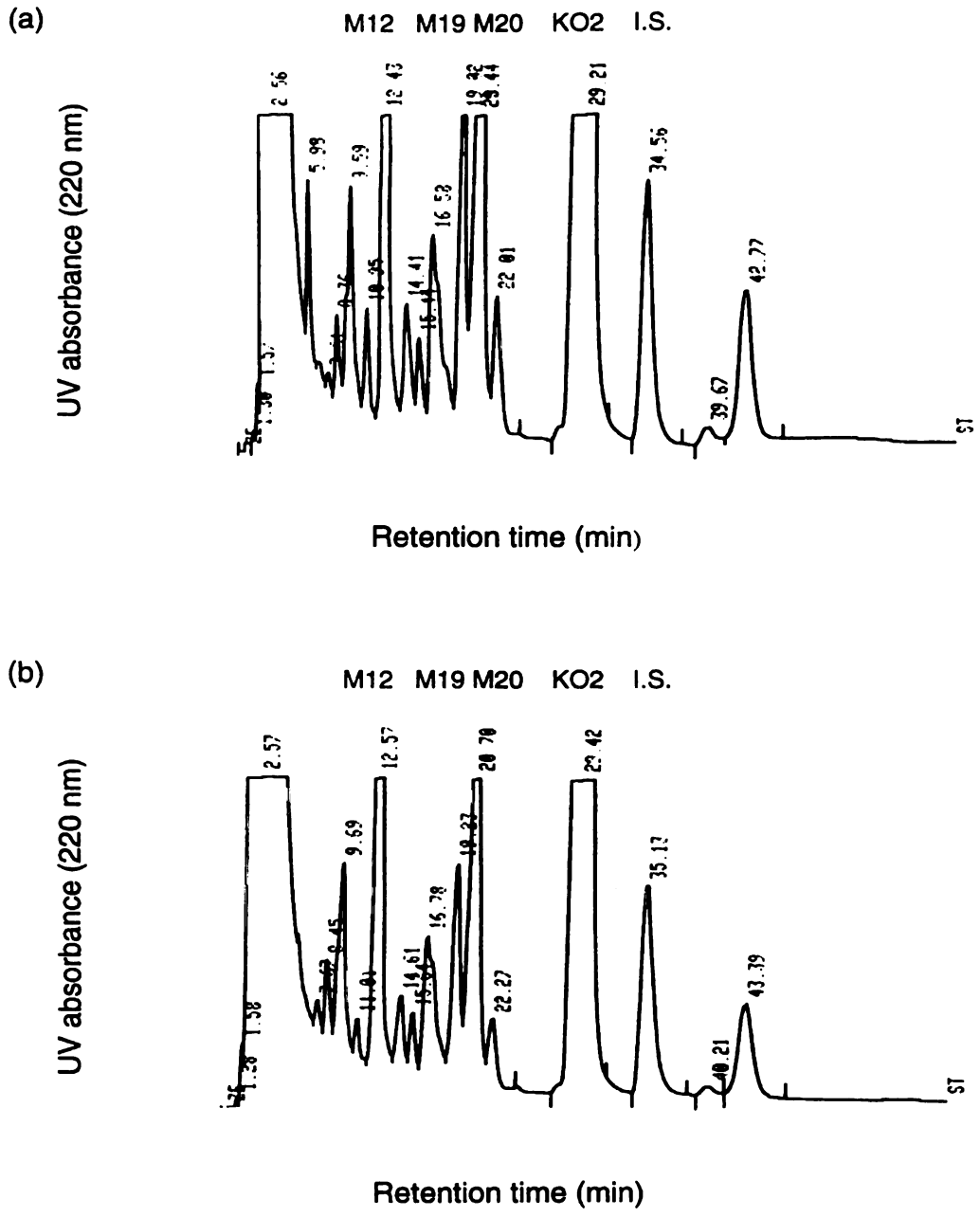

Figure 2.3.1.1 Typical HPLC chromatographs of K02 and its metabolites formed using *in vitro* incubation systems. (a) human liver microsomes, (b) cDNA-expressed human CYP3A4. K02 concentration is 100 μM in both cases.

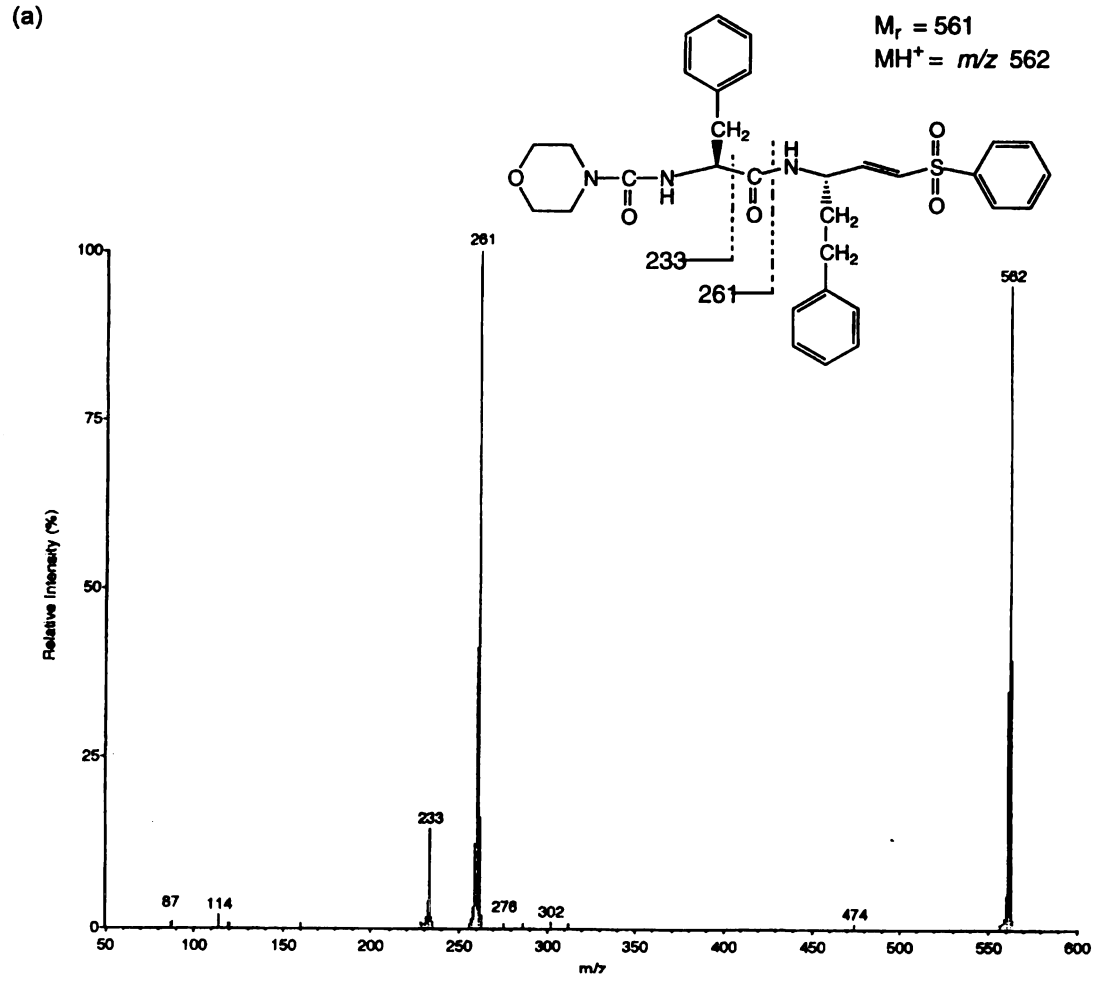

Figure 2.3.1.2 Tandem mass spectra of K02 and its three major primary hydroxylated metabolites with corresponding deduced structures. (a) K02, (b) M12, (c) M19, (d) M20.

(b)

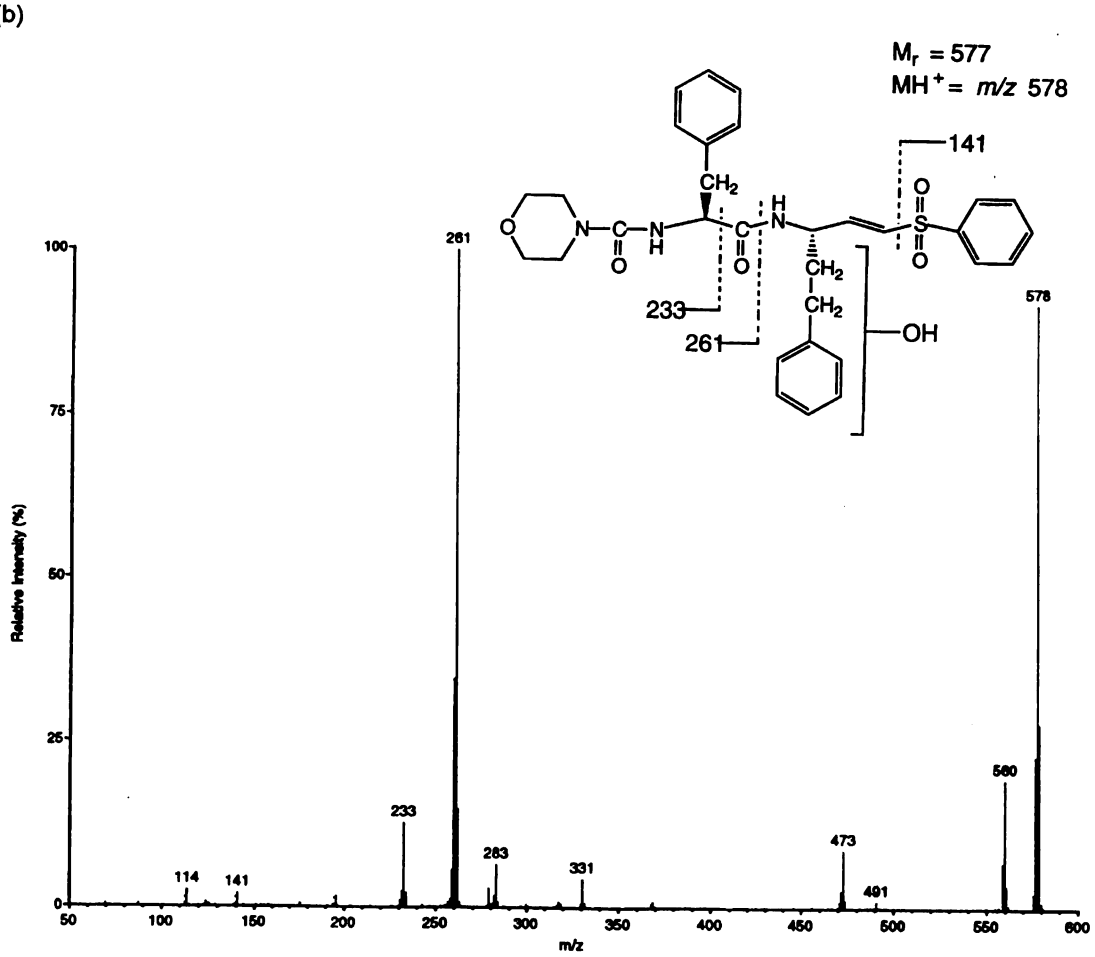
M_r = 577
MH^+ = *m/z* 578
141
233
261
OH
Relative Intensity (%)
m/z
261
578
560
233
473
263
331
491
114
141

(c)

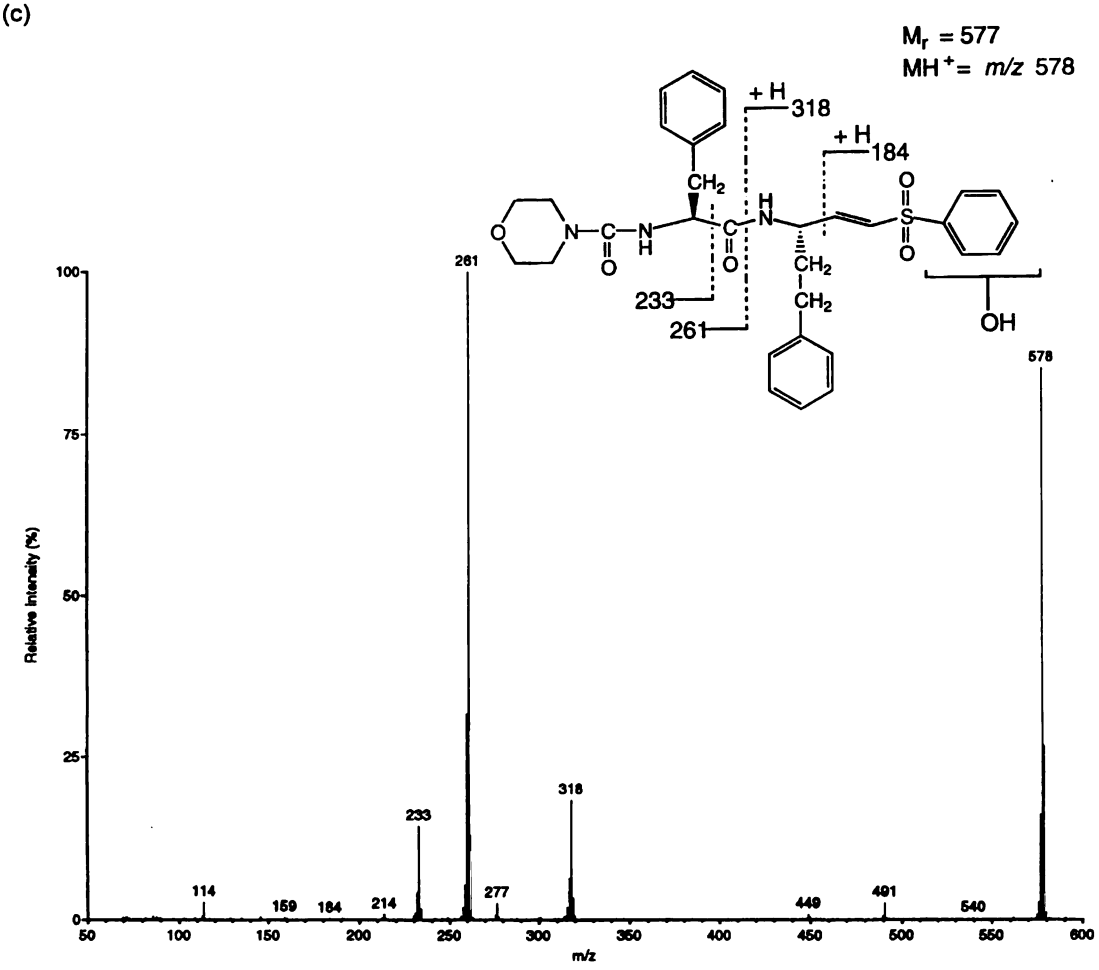
M_r = 577
MH^+= *m/z* 578
+ H
318
+ H
184
233
261
OH
Relative Intensity (%)
m/z
261
318
233
578
114
159
184
214
277
449
491
540

(d)

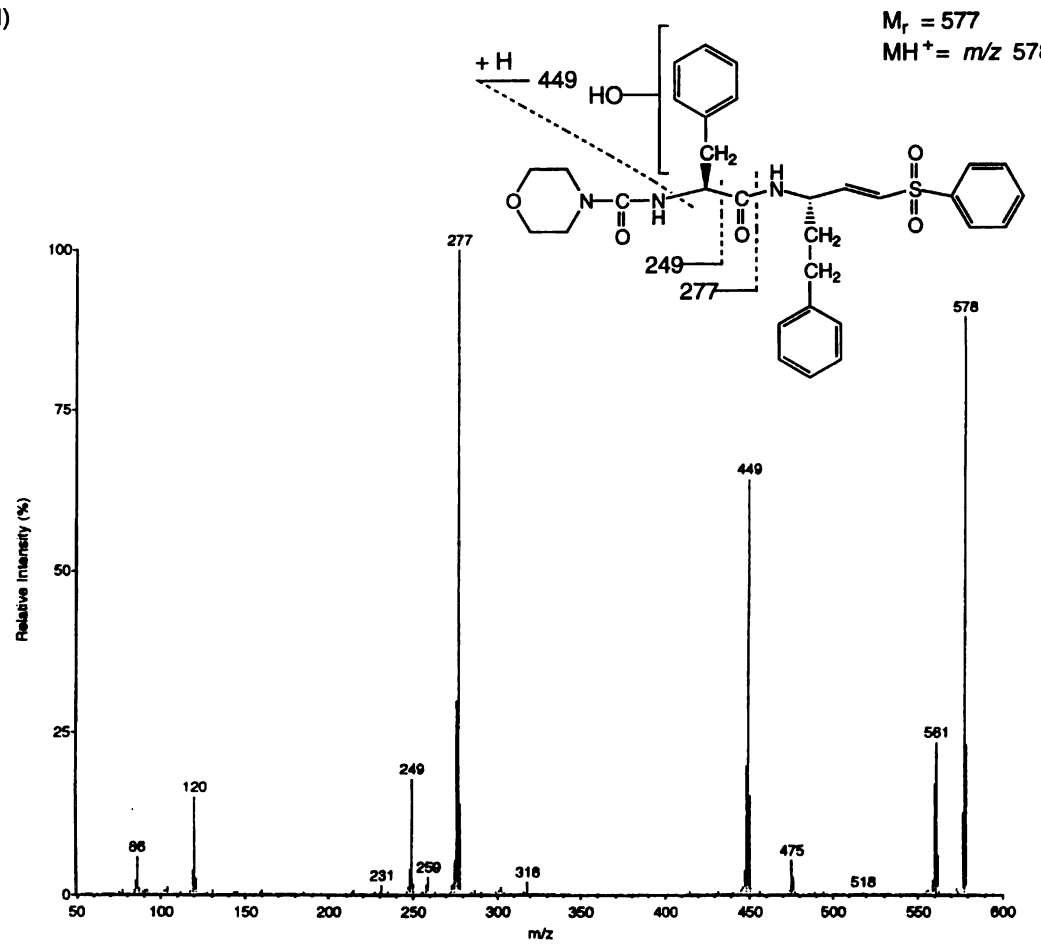
M_r = 577
MH^+ = *m/z* 578
+ H
449
HO
CH_2
249
277
CH_2
CH_2
Relative Intensity (%)
m/z
277
449
578
581
249
120
86
231
259
316
475
518

CYP3A4, the Primary Enzyme Responsible for K02 Biotransformation in Human Liver Microsomes

Chemical Inhibition Study. Ketoconazole, a reversible inhibitor of CYP3A4 strongly inhibits the formation of M12, M19 and M20 with IC_{50} values in the range of 1-4 μM (Figure 2.3.1.3). Quinidine, 7,8-benzoflavone and sulfaphenazole, selective chemical inhibitors of CYP2D6, CYP1A2 and CYP2C9 at their respective recommended inhibitor concentrations (Halpert *et al.*, 1994), had no significant effects on the formation of M12, M19 and M20 (Figure 2.3.1.4).

Immunoinhibition Study. Rabbit CYP3A polyclonal antibody(Gorski *et al.*, 1994), known to cross-react with human CYP3A4, exhibited concentration dependent inhibitory effects on M12, M19 and M20 formation. At a concentration of 200 μ l/mg microsomal protein, this antibody showed 75% -94% inhibitory effects on M12, M19 and M20 formation (Figure 2.3.1.5).

Metabolism by cDNA-expressed CYP3A4. The HPLC chromatograph of the metabolite profile of K02 in a cDNA-expressed human CYP3A4 (co-expressed with CYP reductase) system is shown in Figure 2.3.1.1b. Identical metabolite profiles are observed for HPLC chromatographs obtained following K02 incubations in human liver microsomes and cDNA-expressed human CYP3A4 (Figures 2.3.1.1a and b). The formations of M12, M19 and M20 appear to follow single Michaelis-Menten kinetics with the cDNA-expressed enzyme. The corresponding K_m and V_{max} values are summarized in Table 2.3.1.1.

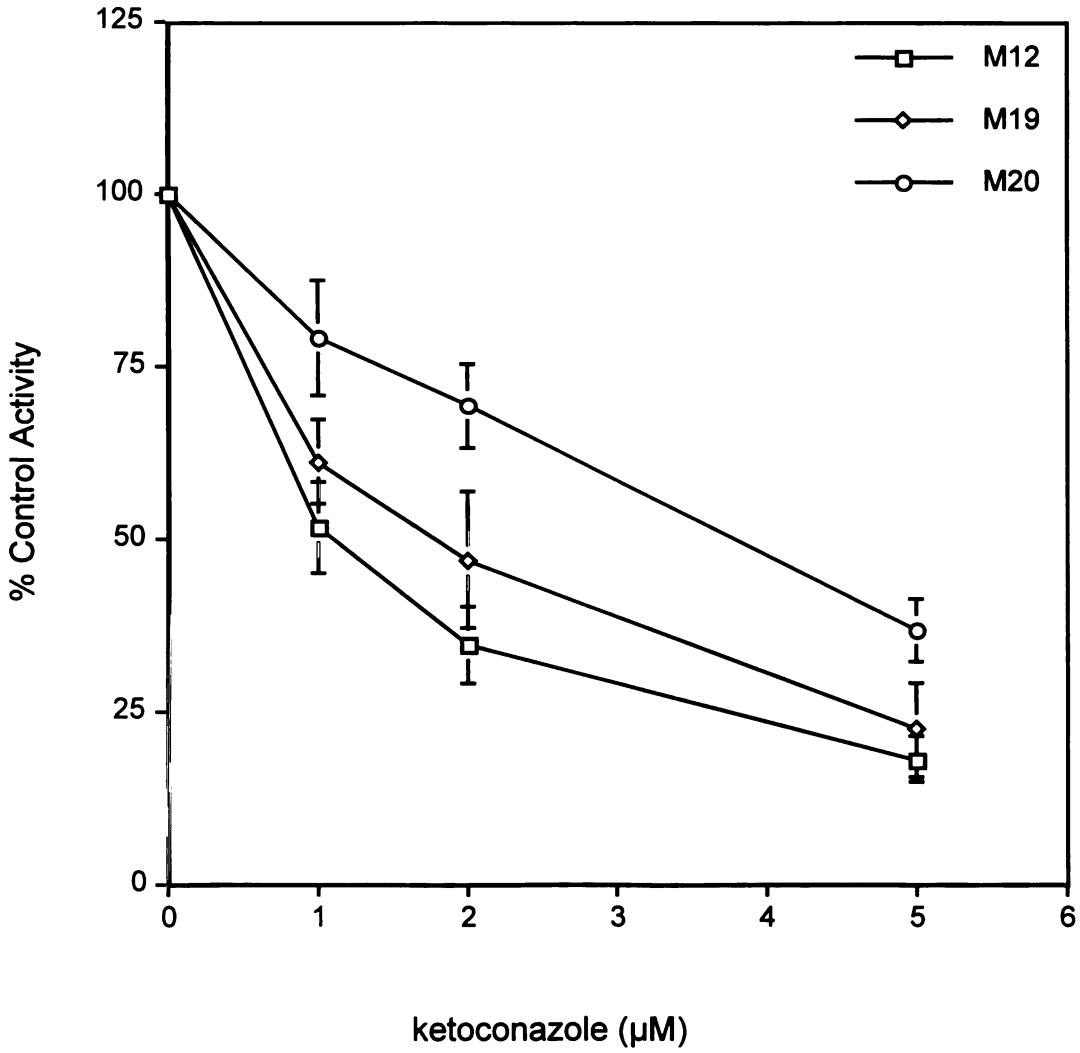

Figure 2.3.1.3 Effect of ketoconazole on the formation in human liver microsomes of the three major primary metabolites of K02. Values are mean of duplicate incubations ± standard deviation.

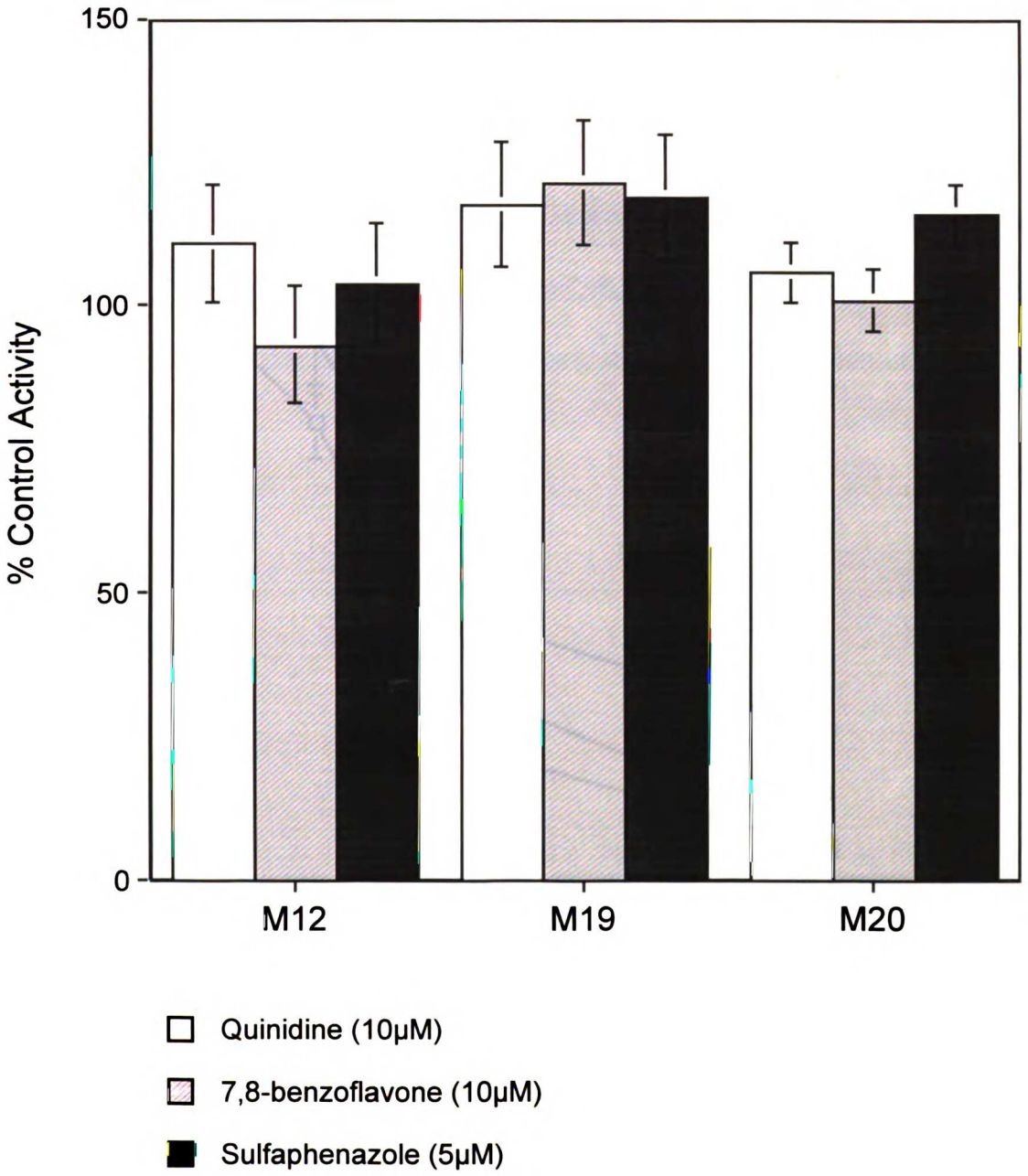

Figure 2.3.1.4 Effects of various selective inhibitors of CYPs on the formation in human liver microsomes of the three major primary metabolites of K02. Values are mean of duplicate incubations ± standard deviation.

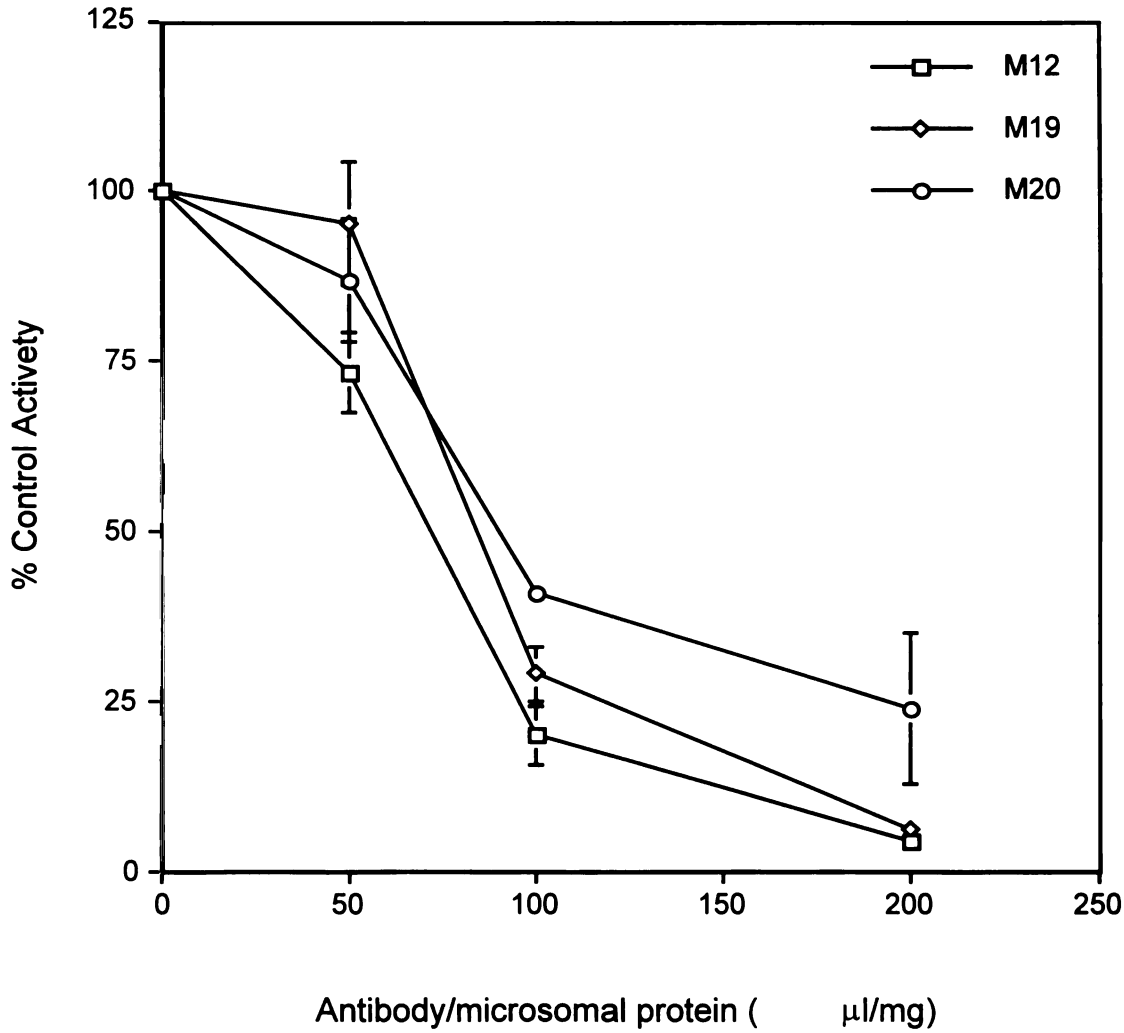

Figure 2.3.1.5 Effect of rabbit anti-human CYP3A polyclonal antibody on the formation in human liver microsomes of the three major primary metabolites of K02. Values are mean of duplicate incubations ± standard deviation.

Inhibition of 1'-Hydroxyl-Midazolam Formation by K02 in Human Liver Microsomes. The Lineweaver-Burk plot shown in Figure 2.3.1.6 demonstrates that K02 competetively inhibits the formation of 1'-hydroxyl-midazolam, a major metabolite formed in humans and catalyzed by CYP3A4. The concentration range of midazolam was 12.5 - 100 μM. The K_m of 1'-hydroxyl-midazolam was determined to be 11.9 ± 0.6 μM, and the K_i of K02 was found to be 12.1 ± 0.2 μM by nonlinear regression analysis using PCNONLIN v.4.0 (Statistical Consultants Inc., Lexington, KY) based on a simple competitive inhibition Michaelis-Menten model.

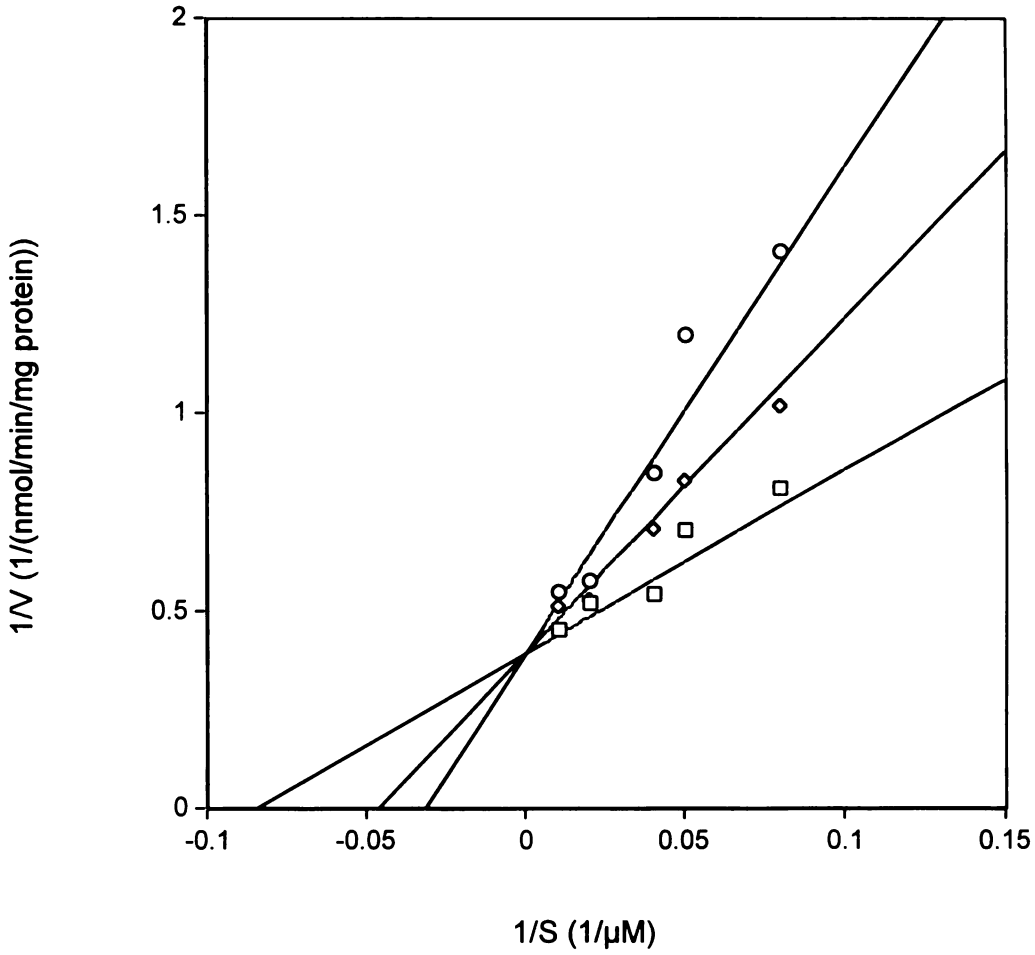

Figure 2.3.1.6 Lineweaver-Burk plot showing that K02 competitively inhibits 1'-hydroxymidazolam formation in human liver microsomes. Midazolam concentrations are in the range of 12.5 μM - 100 μM, (□) 0 μM K02, (◊) 10 μM K02, (O) 20 μM K02. Solid lines depict fit of data by nonlinear regression analysis using PCNONLIN v.4.0 (Statistical Consultants Inc., Lexington, KY) based on a simple competitive inhibition Michaelis-Menten model. The corresponding kinetic parameters are calculated to be V_{max} = 2.6±0.1 nmol/min/mg protein, K_m = 11.9±0.6 μM, and K_i = 12.1±0.2 μM.

2.3.2 Metabolism of K02 in Rat Liver and Intestinal Microsomes

HPLC chromatographs of the K02 biotransformation profile following K02 incubations in rat liver and intestinal microsomes are shown in Figures 2.3.2.1a and b, respectively. The catalytic activity for K02 oxidation in rat intestinal microsomes is about 10% of that in rat liver microsomes, mainly due to the low concentration of cytochrome P450s in enterosomes. M20, a major metabolite formed in these microsomal incubation systems, was chosen for the identification of the major CYPs involved in K02 biotransformation in the rat liver and intestinal microsomes. Chemical and immunoinhibition of M20 formation in rat liver and intestinal microsomes are demonstrated in Figures 2.3.2.2 and 2.3.2.3, respectively. Ketoconazole, a reversible inhibitor of CYP3A4 strongly inhibited the formation of M20. Quinidine, 7,8-benzoflavone and sulfaphenazole, selective chemical inhibitors of CYP2D6, CYP1A2 and CYP2C9 at their respective recommended inhibitor concentrations, had no significant effects on the formation of M20. Rabbit anti-rat CYP3A2 polyclonal antibody also significantly inhibited M20 formation.

(a)

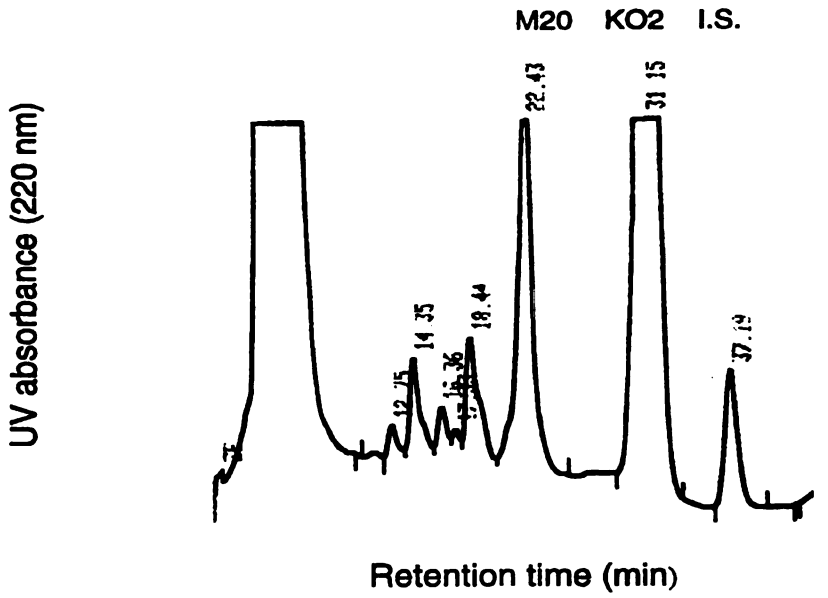

(b)

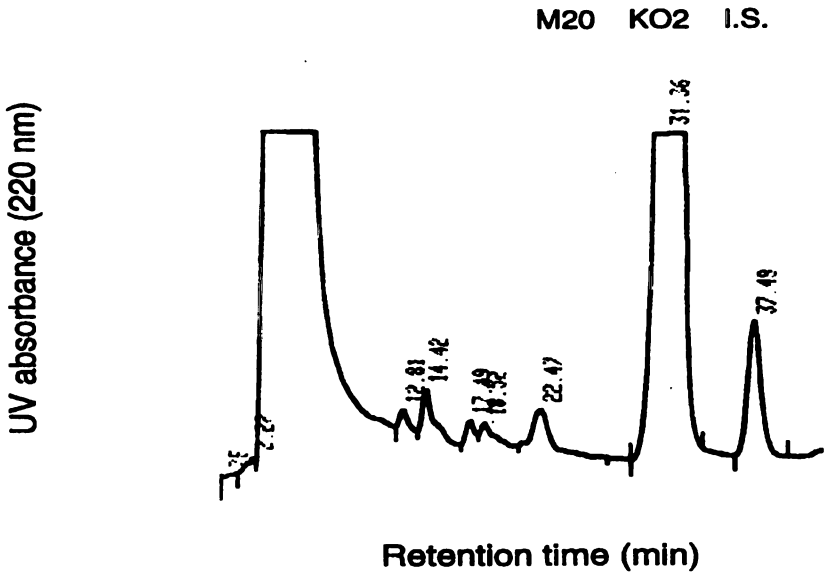

Figure 2.3.2.1 Typical HPLC chromatographs of K02 and its metabolites formed using *in vitro* incubation systems. (a) rat liver microsomes, (b) rat intestinal microsomes. K02 concentration is 100 μM in both cases.

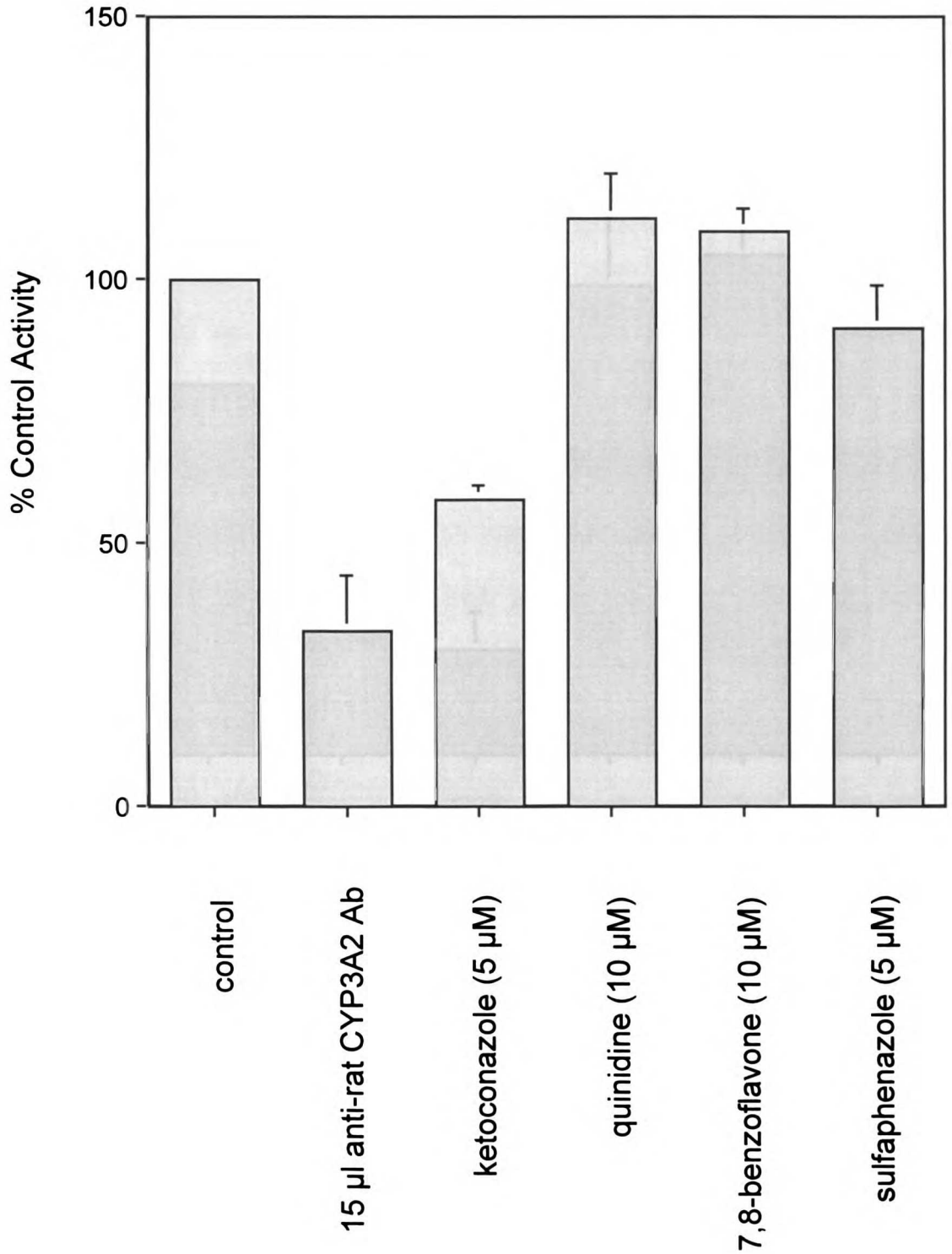

Figure 2.3.2.2 Chemical and immunoinhibition of M20 formation in rat liver microsomes. K02 concentration is 50 µM. Values are means of three measurements ± standard deviation

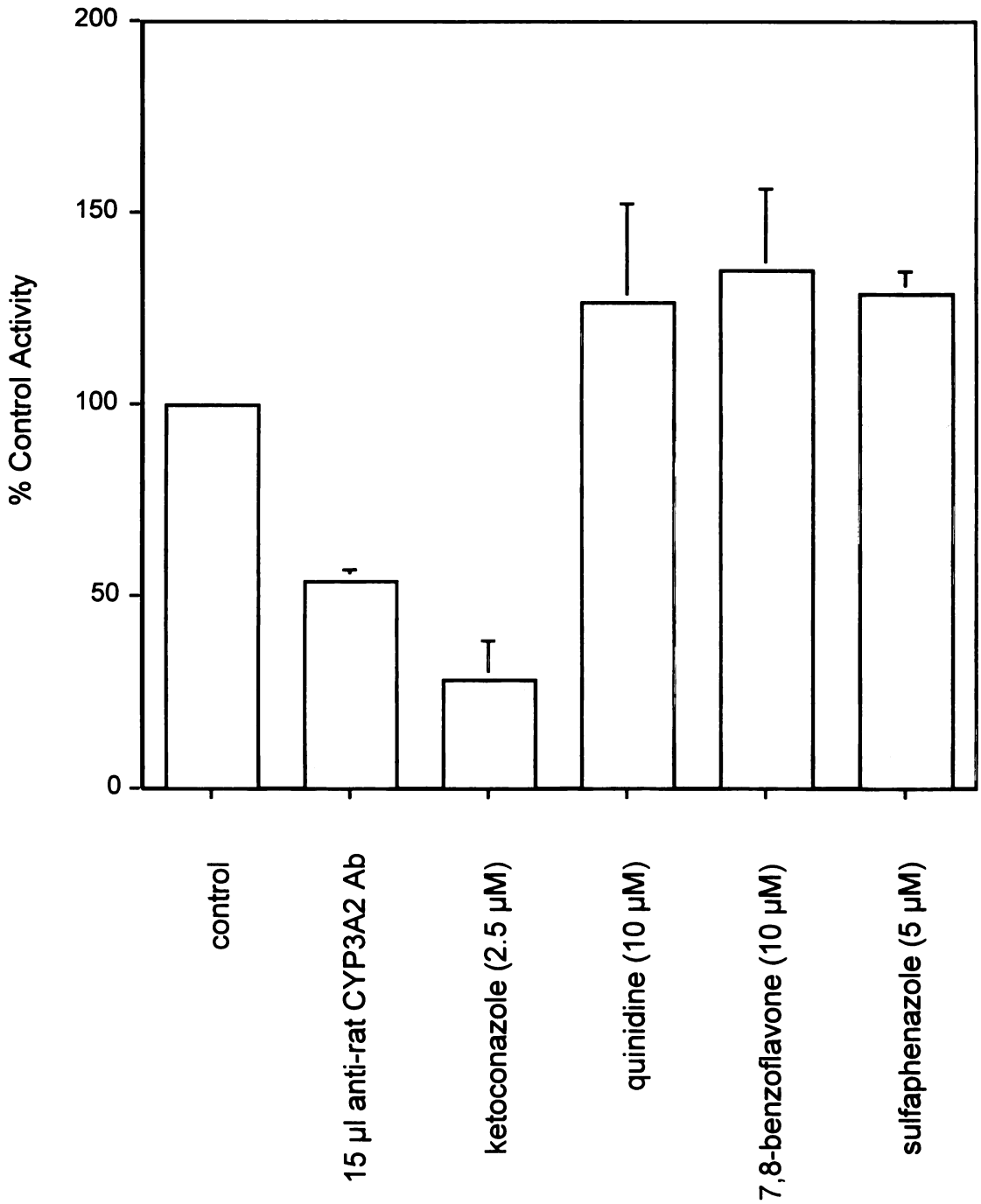

Figure 2.3.2.3 Chemical and immunoinhibition of M20 formation in rat intestinal microsomes. K02 concentration is 50 µM. Values are means of three measurements ± standard deviation

2.4 Discussion

K02 is the first vinylsulfone peptidomimetic that has been subjected to biotransformation studies using human liver, rat liver and intestinal microsome preparations. K02 and other vinylsulfone peptidomimetics of its class act as potent inhibitors of cathepsins B and L, two cancer associated cysteine proteases, cathepsin K, cathepsin S, and of cruzain, the major cysteine protease present in *T. cruzi*. The study described here demonstrates that K02 is a substrate of CYP3A and that CYP3A plays the primary role in the oxidative biotransformation of K02 in human liver as well as in rat liver and intestinal microsomal preparations. This conclusion is based on the results of an integrated *in vitro* approach utilizing 1) selective CYP chemical inhibitors; 2) immunoinhibition with CYP3A antibody; and 3) cDNA-expressed human CYP3A4. Both ketoconazole, a CYP3A selective inhibitor, and rabbit anti-CYP3A antibody demonstrate potent and concentration dependent inhibitory effects on the formation of three major primary hydroxylated metabolites of K02, designated M12, M19 and M20. The IC_{50}s of ketoconazole were in the range of 1-4 μM, which is a typical value for this potent reversible CYP3A inhibitor. Representative chemical inhibitors to other major cytochrome P450 enzymes responsible for human drug metabolism, CYP2D6 (quinidine), CYP2C9 (7,8-benzoflavone), and CYP1A2 (sulfaphenazole), at their recommended concentrations, showed no significant effects on K02 metabolite formation.

Incubation of K02 with cDNA-expressed human CYP3A4 demonstrates an almost identical metabolite profile with that obtained in human liver microsomes. However, the K_m and V_{max} values obtained in these two incubation systems are not exactly comparable, with differences of up to 4-fold. We speculate that the CYP conformations and/or the interactions of NADPH cytochrome P450 reductase with CYP are not exactly the same in these two systems due to differing conditions of the microsomal membranes and that protein binding characteristics may differ in these two microsomal incubation systems. K02 also competetively inhibits the formation of 1'-hydroxylmidazolam, the major midazolam metabolite in human, which is catalyzed by CYP3A4. This suggests the potential for drug-drug interactions of K02 with other CYP3A substrates when the drugs are administered concomitantly. We confirmed that CYP3A is also the major CYP enzyme for K02 oxidation in rat liver and intestinal microsomes. Ketoconazole, a potent CYP3A inhibitor, can significantly inhibit K02 biotransformation in rat liver and intestinal microsomes. Although *in vitro* microsomal incubations demonstrate that the catalytic activity of rat intestinal microsomes is much less than that of rat liver microsomes, we believe this may not quantitatively reflect the relative activity of K02 hepatic and intestinal metabolism in *vivo* due to the difficulty of preparing and maintaining enterosomes *in vitro*.

The three major oxidation sites of K02 catalyzed by CYP3A are hydroxylation at phenylalanine, homophenylalanine and vinylsulfone benzene side chains. The major oxidative metabolites of HIV protease inhibitors are

hydroxylated products at side chains of the parent compounds and N-deakylation products(Chiba *et al.*, 1997; Fitzsimmons and Collins, 1997; Kumar *et al.*, 1996). Although K02 and HIV protease inhibitors target different enzymes and differ in chemical structure, these peptidomimetics are all CYP3A substrates and the oxidation reactions catalyzed by CYP3A are similar, i.e., hydroxylation and/or N-dealkylation on side chains of peptidomimetics. Due to lack of an accurate three-dimensional structure of the active site of CYP3A, it is difficult to precisely predict the oxidative sites of CYP3A substrates.

This study provides valuable feedback for early drug discovery and development for this class of vinylsulfone peptidomimetics.

2.5 Summary

Here we investigated the disposition features of K02 using *in vitro* systems, characterizing the drug's interaction with human cytochrome P450 3A (CYP3A). An HPLC assay was developed to analyze K02 and its metabolites formed in human liver microsomes. Three major primary metabolites were determined by LC/MS/MS to be hydroxylated products of the parent compound. A rabbit CYP3A polyclonal antibody (200μl antibody / mg microsomal protein) exhibited 75% - 94% inhibition of the formation of these three hydroxylated metabolites. Ketoconazole (5μM), a selective CYP3A inhibitor, produced up to

75% inhibitory effect, while other CYP specific inhibitors (quinidine (2D6), 7,8-benzoflavone (1A2) and sulfaphenazole (2C9)) showed no significant effects. An identical metabolite formation profile for K02 was observed for cDNA-expressed human CYP3A4 (Gentest). Formation of 1'-hydroxymidazolam, the primary human midazolam metabolite, was markedly inhibited by K02 via competitive processes which suggests the potential for drug-drug interactions of K02 with other CYP3A substrates. Similar results were obtained in rat liver and intestinal microsomal incubation systems. Collectively, these data demonstrate that K02 is a substrate for CYP3A and that CYP3A is the principle enzyme responsible for K02 oxidation by *in vitro* microsomal systems in human and rat.

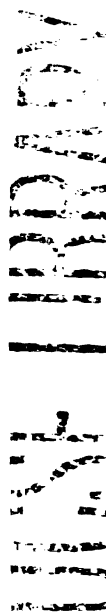

Chapter 3 K02 is a Substrate for P-gp: the Transport Properties of K02 Across MDR1-MDCK and Caco-2 Cell Monolayers

3.1 Introduction

In the kidney, intestine, liver and pancreas, P-glycoprotein is expressed in a polarized manner. It is located on the apical surfaces of proximal tubule cells of the kidney, intestinal epithelial cells, biliary face of hepatocytes and small ductules of the pancreas(Thiebaut *et al.*, 1987). P-gp functions as an ATP-dependent drug efflux pump and actively excretes a variety of structurally unrelated compounds out of cells and into the lumen of excretory organs.

The availability of several P-gp polarized-expressed epithelial cell lines, such as MDR1 transfected MDCK and LLC-PK1cell lines, and the wild-type Caco-2 cell line, makes it possible to characterize P-gp mediated transport properties of new drug candidates using *in vitro* cell cultures in the Transwell system(Hunter *et al.*, 1993; Pastan *et al.*, 1988; Tanigawara *et al.*, 1992).

I have characterized the transport kinetics and drug interactions of K02 in P-gp-transfected MDR1-MDCK cells and wild-type Caco-2 cells, a cell line selected from human colon adrenocarcinoma with endogenous P-gp expression. Caco-2 has been used as an *in vitro* model for evaluating intestinal drug absorption since it resembles the small intestine in many aspects(Hidalgo *et al.*, 1989). We believe the present study will help us to define the role of P-gp in the pharmacokinetics of K02.

3.2 Materials and Methods

The MDR1-MDCK cell line was generously provided by Dr. Ira Pastan of the National Cancer Institute(Pastan *et al.*, 1988). The Caco-2 cell line (HTB-37) was purchased from American Type Culture Collection (ATCC) (Rockville, MD). ^{14}C-K02 (27.6 Ci/mol) was kindly supplied by Dr. James Palmer of Arris Pharmaceutical Corporation (South San Francisco, CA). Cyclosporine was a gift from Sandoz Pharma (Basel, Switzerland). Vinblastine and verapamil were obtained from Sigma Chemical Co. (St. Louis, MO). Ketoconazole was purchased from USPC (Rockville, MD). ^{3}H Mannitol (27 Ci/mol) was purchased from Amersham (Arlington Heights, IL). LU-49888 (28 Ci/mmol), a ^{3}H-labeled photoaffinity analogue of verapamil was kindly supplied by Dr. Xiaodong Qian of BASF (Cambridge, MA). Azidopine (44 Ci/mmol) was obtained from Amersham (Arlington Heights, IL). Other chemicals were of reagent grade and also purchased from Sigma.

Photoaffinity Labeling of P-gp and Autoradiography. Membrane samples containing P-gp (MDR1) prepared from CEM_{5k} cell culture were kindly supplied by Dr. Xiaodong Wang of BASF (Cambridge, MA). CEM_{5k} is a derived drug resistant cell line of human leukemic lymphoblasts selected by vinblastine(Beck *et al.*, 1986). Membrane protein (200 μg) was preincubated with 100nM ^{3}H-LU-49888 (about 2 μCi) (Qian and Beck, 1990), or 50 nM Azidopine (2 μCi), in the

presence or absence of K02, in a buffer containing 250 mM sucrose and 10 mM Tris-HCl, pH 7.4, at room temperature for 30 min and then was irradiated with UV light (254 nm) at a distance of 10 cm for 10 min at 4°C. Photolabeled proteins were diluted with Laemmli sample buffer (1:1) and separated by one-dimensional 4-15% Tris-Glycine SDS-PAGE (Biorad, Richmond, CA). After staining with Coomassie blue and destaining, the gels were soaked in Amplify (Amersham, Arlington Heights, IL) for 30 min and dried under vacuum at 75°C. The dried gels were exposed to Hyperfilm-ECL (Amersham, Arlington Heights, IL) for 4-5 days at -80°C and developed. Densitometric readings of autoradiographs were made using a Pharmacia LKB UltroScan XL densitometer (Pharmacia LKB, Alameda, CA).

Cell Cultures. MDR1-MDCK cells were maintained in culture in Dulbecco's modified Eagle's medium(DMEM) supplemented with 10% fetal calf serum and 80 ng/ml colchicine. Caco-2 cells were in culture in Minimum essential medium Eagle with 2 mM L-glutamine and Earle's BSS containing 1.5 g/L sodium bicarbonate, 0.1 mM non-essential amino acids, and 1.0 mM sodium pyruvate, and with 10% fetal bovine serum. For transport experiments, MDR1-MDCK and Caco-2 cells were grown as epithelial layers by seeding onto permeable filter matrices of Transwell inserts (4.7 cm^2 growth area, about 10^6 cells/insert, Corning Costar Corporation, Cambridge, MA) in 6-well cluster plates for 4-5 and 18-21 days, respectively. The integrity of the cell monolayers were measured by

transepithelial electrical resistance (TEER) using a Millipore Millicell-ERS resistance system (Millipore Corporation, Bedford, MA) and the flux of ^{3}H-mannitol.

Protein Assay. The cell monolayers grown on the transwell inserts were solubilized in 1N NaOH for more than 1 hour and neutralized by 1 N HCl. The protein contents were determined by the method of Bradford using a Biorad Protein Assay Kit with albumin protein standard (Biorad, Richmond, CA).

Western Blot. The relative P-glycoprotein expression level in MDR1-MDCK and Caco-2 was measured by Western blot. MDR1-MDCK and Caco-2 cells were grown in culture for the same time periods as those used in transport experiments. The cells were removed from the T75 flask by scraping into phosphate-buffered saline. The cells were pelleted at 10,000 x g and resuspended in storage buffer (100 mM potassium phosphate, pH 7.4, 1.0 mM EDTA, 20% glycerol, 1 mM dithiothreitol, 20 μM butylated hydroxytoluene and 0.5 mM phenylmethylsufonyl fluoride), and lysates were generated by sonication. Lysates (50 μg) were resuspended in Laemmli sample buffer, loaded onto 4-15% polyacrylamide gel (Biorad, Richmond, CA), and electrophoresed. Proteins were transferred to nitrocellulose and then incubated sequentially with P-gp mouse monoclonal C219 (Signet Laboratories, Inc., Dedham, MA) and peroxidase

conjugated anti-mouse IgG (Gibco BRL, Gaithersburg, MD) and developed with the Amersham ECL detection system (Arlington Heights, IL).

Measurement of Bidirectional Transepithelial K02 Fluxes. The detailed experimental procedure was adapted from Hunter(Hunter *et al.*, 1993). Briefly: 1.5 ml and 2.5 ml serum-free medium were pipeted into insert cups (apical solution) and 6-well plates (basolateral solution), respectively. The medium on either the apical or basolateral side of the monolayers contained 10 μM ^{14}C K02. The monolayers were then incubated at 37°C for up to 3 hours. For the temperature dependence study, the monolayers were also incubated at 4°C for up to 3 hours. 50 μl of solution was taken from the receiving side every 30 minutes and subjected to liquid scintillation counting (Beckman LS1801 scintillation counter, Beckman Instruments, Inc., Palo Alto, CA). All P-gp substrates/inhibitors used to assess the inhibitory effects on K02 bidirectional transport were applied to the basolateral side at various concentrations.

Cellular Accumulation Measurements. At the end of 3-hour transport experiments, the medium was removed and the monolayers were washed three times with iced-cold phosphate-buffered saline. The filters holding the monolayer were detached from the inserts and the cells solubilized with 10 ml scintillation counting fluid overnight and then counted.

3.3 Results

3.3.1 Inhibition of Photoaffinity Labeling of P-gp by K02

K02 significantly inhibits the photoaffinity labeling of P-glycoprotein with azidopine and LU-49888, a photoaffinity analogue of verapamil, as depicted in the autoradiograph shown in Figure 3.3.1.1 Densitometric readings of labeled-P-gp bands in the absence and presence of K02 (10μM) on the autoradiographs yielded 80% and 74% (lanes 2 and 6) inhibition of LU-49888 and azidopine labeling, respectively, compared with controls (0 μM K02, lanes 1 and 5).

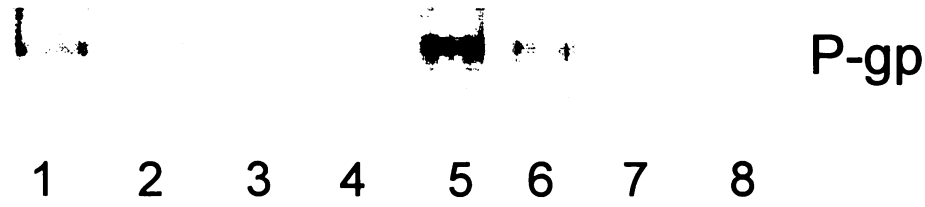

Figure 3.3.1.1 Effects of K02 on photoaffinity labeling of P-glycoprotein by azidopine and LU-49888. Lanes 1, 2, 3 and 4, LU-49888, lanes 5, 6, 7 and 8, azidopine. Lanes 1 and 5, 0 μM K02; lanes 2 and 6, 10 μM K02; lanes 3 and 7, 50 μM K02; lanes 4 and 8, 100 μM K02.

3.3.2 K02 Bidirectional Transepithelial Fluxes

The protein contents of MDR1-MDCK and Caco-2 cell monolayers were approximately 10 mg/filter. The densitometric reading of the Western blots showed that the P-gp expression level in MDR1-MDCK cells was about 10-fold that in Caco-2 cells (Figure 3.3.2.1). As depicted in Figure 3.3.2.2 (solid lines), the basolateral to apical (B-A) flux of 10 μM ^{14}C-K02 across MDR1-MDCK cell monolayers was markedly greater than its apical to basolateral (A-B) flux (ratio = 39). In Caco-2 monolayers (dashed lines), the B-A flux was reduced about 50% compared to that of MDR1-MDCK and the A-B flux was increased about 8-fold. The corresponding B-A to A-B flux ratio in Caco-2 cells is 2.5.

Caco-2 MDR1-MDCK MDCK

Figure 3.3.2.1 Western blots of P-gp-expressed cell lines using mouse monoclonal P-gp antibody C-219.

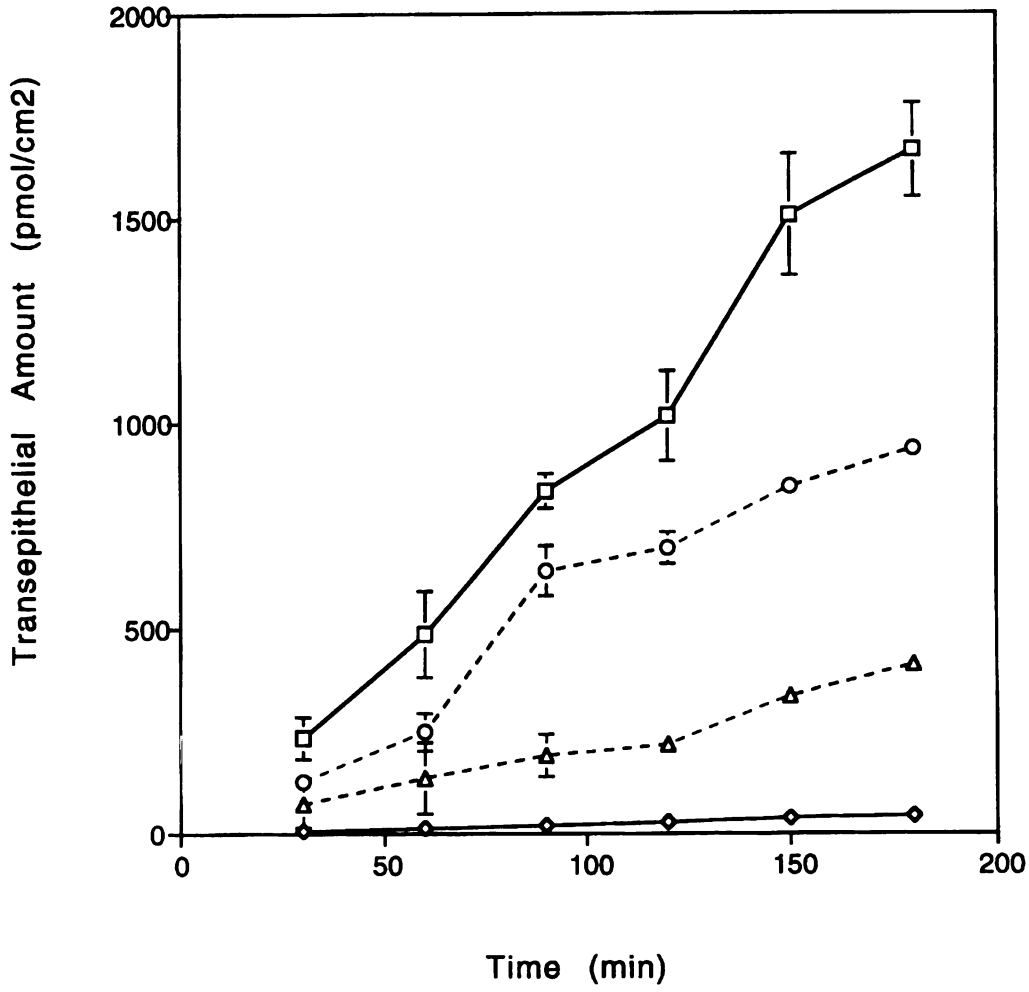

Figure 3.3.2.2 Bidirectional transepithelial transport of K02 across MDR1-MDCK and Caco-2 cell monolayers. ^{14}C-K02 is 10 μM. Solid lines depict basolateral to apical (connecting squares) and apical to basolateral (connecting diamonds) transport in MDR1-MDCK cells. Dashed lines depict basolateral to apical (connecting circles) and apical to basolateral (connecting triangles) transport in Caco-2 cells. Values are means of three measurements ± standard deviation.

3.3.3 Temperature Dependence of K02 Bidirectional Transepithelial Fluxes

This specific K02 B-A transport was temperature dependent. As demonstrated in Figure 3.3.3.1, the ratio of B-A flux at 37 °C to that at 4 °C is about 15 in MDR1-MDCK cells and 4 in Caco-2 cells.

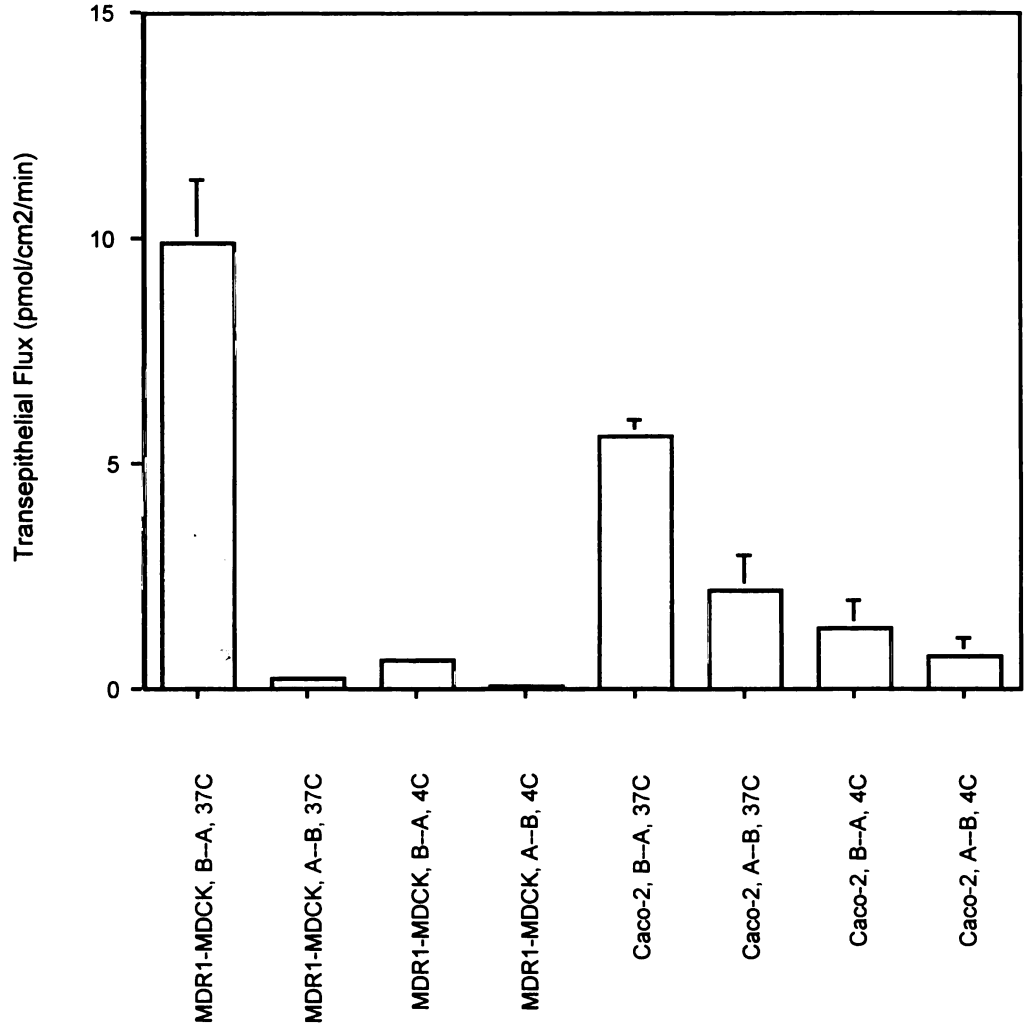

Figure 3.3.3.1 Temperature dependence of bidirectional transepithelial flux of K02 in MDR1-MDCK and Caco-2 cell monolayers. ^{14}C K02 is 10 μM. Values are mean of three measurements ± standard deviation.

3.3.4 Basolateral to Apical (B-A) Transport of K02 is Concentration Dependent and Saturable

The B-A transport of K02 in either MDR1-MDCK or Caco-2 cell monolayers were concentration dependent, saturable and followed simple Michaelis-Menten type kinetics (Figures 3.3.4.1 and 3.3.4.2). The apparent Michaelis-Menten constant and maximum velocity values for this B-A transport were 69.1±19.5 μM and 148.9±16.3 pmol/min/cm^2 in MDR1-MDCK and 71.8 ±45.9 μM and 35.3±9.0 pmol/min/cm^2 in Caco-2, respectively.

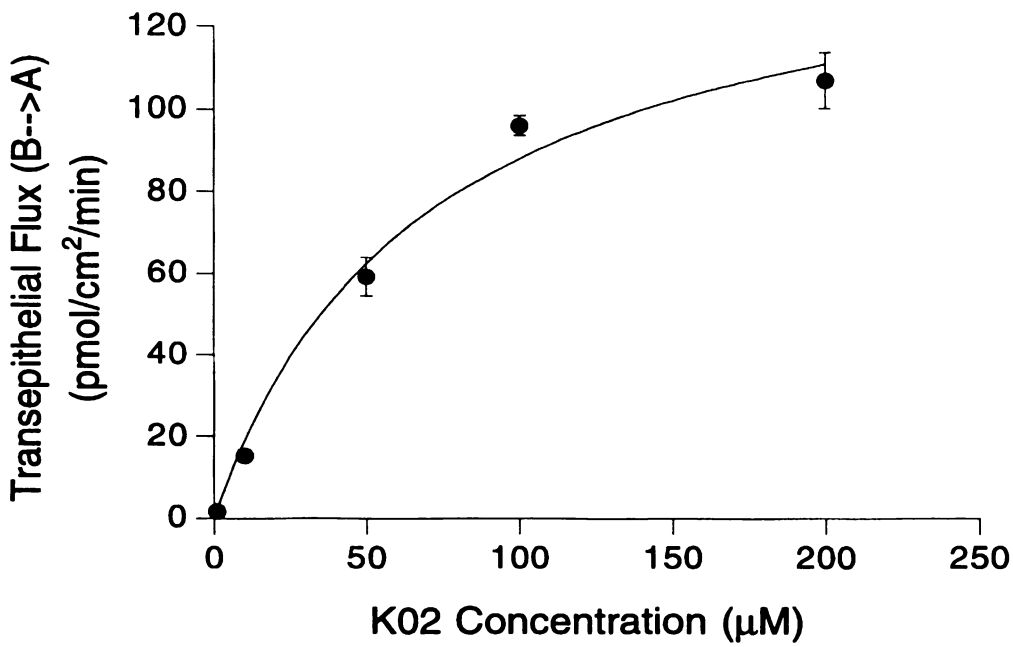

Figure 3.3.4.1 Kinetic analysis of K02 basolateral to apical flux in MDR1-MDCK cell monolayers. Values are mean of three measurements ± standard deviation. Curve fitted assuming Michaelis-Menten kinetics.

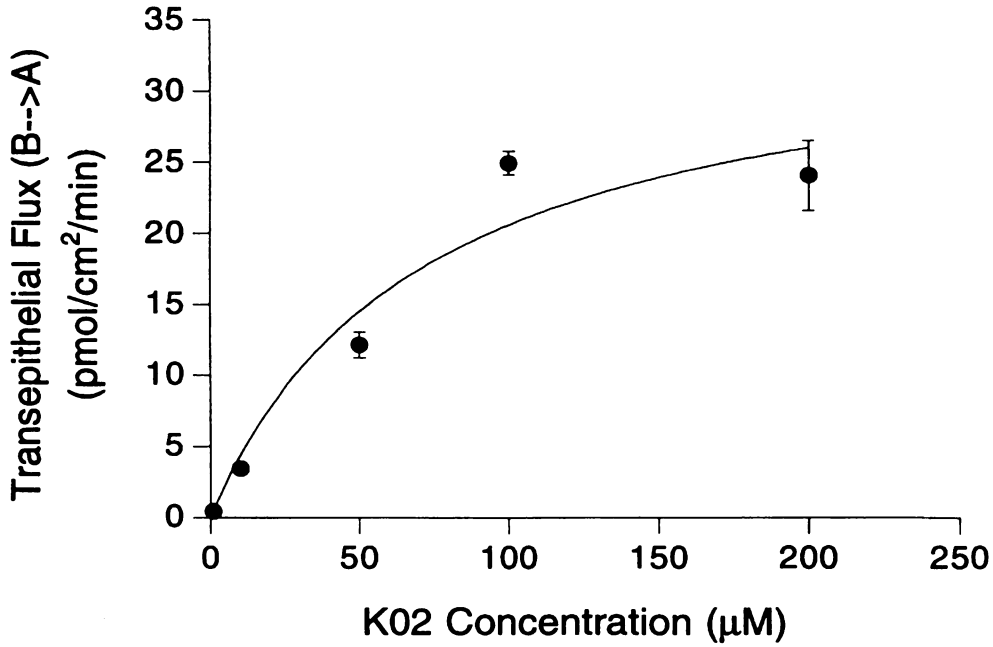

Figure 3.3.4.2 Kinetic analysis of K02 basolateral to apical flux in Caco-2 cell monolayers. Values are mean of three measurements ± standard deviation. Curve fitted assuming Michaelis-Menten kinetics.

3.3.5 Inhibitory Effects of P-Glycoprotein Substrates/Inhibitors on K02 Bidirectional Transepithelial Fluxes

The inhibitory effects of P-glycoprotein substrates/inhibitors on K02 bidirectional transepithelial fluxes in both MDR1-MDCK and Caco-2 cells were investigated. As illustrated in Figures 3.3.5.1a-d, this specific B-A transport in MDR1-MDCK was significantly inhibited by the P-gp substrates cyclosporine

(47.0 % inhibition at 10 μM), vinblastine (48 % inhibition at 25 μM), verapamil (42.3 % inhibition at 100 μM) and ketoconazole (36 % inhibition at 100 μM), while the K02 A-B transport increased. Similar results were observed in Caco-2 cells, the K02 B-A transport was inhibited by cyclosporine, vinblastine, verapamil and ketoconazole, while the K02 A-B transport increased. Typical representative IC_{50} curves are presented in Figure 3.3.5.2a-d. Table 3.3.5.1 summarizes the IC_{50} values of various P-gp substrates/inhibitors for K02 B-A transport in MDR1-MDCK and Caco-2 cells.

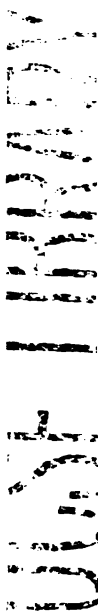

(a)

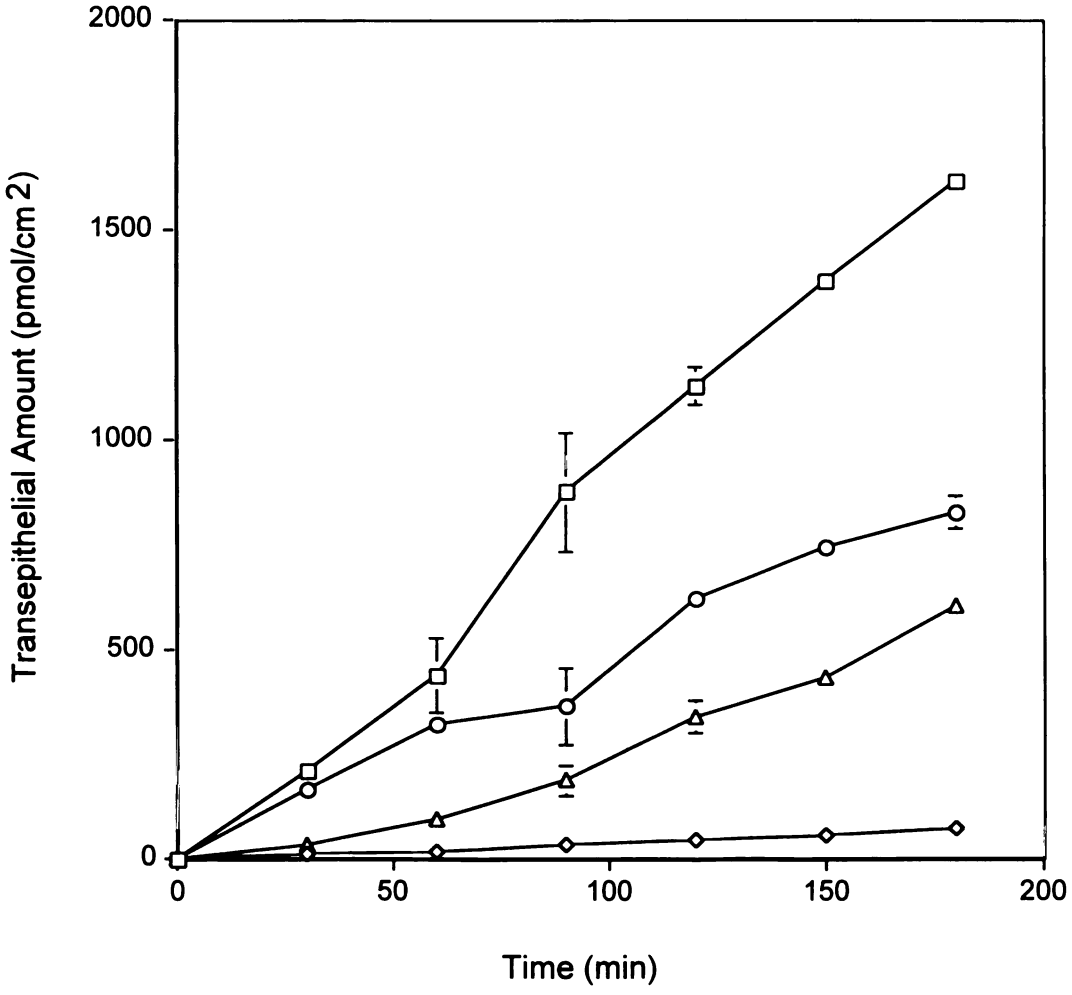

Figures 3.3.5.1 Effects of P-gp inhibitors on bidirectional transport of K02 in MDR1-MDCK cell monolayers. ^{14}C K02 is 10 μM. (a) 10 μM cyclosporine A, (b) 25 μM vinblastine, (c) 100 μM verapamil, (d) 100 μM ketoconazole. Solid lines depict basolateral to apical (connecting squares) and apical to basolateral (connecting diamonds) transport in the absence of inhibitors Solid lines depict basolateral to apical (connecting circles) and apical to basolateral (connecting triangles) transport in the presence of inhibitors in the basolateral compartment. Values are means of three measurements ± standard deviation.

(b)

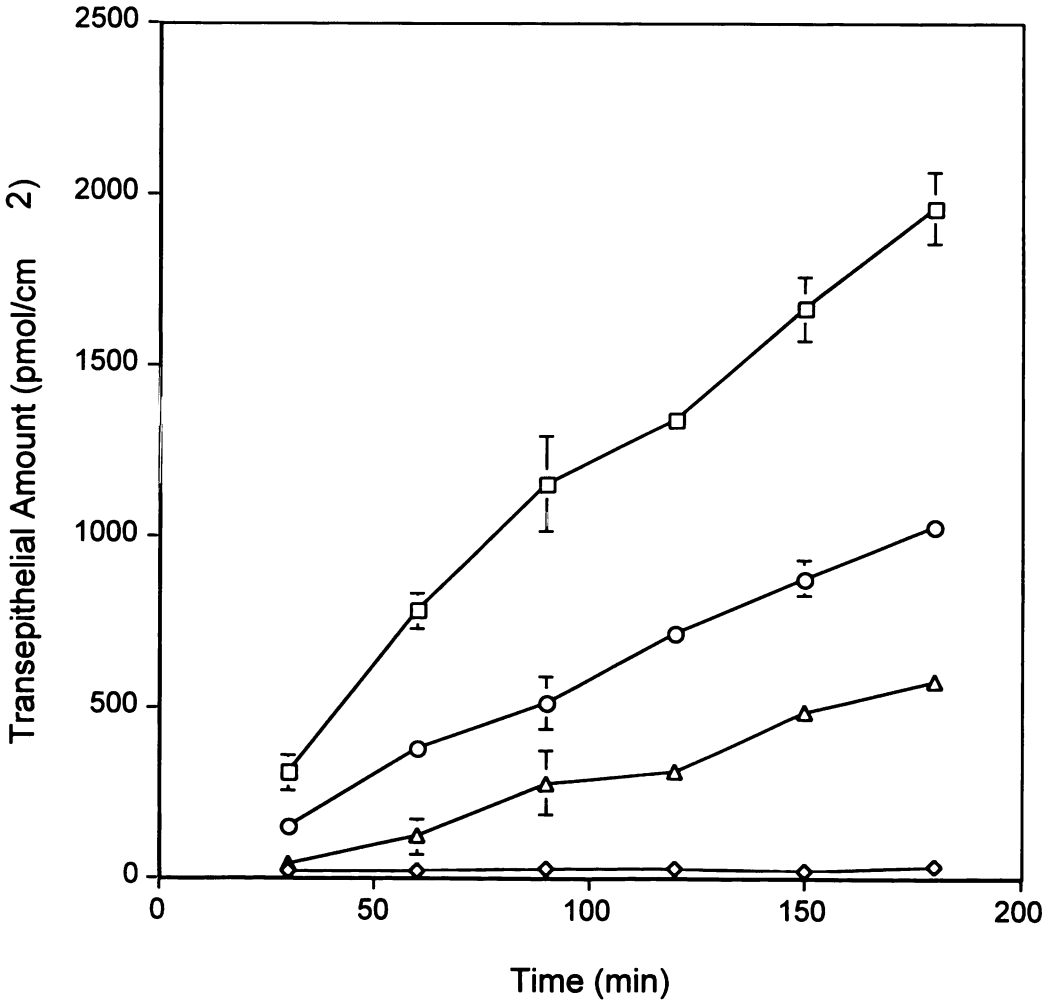
2500
2000
1500
1000
500
0
0
50
100
150
200
Transepithelial Amount (pmol/cm 2)
Time (min)

(c)

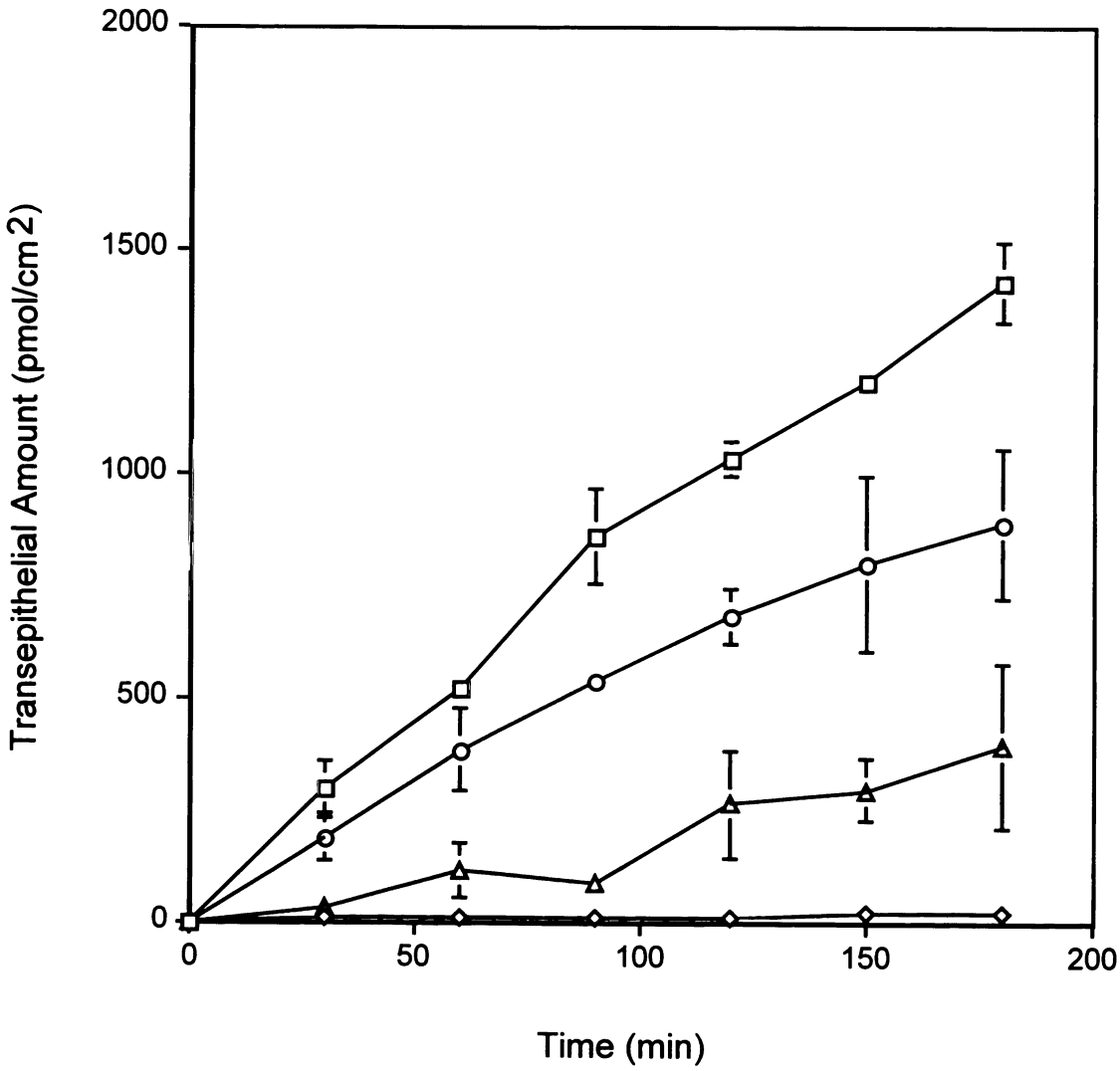
2000
1500
1000
500
0
Transepithelial Amount (pmol/cm 2)
0
50
100
150
200
Time (min)

(d)

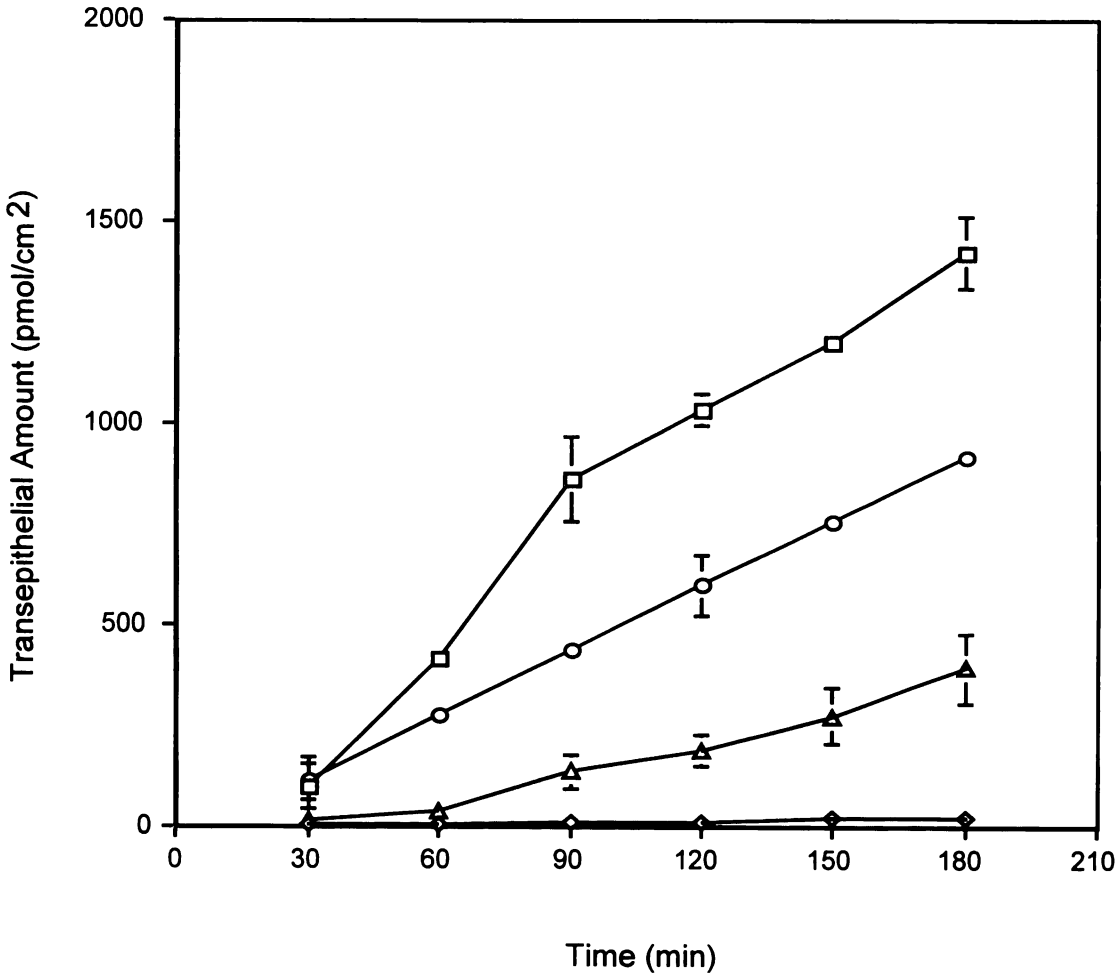
2000
1500
1000
500
0
Transepithelial Amount (pmol/cm 2)
0
30
60
90
120
150
180
210
Time (min)

(a)

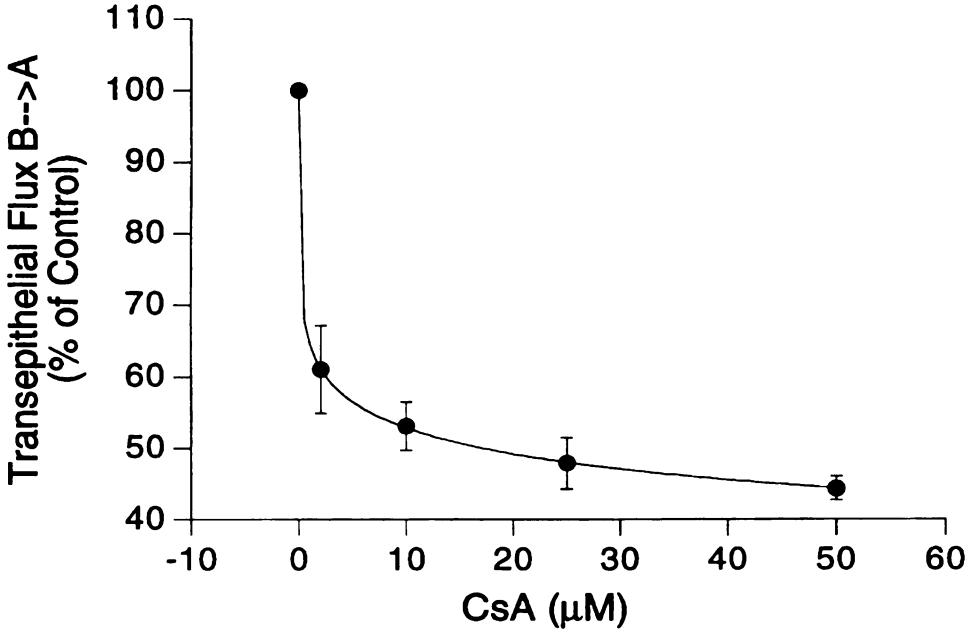

Figure 3.3.5.2 Concentration dependence of cyclosporine (a), vinblastine (b), verapamil (c) and ketoconazole (d) on K02 basolateral to apical flux in MDR1-MDCK cell monolayers. ^{14}C K02 is 10 μM. Values are mean of two measurements ± standard deviation.

(b)

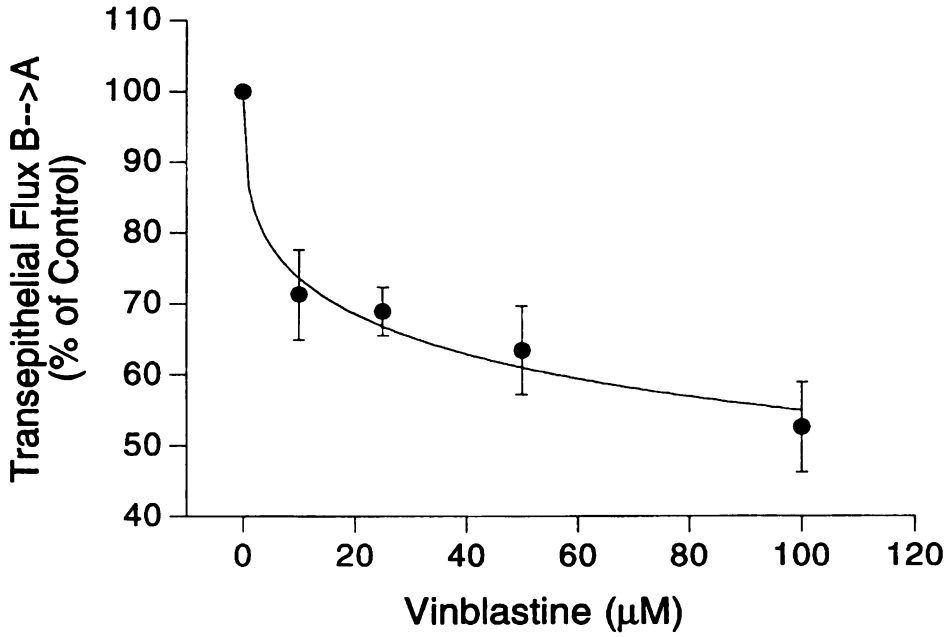
Transepithelial Flux B-->A
(% of Control)
110
100
90
80
70
60
50
40
0
20
40
60
80
100
120
Vinblastine (μM)

(c)

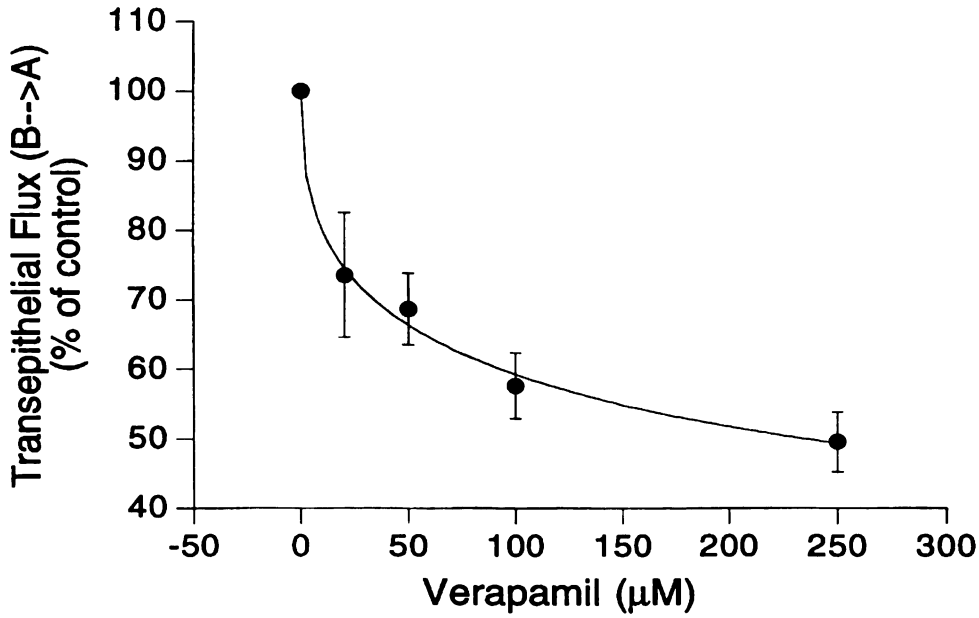
Transepithelial Flux (B-->A)
(% of control)
110
100
90
80
70
60
50
40
-50
0
50
100
150
200
250
300
Verapamil (μM)

(d)

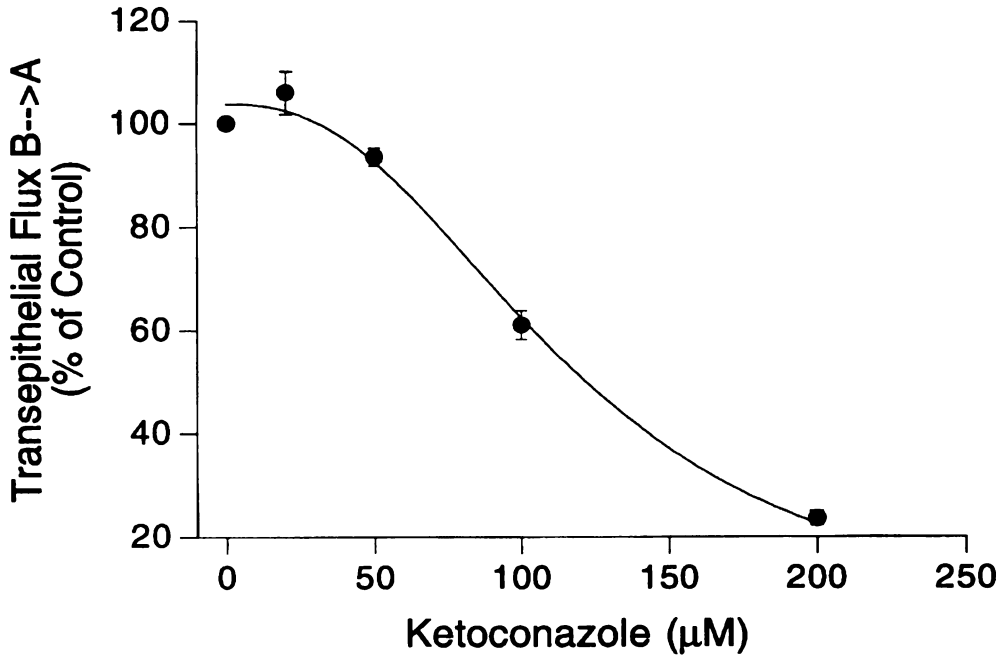

Table 3.3.5.1 IC_{50}s of P-gp inhibitors for K02 transepithelial flux (B→A) across MDR1-MDCK and Caco-2 cell monolayers

Inhibitor	MDR1-MDCK	Caco-2
Cyclosporine	17.1 ± 0.7	94.0 ± 15.7
Vinblastine	75.9 ± 13.0	162 ± 50
Ketoconazole	119 ± 10	237 ± 28
Verapamil	236 ± 63	399 ± 19

3.3.6 Cellular Accumulation of K02

Figure 3.3.6.1 depicts the bidirectional cellular accumulation of K02 in the absence and presence of P-gp substrates/inhibitors in MDR1-MDCK cells. The 3-hour cellular accumulation from B-A is about 5 times of that from A-B in MDR1-MDCK cells in the absence of P-gp substrates/inhibitors. Both B-A and A-B K02 accumulation increased and their ratios decreased with increasing ketoconazole and verapamil concentrations. In Caco-2 cells, B-A and A-B accumulation (109±3 and 115±3 pmol/cm^2, respectively) exhibited no significant difference and both B-A and A-B accumulation increased to a similar plateau (139±4 and 140±3 pmol/cm^2, respectively) in the presence of 10 μM cyclosporine.

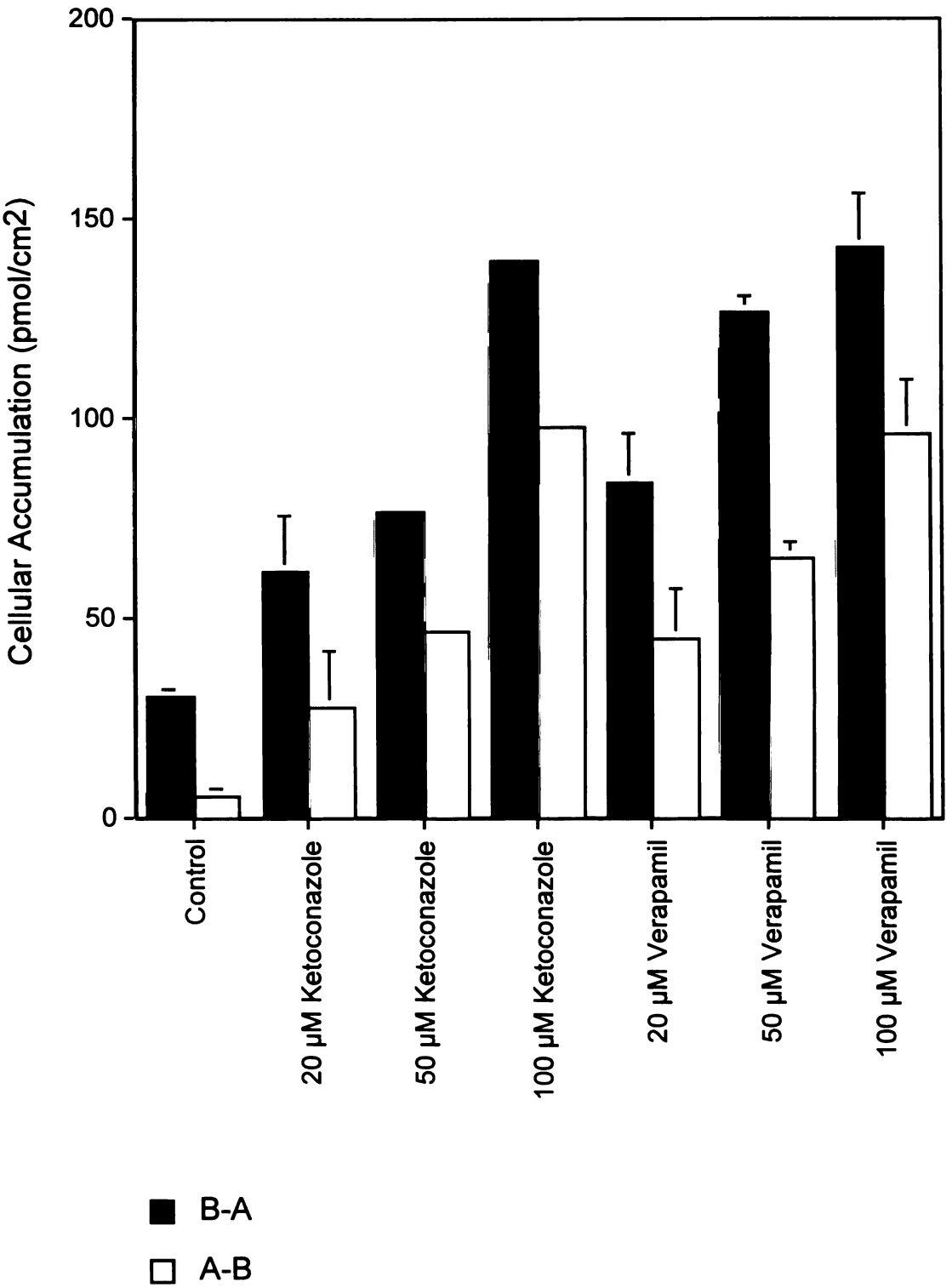

Figure 3.3.6.1 Cellular accumulation of K02 in MDR1-MDCK cell monolayers. Values are mean of three measurements ± standard deviation

3.4 Discussion

K02 strongly inhibits the photoaffinity labeling of P-glycoprotein with azidopine and LU-49888, a photoaffinity analogue of verapamil. Verapamil is a documented inhibitor and substrate of P-gp, which has been clinically co-administered with many cancer drugs as a P-gp inhibitor to overcome or alleviate multidrug resistance in cancer chemotherapy(Futscher *et al.*, 1996). This study demonstrates that K02, at least, is a P-gp inhibitor.

P-glycoprotein expressed in the MDR1-MDCK and Caco-2 cells has been shown to be localized on the apical side of the epithelia by immunohistochemistry and confocal laser scanning microscopy, respectively. This polarized P-gp expression in epithelial cell monolayers provide an essential tool for characterization of P-gp mediated transport properties of new potential therapeutic agents under drug development. MDR1-MDCK cell monolayers provide a unique tool for characterization of P-gp-mediated drug transport properties since the transfected-P-gp (MDR1) expression level is much higher than that of any endogenous transporter present in MDCK cells. While in Caco-2 cells, we can obtain information about drug absorption which is much closer to the real *in vivo* situation and assess the role of P-gp among other endogenous transporters. K02 basolateral to apical (B-A) transepithelial flux is significantly greater than its apical to basolateral (A-B) flux both in MDR1-MDCK and Caco-2 cells. K02 B-A flux in MDR1-MDCK is greater than its counterpart in Caco-2, while K02 A-B flux in MDR1-MDCK is much less than that in Caco-2. These

results are consistent with our observation obtained from Western blots that there is markedly higher expression of P-gp in MDR1-MDCK than in Caco-2. Both K02 B-A and A-B transport show temperature dependence in MDR1-MDCK and Caco-2 cells. Temperature dependence is a characteristic of carrier-mediated transport. K02 B-A flux is shown to be concentration dependent, saturable and to follow Michaelis-Menten kinetics. The K_m values are almost the same in MDR1-MDCK and Caco-2 which indicates that K02 is also mainly transported by P-gp endogenously expressed in Caco-2 cells. The V_{max} value in MDR1-MDCK is about 4 times greater than that in Caco-2 which again corresponds with our Western blot results. K02 B-A flux in both MDR1-MDCK and Caco-2 is inhibited by various P-gp subtrates and inhibitors. Cyclosporine, an immunosuppressive agent, and a high affinity P-gp substrate, strongly inhibits K02 transport, resulting in decreased K02 B-A flux and increased K02 A-B flux. Tacrolimus and rapamycin, two other macrolide immunosuppresants and P-gp substrates, also exert inhibitory effects on K02 transport, but much weaker than that of cyclosporine. Vinblastine, a cancer chemotherapeutic agent and an avid P-gp substrate, significantly inhibits the P-gp mediated K02 transport. Verapamil, a well-known P-gp reversal agent, dosed concomitantly with other cancer chemotherapeutics to overcome multidrug resistance, also exhibits inhibitory effects on K02 B-A flux. Ketoconazole, a potent CYP3A inhibitor and a reported P-gp reversal agent in P-gp over-expressed multidrug resistant cell lines(Siegsmund *et al.*, 1994), also markedly inhibited K02 B-A flux and increased K02 A-B flux. Although the IC_{50} values for each of the P-gp substrates

applied to MDR1-MDCK and Caco-2 cells are different, the relative potency order remains the same in the two systems, cyclosporine > vinblastine > ketoconazole > verapamil. These studies suggest the potential for drug-drug interactions of K02 when it is co-administratered with other P-gp substrate drugs. All these transport data demonstrate that K02 is a P-gp substrate.

In Caco-2 cells, the K02 A-B flux is 2.19 pmol/min/cm^2. The corresponding apparent permeability[1] is 3.6 • 10^{-6} cm/s. This permeability value is very low and we predict that K02 will be a compound with poor oral bioavailabilty in human. Applying P-gp inhibitors, such as cyclosporine, vinblastine, verapamil and ketoconazole to the system, we can increase this K02 A-B transport, e.g., cyclosporine (66 % increase at 10 μM) and verapamil (64% increase at 100 μM). These results suggest the potential clinical importance of modulation of P-gp in the small intestine to increase the K02 oral bioavailability.

The cellular accumulation of K02 in MDR1-MDCK, in the absence and presence of verapamil and ketoconazole, is consistent with the polarized expression of P-gp on the apical side of the epithelia as well as supporting the vacuum cleaner model of P-gp action(Gottesman and Pastan, 1993). In this model, besides pumping drugs from cytoplasm, P-gp can act on drugs in the membrane, pumping them out of the cell before they enter the cytosol. The model has received considerable experimental support, including recent results from 25 nm resolution electron microscopic reconstituted P-gp structure, which

[1] P_a = flux/(A • C_0). P_a, apparent permeability (cm/s); A, area of cell insert (cm^2); C_0, initial concentration in donor compartment (μM).

identified a cavity on the cytosolic side of P-gp, as well as a hole in the P-gp membrane inserting portion(Rosenberg *et al.*, 1997). These results indicate that P-gp can translocate its substrates either from the cytosol or in the membrane. Since P-gp is highly expressed on the apical side of MDR1-MDCK, in the K02 A-B accumulation studies, P-gp can countertransport K02 back to the apical compartment within the apical side of the cell membrane before K02 enters the cytosol. For K02 B-A accumulation, K02 must first diffuse into cytosol from the basolateral side, and then encounter and be pumped out by P-gp on the apical side of the cells. Due to the high level of expression of P-gp in MDR1-MDCK, we observed that K02 B-A accumulation was 5-times that of K02 A-B accumulation. Both K02 B-A and A-B accumulation increased and their ratios decreased with increasing concentrations of P-gp inhibitors (verapamil and ketoconazole) by inhibiting P-gp. In Caco-2 cells, since the P-gp expression is much lower than that in MDR1-MDCK cells and the resulting ability to pump K02 directly from the apical membrane when K02 diffuses from the apical side into the cell is much weaker than that in MDR1-MDCK cells, we were not able to observe the difference between K02 A-B and B-A accumulation, but we did observe that accumulation in both directions increased and reached a similar plateau upon adding the P-gp potent inhibitor, cyclosporine to the system. We also observed that both K02 A-B and B-A accumulation in Caco-2 were much higher than those respective measures in MDR1-MDCK, which is consistent with the P-gp expression level.

Comparing K02 transport properties in MDR1-MDCK and Caco-2 cells, we can conclude that MDR1-MDCK cells provide an excellent tool for characterization of P-gp-mediated transport for new chemical entities which are potential therapeutic agents under drug development, while Caco-2 cells provide information which may better predict *in vivo* drug absorption, by evaluating the permeability of compounds (from A-B flux to mucosa to serosa flux). We expect that transfected cell lines over a wide spectra of physiologically important transporters, such as ATP-dependent transporters, P-gp, MRP(Almquist *et al.*, 1995), cMOAT(Ito *et al.*, 1997), dipeptide transporters(Adibi, 1997), and organic cation transporters(Zhang *et al.*, 1997), will become standard tools for biochemical characterization of transport properties of a desired specific transporter with drug candidates. Caco-2 cells with endogenous P-gp expression, but also including some of the above-mentioned various classes of transporters, will provide clinically relevant information of drug absorption and the relative contribution of individual transporter present to the overall drug transport. All of these cell lines will be the basis for development of high throughput screening (HTS) strategies for accelerating earlier pharmacokinetic predictions.

3.5 Summary

Here we determined that K02 is a substrate of P-gp and characterized the transport properties of K02 across monolayers of P-gp-expressed MDR1 transfected MDCK cells (MDR1-MDCK) and Caco-2 cells. MDR1-MDCK and Caco-2 cells, grown to confluence on Transwell insert membranes, were used to investigate transcellular transport of ^{14}C-K02. The basolateral to apical (B-A) flux of 10 μM ^{14}C-K02 across MDR1-MDCK cells was markedly greater than its apical to basolateral (A-B) flux (ratio = 39). This specific B-A transport was temperature dependent and saturable. The ratio of B-A flux at 37 °C to that at 4 °C is about 15. The apparent Michaelis-Menten constant and maximum velocity values for the B-A transport were 69.1±19.5 μM and 148.9±16.3 pmol/min/cm^2. This B-A flux was significantly inhibited by P-gp substrates/inhibitors, e.g., cyclosporine (IC_{50} = 17.1±0.7 μM), vinblastine (IC_{50} = 75.9±13.0 μM) and verapamil (IC_{50} = 236±63 μM). In Caco-2 cell monolayers, the B-A flux was reduced about 50% compared to that in MDR1-MDCK and the A-B flux was increased about 8-fold. The apparent Michaelis-Menten constant and maximum velocity values for the B-A transport were 71.8±45.9 μM and 35.3±9.0 pmol/min/cm^2. This B-A flux was also significantly inhibited by P-gp substrates/inhibitors. Western blots showed that the P-gp expression level in MDR1-MDCK cells were about 10-fold that in Caco-2 cells. In conclusion, K02 is a substrate of P-gp and K02 is transported by P-gp in both MDR1-MDCK and Caco-2 cells.

Chapter 4 Attempts to Identify Photoaffinity Substrate Labeling Site(s) of P-Glycoprotein with LU-49888 and Azidopine

4.1 Introduction

P-gp encoded by the MDR1 gene in human has 1280 amino acid residues. Hydropathy analysis and sequence alignment with known conserved ATP-binding regions reveal that P-gp is composed of two homogenous cassettes, with each cassette containing six transmembrane domains followed by an intracelular ATP binding domain(Gottesman and Pastan, 1993). Photoaffinity labeling and mutagenesis studies suggest that transmembrane domain 6 (TM6) in the first ATP-binding cassette (ABC) and transmembrane domain 12 (TM12) in the second ABC are likely to form part of the substrate binding domains(Greenberger, 1993; Morris *et al.*, 1994; Zhang *et al.*, 1995). These studies, however, have not precisely described the specific amino acid residues involved in P-gp-substrate interactions. Recently, two independent studies indicated the existence of two nonidentical and positively cooperative drug-interaction sites in P-gp based on the kinetics of interactions of various P-gp substrates/inhibitors with photoaffinity labeling and fluorescent P-gp substrate transport(Dey *et al.*, 1997; Shapiro and Ling, 1997). The goal of this work was to identify the photoaffinity labeling sites of P-gp with azidopine or LU-49888, a photoaffinity analogue of verapamil and to understand how chemotherapeutic drugs interact with P-gp. Azipodine and LU-49888 (Figure 4.1.1) are two known P-gp photoaffinity labeling agents used in various biochemical characterizations of P-gp(Friche *et al.*, 1993; Hu *et al.*, 1996; Qian and Beck, 1990).

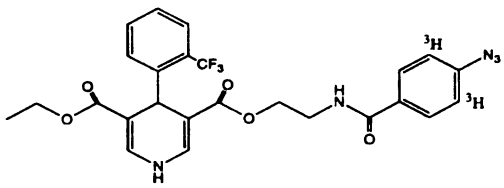

Azidopine

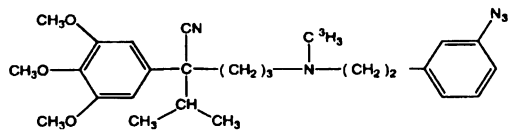

LU-49888

Figure 4.1.1 Chemical structures of azidopine and LU-49888.

Photoaffinity labeling for the formation of covalent bonds between macromolecules and their substrate analogue probes, such as photoaffinity labeling agents, has been widely employed in the biochemical community as a useful tool for structural and functional characterizations of biological systems(Bayley and Staros, 1984). Photoaffinity labeling agents are structural analogues of natural substrates with similar inherent affinities for binding sites. These ligands contain photoreactive groups which are capable of forming covalent bonds at binding sites of macromolecules when photoactivated by UV light(Bayley and Staros, 1984) (Figures 4.1.2 and 4.1.3).

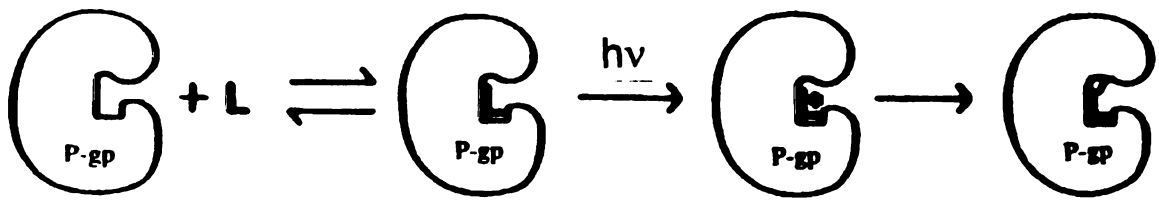

Figure 4.1.2 Idealized photoaffinity labeling of a receptor R by a photoaffinity reagent L(Bayley and Staros, 1984).

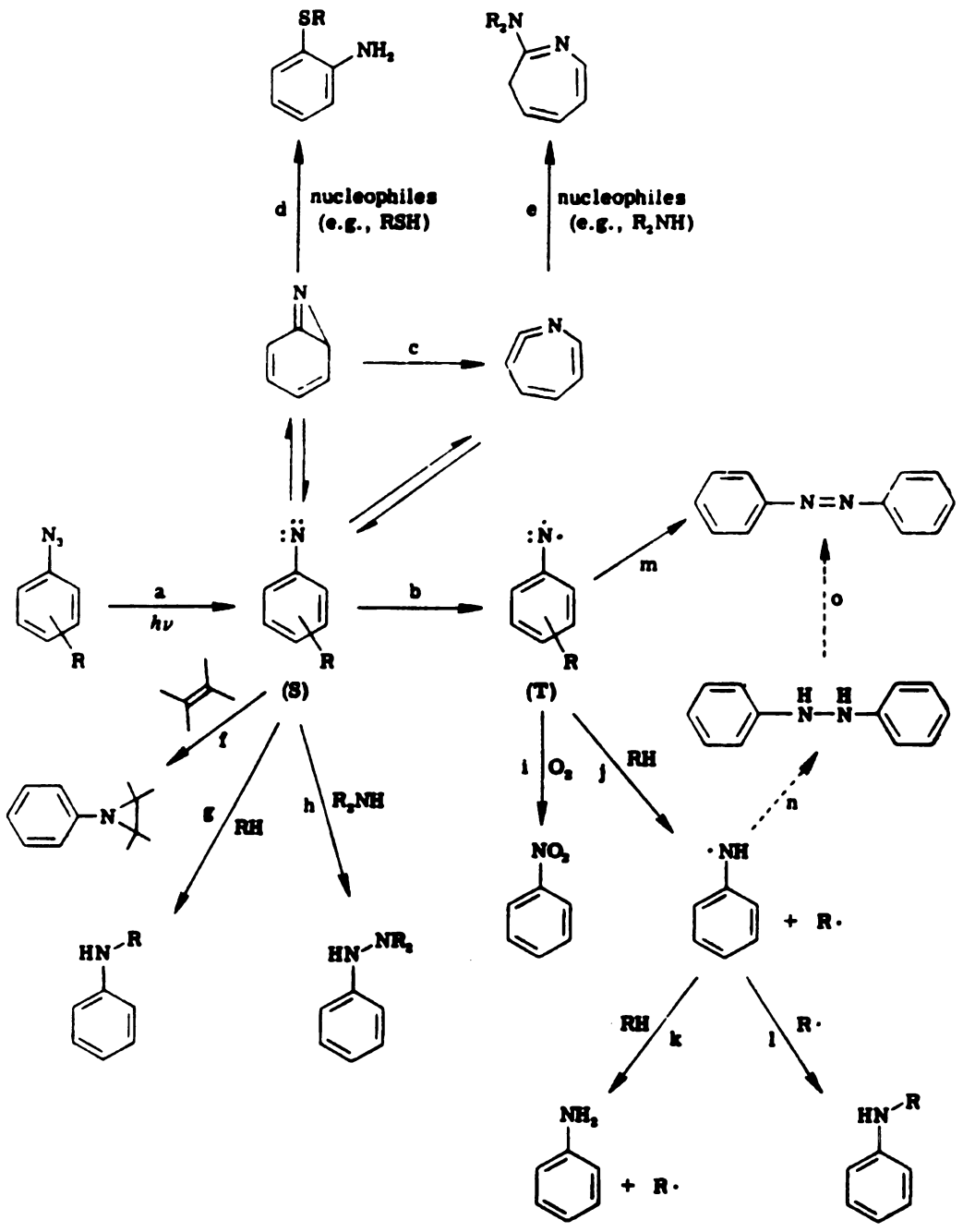

Figure 4.1.3 Photochemistry of aryl azides. The common pathways of aryl azides as photoaffinity labeling agents to form covalent linkages with macromolecules at binding sites are through d and e by reacting with nucleophilic amino acid residues of macromolecules within the binding site(Bayley and Staros, 1984).

4.2 Materials and Methods

Chemicals. LU-49888 (85 Ci/mmol), a ^{3}H-labeled photoaffinity analogue of verapamil was kindly supplied by Dr. Xiaodong Qian of BASF (Cambridge, MA). Azidopine (56 Ci/mmol) was obtained from Amersham (Arlington Heights, IL). Other chemicals were of reagent grade and purchased from Sigma (St. Louis, MO). All solvents were of HPLC grade and obtained from Fisher Scientific (Santa Clara, CA).

Preparation of Plasma Membranes. Membrane samples containing P-gp (MDR1) prepared from a CEM_{5k} cell culture were kindly supplied by Dr. Xiaodong Wang of BASF (Cambridge, MA). CEM_{5k} is a derived drug resistant cell line of human leukemic lymphoblasts selected by vinblastine. Membrane fractions were prepared by a nitrogen cavitation method as described by Qian and Beck (1990). The membrane contained approximately 1% (w/w) of P-gp as a fraction of total membrane protein.

Photoaffinity Labeling. Membrane protein (200 μg/0.5 ml) was preincubated with 100 nM ^{3}H-LU-49888 (4.25 μCi), or 100 nM Azidopine (2.8 μCi), in the presence or absence of P-gp inhibitors (vinblastine or verapamil), in a buffer containing 250 mM sucrose and 10 mM Tris-HCl, pH 7.4, at room temperature for 30 min and then was irradiated with UV light (254 nm) at a distance of 10 cm for 10 min

at 4°C. For studies to prepare labeled peptides, 700 μg membrane protein and 4 μCi Azidopine or LU-49888 in 200 μl buffer were used in the incubation.

Immunoprecipitation. Immunoprecipitation was performed according to the methods of Safa (1988) and Cornwell (1987), with minor modification. Briefly, after photoaffinity labeling, membrane proteins were solubilized in 200 μl deoxycholate/Triton X-100 buffer (20 mM Tris-HCl, pH 8.0; 140 mM NaCl; 0.5% deoxycholate; 0.1% Triton X-100) for 30 min at 4°C. Solubilized samples were then incubated overnight with 50 μg of either nonspecific mouse myeloma IgG1 (Sigma, St. Louis, MO) or C219 monoclonal antibody (Signet, Dedham, MA). Protein A-Sepharose CL-4B (Sigma, St. Louis, MO) was then added to the tubes and incubated for 2 hours at 4°C, after which the immune complexes were washed with deoxycholate/Triton X-100 buffer 5 times. The final pellets were resuspended in Laemmli sample buffer and the Sepharose beads were removed by centrifugation. Supernatants were then analyzed by SDS-PAGE followed by autoradiography.

Autoradiography. Photolabeled proteins were diluted with Laemmli sample buffer (1:1) and separated by one-dimensional 4-15% Tris-glycine SDS-PAGE (Biorad, Richmond, CA). After staining with Coomassie blue and destaining, the gels were soaked in Amplify (Amersham, Arlington Heights, IL) for 30 min and dried under vacuum at 75°C. The dried gels were exposed to Hyperfilm-ECL

(Amersham, Arlington Heights, IL) for 4-5 days at -80°C and developed. Densitometric readings of autoradiographs were made using a Pharmacia LKB UltroScan XL densitometer (Pharmacia LKB, Alameda, CA).

Trypsin Digestion. Photolabeled P-gp was extracted from the membrane in 50 mM NH_4HCO_3, pH 8.0, containing 2% β-octyl glucoside for 2 hours at room temperature. P-gp was then digested with 900 μg/ml TPCK-treated trypsin (Sigma, St. Louis, MO) overnight at 37°C.

HPLC Fractionation of Peptides. The HPLC gradient system consisted of solvent A, 0.1% TFA in 5% acetonitrile/water; solvent B, 0.08% TFA in 90% acetonitrile/water. The gradient time profile is shown in Figure 4.3.2.1b. A protein & peptide C-18 analytical column (Vydac, Hesperia, CA) was used with a flow rate of 1 ml/min. The eluted fractions were collected at 1 min/fraction and 50 μl aliquots were subjected to scintillation counting. The radioactive fractions were concentrated by SpeedVac to a final volume of 10 μl, mixed with 10 μl of 5% TFA, 50% acetonitrile solution and 1μl of the mixture was subjected to mass spectrometric analysis.

Mass Spectrometric Analysis. MALDI-TOF mass spectrometry using Voyager Elite XL Biospectrometry Workstation (PerSeptive Biosystems, Framingham, MA) was employed to analyze radioactive peptide fractions.

4.3 Results

4.3.1 P-gp is Specifically Labeled by LU-49888 and Azidopine

The autoradiograph shown in Figure 4.3.1.1 demonstrates that the band photoaffinity labeled by LU-49888 can be immunoprecipitated by P-gp monoclonal antibody C-219, but not by IgG1, an isoform of C-219 which was used as the control antibody.

Figure 4.3.1.1 Autoradiograph: C-219 immunoprecipitates LU-49888 labeled P-gp. Lane 1, without immunoprecipitation; lane 2, immunoprecipitation with nonspecific antibody, mouse IgG1; lane 3, immunoprecipitate with P-gp monoclonal antibody, C-219.

Vinblastine and verapamil, two P-gp substrates, significantly inhibit the photoaffinity labeling of P-gp by LU-49888 (Figure 4.3.1.2a) and azidopine (Figure 4.3.1.2b)

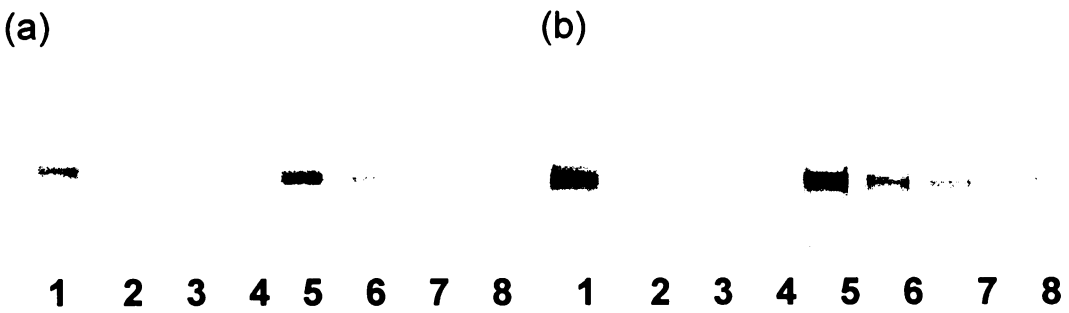

Figure 4.3.1.2 Effects of vinblastine and verapamil on photoaffinity labeling of P-gp by LU-49888 and azidopine. (a) LU-49888, (b) azidopine. Lanes 1 and 5, control; vinblastine: lane 2 (2 μM), lane 3 (20 μM) and lane 4 (200 μM); verapamil: lane 6 (2 μM), lane 7 (20 μM) and lane 8 (200 μM).

4.3.2 Proteolytic Digestion of Labeled P-gp and HPLC Separation of Labeled Peptides

HPLC chromatographs of peptides from trypsin digestion of LU-49888 and azidopine labeled P-gp are shown in Figures 4.3.2.1 and 4.3.2.2, respectively. Panel a of each figure is the chromatograph by UV detection at 214 nm and panel b is the histogram by liquid scintillation counting of aliquots of eluted HPLC fractions. The liquid scintillation counting histogram in Figure 4.3.2.1 demonstrates that fraction number 60 may contains LU-49888 labeled P-gp peptides. The liquid scintillation counting histogram in Figure 4.3.2.2b demonstrates that fraction numbers 17, 20, 22, 24 and 43 may contain azidopine

labeled P-gp peptides. These fractions were collected and concentrated by SpeedVac for mass spectrometry analysis.

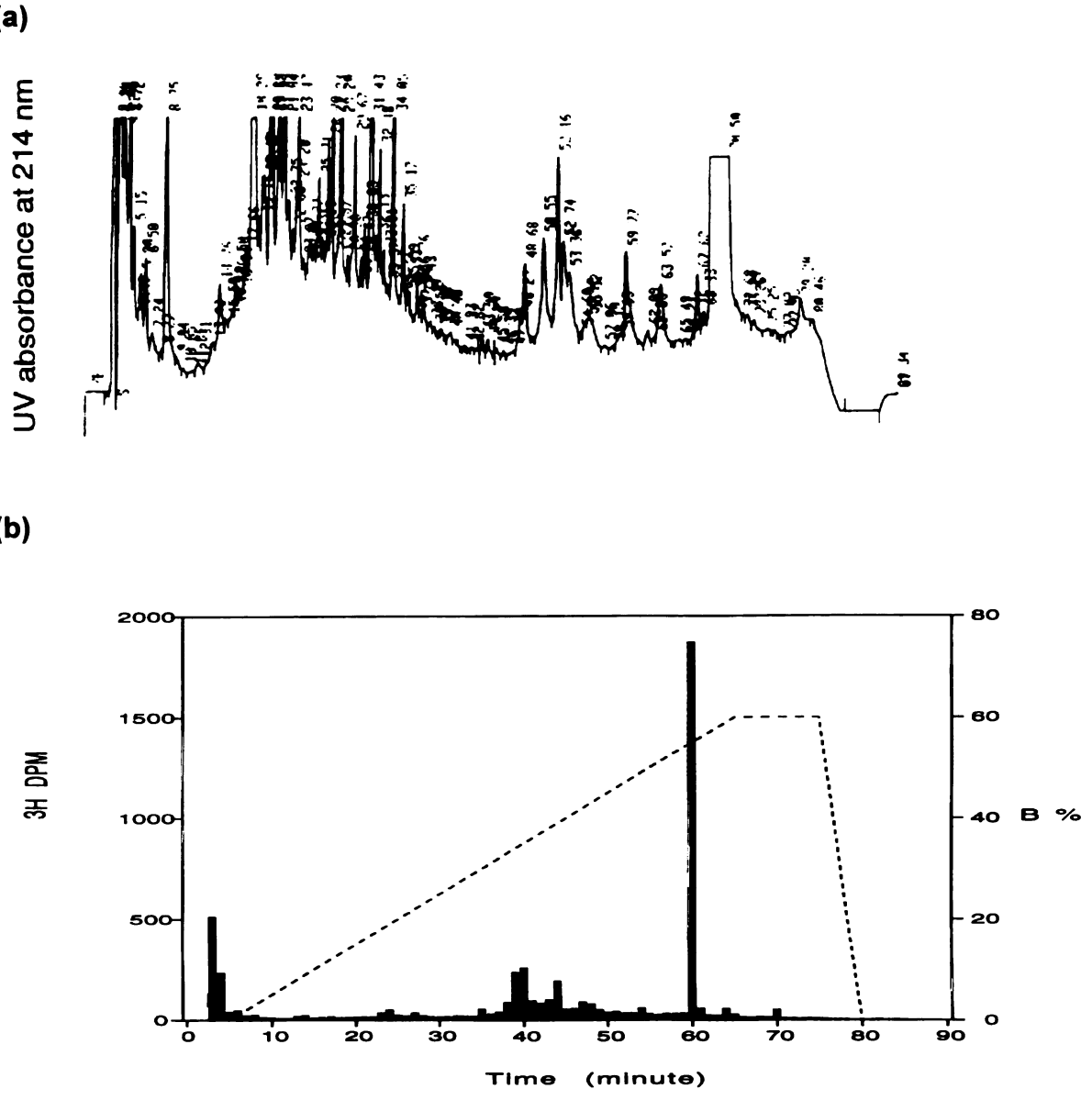

Figure 4.3.2.1 HPLC chromatographs of peptides from trypsin digestion of LU-49888 labeled P-gp. (a) chromatograph by UV detection at 214 nm, (b) histogram by liquid scintillation counting. The HPLC gradient time profile is shown in (b).

(a)

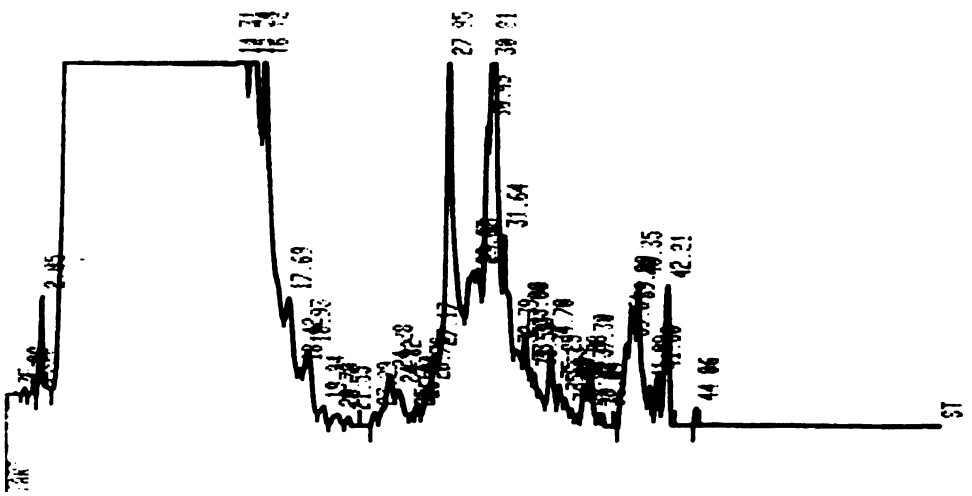

(b)

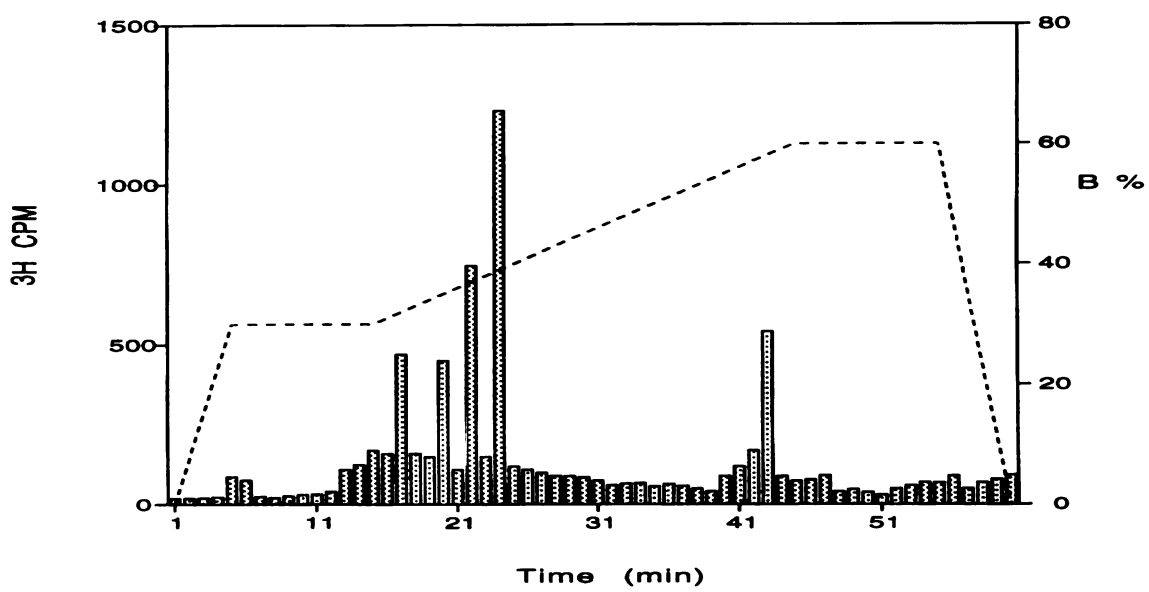

Figure 4.3.2.2 HPLC chromatographs of peptides from trypsin digestion of azidopine labeled P-gp. (a) chromatograph by UV detection at 214 nm, (b) histogram by liquid scintillation counting. The HPLC gradient time profile is shown in (b).

4.3.3 Mass Spectrometric Analysis of Labeled Peptides

The mass spectra of fractions 17, 20, 22, 24 and 43 of azidopine labeled P-gp peptides are shown in Figure 4.3.3.1 by MALDI-TOF mass spectrometry.

(a)

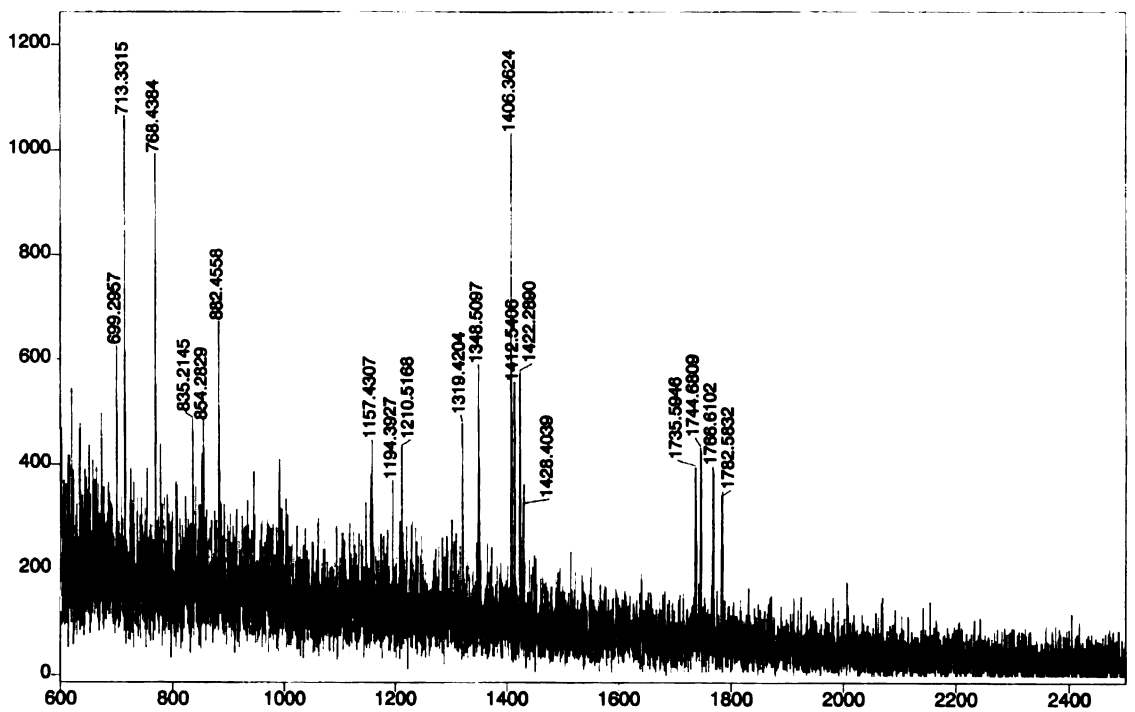

Method: KCRDECZE | Accelerating Voltage: 20000 | Laser : 1500 | Mirror Ratio: 1.060
Mode: Reflector | Grid Voltage: 70.000 % | Scans Averaged: 99 | PSD Mirror Ratio:
Sampling Rate: 0.5 nsec | Guide Wire Voltage: 0.050 % | Pressure: 1.57e-07 | Timed Ion Selector: 857.1 OFF
Detector Range: 200 mV | Delay: 100 ON | Low Mass Gate: 400.0 | Negative Ions: OFF

Figure 4.3.3.1 MALDI-TOF mass spectra of HPLC fractions of azidopine labeled P-gp peptides. (a) fraction 17, (b) fraction 20, (c) fraction 22, (d) fraction 24 and (e) fraction 43.

(b)

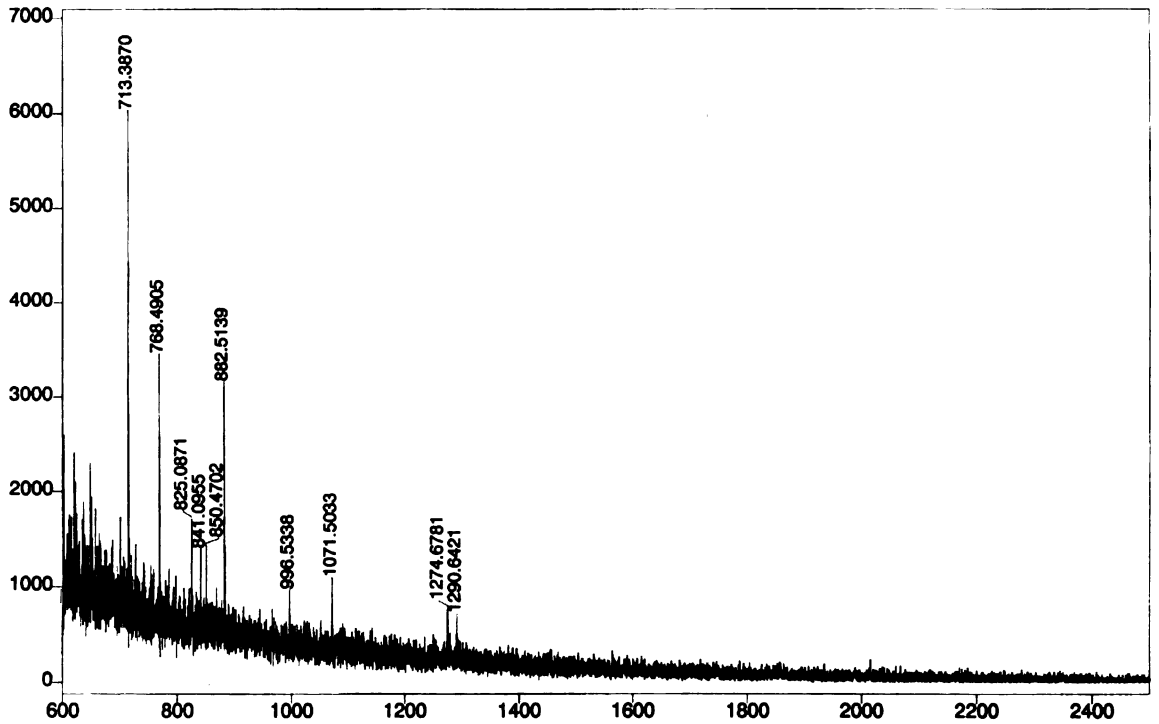

Method: KCRDECZE	Accelerating Voltage: 20000	Laser : 1500	Mirror Ratio: 1.060
Mode: Reflector	Grid Voltage: 70.000 %	Scans Averaged: 77	PSD Mirror Ratio:
Sampling Rate: 0.5 nsec	Guide Wire Voltage: 0.050 %	Pressure: 1.58e-07	Timed Ion Selector: 857.1 OFF
Detector Range: 200 mV	Delay: 100 ON	Low Mass Gate: 400.0	Negative Ions: OFF

(c)

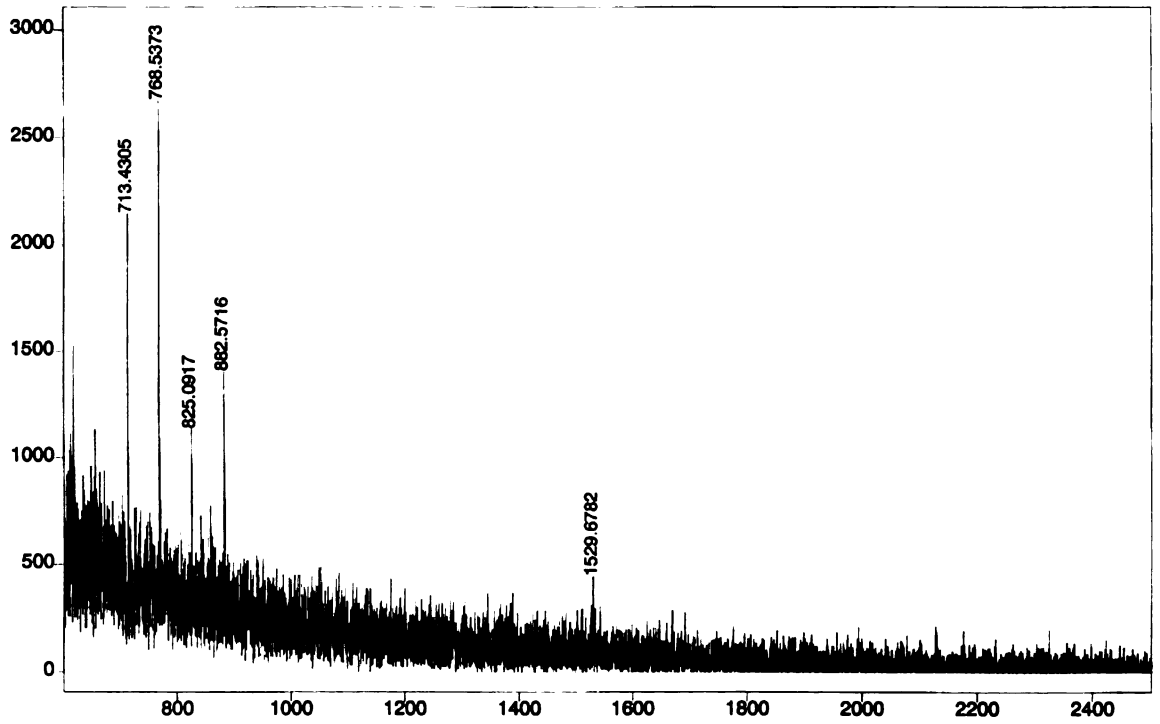

Method: KCRDECZE	Accelerating Voltage: 20000	Laser : 1500	Mirror Ratio: 1.060
Mode: Reflector	Grid Voltage: 70.000 %	Scans Averaged: 45	PSD Mirror Ratio:
Sampling Rate: 0.5 nsec	Guide Wire Voltage: 0.050 %	Pressure: 1.60e-07	Timed Ion Selector: 857.1 OFF
Detector Range: 200 mV	Delay: 100 ON	Low Mass Gate: 400.0	Negative Ions: OFF

(d)

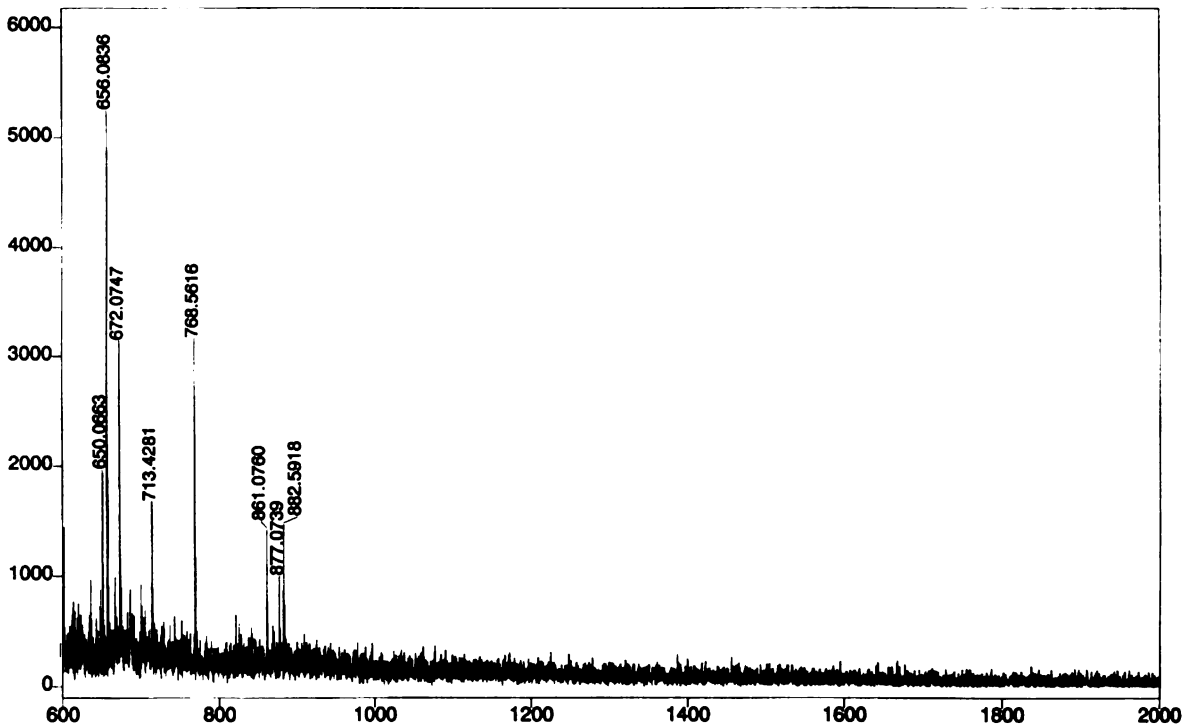

Method: KCRDECZE	Accelerating Voltage: 20000	Laser : 1400	Mirror Ratio: 1.060
Mode: Reflector	Grid Voltage: 70.000 %	Scans Averaged: 63	PSD Mirror Ratio:
Sampling Rate: 0.5 nsec	Guide Wire Voltage: 0.050 %	Pressure: 2.13e-07	Timed Ion Selector: 857.1 OFF
Detector Range: 200 mV	Delay: 100 ON	Low Mass Gate: 400.0	Negative Ions: OFF

(e)

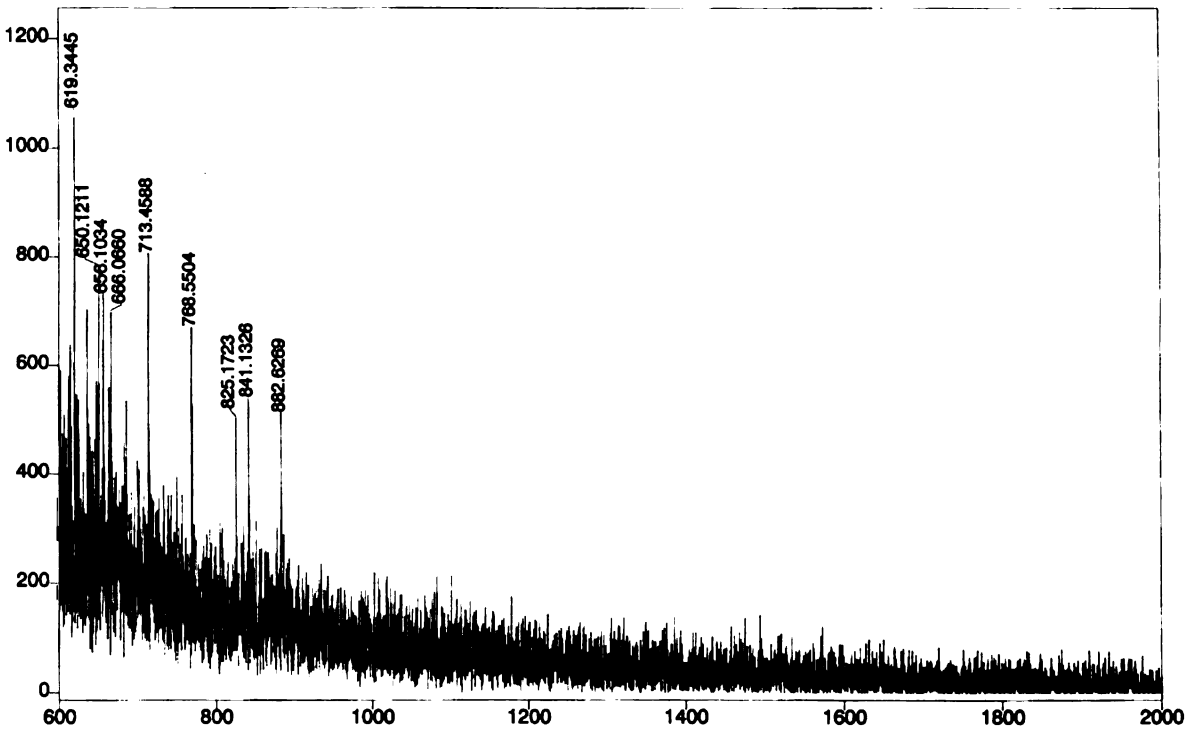

Method: KCRDECZE	Accelerating Voltage: 20000	Laser : 1500	Mirror Ratio: 1.060
Mode: Reflector	Grid Voltage: 70.000 %	Scans Averaged: 105	PSD Mirror Ratio:
Sampling Rate: 0.5 nsec	Guide Wire Voltage: 0.050 %	Pressure: 1.83e-07	Timed Ion Selector: 857.1 OFF
Detector Range: 200 mV	Delay: 100 ON	Low Mass Gate: 400.0	Negative Ions: OFF

4.4 Discussion

The photoaffinity labeling of P-gp by either LU-49888 or azidopine is specific, which was confirmed by inhibition studies with vinblastine and verapamil (Figure 4.3.1.2) and by immunoprecipitation study with monoclonal P-gp antibody C-219 (Figure 4.3.1.1). The extraction of photoaffinity labeled P-gp from membrane with 2% β-octyl glucoside was complete. This was confirmed by comparison to the extraction procedure using stronger surfactants, SDS (0.1%) and Triton X-100 (0.5%) followed by the same trypsin digestion and HPLC analysis procedures. The radiohistograms are identical using either 2% β-octyl glucoside or 0.1% SDS and 0.5% Triton X-100. The trypsin digestion was also complete. After the trypsin digestion, aliquots of the mixture were analyzed by SDS-PAGE and autoradiography. The autoradiographs show a smeared band around 4 KDa and no bands at higher molecular weights were observed. The mass spectrometry analysis of radioactive fractions of azidopine labeled P-gp peptides showed no prospective peptide peaks corresponding to azidopine labeled P-gp peptides. The possible reason for this unsuccessful attempt is that the P-gp content in membrane proteins prepared from CEM_{5k} cell culture is too low, approximately 1% (w/w). This P-gp quantity was demonstrated here to be sufficiently sensitive for radioactive detection, e.g., autoradiography and liquid scintillation counting, but not of sufficient sensitivity for mass spectrometry analysis. We can estimate the amount of each radioactive fraction by assuming

no loss during sample preparation. For example, in fraction 24 of Figure 4.3.2.2, the radioactivity measured in a 50 μl aliquot of the 1 ml sample is 1250 CPM. Assuming that the liquid scintillation counting efficiency for ^{3}H is 0.31, the corresponding radioactivity equals $1.82 \bullet 10^{-9}$ Ci ($1250 / (0.31 \bullet 2.22 \bullet 10^{12})$). Since the specific radioactivity of azidopine is 56 Ci/mmol, we can convert $1.82 \bullet 10^{-9}$ Ci to $3.24 \bullet 10^{-2}$ pmol. The total amount of radiolabeled peptides is 0.65 pmol in this fraction. Only 5% of 0.65 pmol (32 fmol) was introduced into the matrix for mass spectrometric analysis. The actual amount introduced into the mass spectrometer was much less than the calculated 32 fmol due to loss of samples during preparation, e.g., loss at sample transferring. Analyzing the recent success of photoaffinity labeling of hamster P-gp ATP-binding sites by radioactive Mg-8-azido-ADP and peptide sequence analysis using the Edman method (Sankaran *et al.*, 1997) reveals that a large amount of P-gp sample was used in that study (6.7 mg of membrane protein from Chinese hamster ovary cell line CR1R12 where P-gp content is 15-20% (w/w)). For future possible efforts to identify the photoaffinity substrate labeling sites of P-gp, several modifications are proposed: 1) A higher P-gp expression cell line is needed and the enrichment of the P-gp fraction in the total membrane protein preparation should be greater than 10% (w/w). 2) An additional P-gp purification step is needed before trypsin digestion, e.g., after photoaffinity labeling, separate the labeled P-gp from the matrix of membrane proteins using SDS-PAGE and excise the corresponding P-gp band from the gel followed by in-gel digestion of the P-gp

gel band with trypsin and extraction of labeled peptides. 3) A microbore HPLC system is recommended to separate the labeled P-gp peptides for mass spectrometry instead of an analytical HPLC system so as to increase concentrations of labeled peptides.

Chapter 5 Pharmacokinetics of K02 in Male Sprague-Dawley Rats and the Effects of CYP3A and/or P-gp Inhibitors on K02 Oral Bioavailability

5.1 Introduction

CYP3A is the major subfamily of hepatic and intestinal CYP enzymes leading to drug oxidative biotransformation both in humans and rats(Benet *et al.*, 1996a; Kolars *et al.*, 1992a; Kolars *et al.*, 1994; McKinnon *et al.*, 1995). Intestinal first-pass metabolism mediated by CYP3A has been shown to be clinically important for several drugs, such as cyclosporine, tacrolimus and midazolam(Floren *et al.*, 1997; Hebert *et al.*, 1992; Thummel *et al.*, 1996).

P-gp expressed on the apical surfaces of columnar epithelial cells of the jejunum and the lumenal surface of biliary hepatocytes has recently been considered to work as an active efflux drug transporter and contributes to both the hepotic and intestinal first-pass effects. Studies utilizing mdr1a and/or mdr1b gene disruptions in mice (knockout mice) have helped to elucidate the influence of P-gp on the pharmacokinetics of therapeutic agents which are P-gp substrates(Schinkel *et al.*, 1995b; Schinkel *et al.*, 1997; Sparreboom *et al.*, 1997; van Asperen *et al.*, 1996). Pharmacokinetic studies employing inhibitors of P-gp along with P-gp-substrate drugs also demonstrate the importance of P-gp in drug absorption, distribution, elimination and toxicity(van Asperen *et al.*, 1997).

A striking overlap of substrate specificity and tissue distribution for CYP3A and P-gp (Wacher *et al.*, 1995) suggests that CYP3A and P-gp may play complementary roles in drug absorption, disposition, metabolism and elimination by biotranformation and countertransport, especially in the villi of the small

intestine. Our hypothesis is that CYP3A and P-gp act synergistically in the small intestine as a barrier to limit oral drug bioavailability.

The purpose of this study was to quantify the effects of CYP3A and/or P-gp inhibitors, on the oral bioavailability of K02, a CYP3A and P-gp substrate.

5.2 Materials and Methods

Materials. K02 and ^{14}C-K02 (27.6 Ci/mol) were kindly supplied by Dr. James Palmer of Arris Pharmaceutical Corporation (South San Francisco, CA). Ketoconazole was purchased from USPC (Rockville, MD). Midazolam was a gift from Hoffmann-LaRoche (Nutley, NJ). D-alpha tocopheryl polyethylene glycol 1000 succinate (TPGS) was purchased from Eastman Chemical Company (Kingsport, TN). Other chemicals were of reagent grade and also purchased from Sigma. All solvents were of HPLC grade and obtained from Fisher Scientific (Santa Clara, CA).

In Vivo Pharmacokinetic Studies. Male SD rats (B&K, Fremont, CA, 8-10 weeks old) were studied. All rats had an indwelling cannula (0.020 in. ID/0.037 in. OD Silastic® laboratory tubing, Dow Corning, Midland MI) implanted in the right jugular vein for blood sampling as described by Upton (1975). The surgery was performed under ketamine/xylazine/acetylpromazine (22/2.5/0.75 mg/kg, IP)

anesthesia. For the rats receiving a K02 intravenous (IV) dose, a separate cannula was implanted in the left jugular vein for K02 administration. The surgery was performed one day before the study. Each group of rats (n=3-6) were administered a single dose of K02 (10 mg/kg) IV or (30 mg/kg) orally by gavage with or without a concomitant oral (PO) dose of the interaction drug, i.e., ketoconazole (20 mg/kg), midazolam (20 mg/kg) or TPGS (8 IU/kg). K02 and interaction drug were administered as solutions in DMSO:0.17% sodium phosphate, 0.08% citric acid anhydrous:propylene glycol (10:20:70, v:v:v). Blood samples (100-200 μl) were collected from 2 min to 8 hrs following administration through the right jugular vein cannula.

LC/MS/MS Determination of K02 Plasma Concentrations. A SCIEX API III tandem mass spectrometer equipped with a heated nebulizer was operated in the positive mode with multiple reaction monitoring for determining the K02 concentrations. The K02 samples were prepared by direct protein precipitation of rat plasma with acetonitrile. The accuracy and the precision of the assay over the K02 concentration range of 1 ng/ml to 8 μg/ml were validated.

Pharmacokinetic Analysis. Non-compartmental methods (systems analysis) were employed to calculate the K02 pharmacokinetic parameters. A two-compartment model with elimination from the central compartment was used to fit the IV data for K02 using a pharmacokinetic analysis program (MULTI) with

Damping Gauss-Newton algorithm (Izumi *et al.*, 1996). The same program was also used to attempt to fit the K02 IV and PO data simultaneously assuming first order absorption.

5.3 Results

5.3.1 Pharmacokinetics of K02 in Male SD Rats

K02 plasma concentration versus time curves for IV (10 mg/kg) and PO (30 mg/kg) administration are depicted in Figures 5.3.1.1 and 5.3.1.2, respectively, by circles connected by solid lines. Pharmacokinetic parameters of K02 calculated by non-compartmental methods are listed in Table 5.3.1.1. The K02 IV data alone fitted to a two-compartment model yielded the pharmacokinetic parameters, V_1, α and β (1.7 l/kg, 0.0707 min^{-1} and 0.0047 min^{-1}). A reasonable fit of simultaneous IV and PO data was obtained yielding an first order absorption rate constant of 0.0153 min^{-1}, a V_1 and α (1.8 l/kg and 0.0714 min^{-1}) close to that obtained for the IV data alone, but a faster elimination constant β (0.0093 min^{-1}) (Figure 5.3.1.3). The K02 protein binding and blood to plasma concentration ratio were measured over a wide concentration range, and found to be concentration independent with f_u = 0.045±0.008 and C_B/C_P = 0.85±0.02.

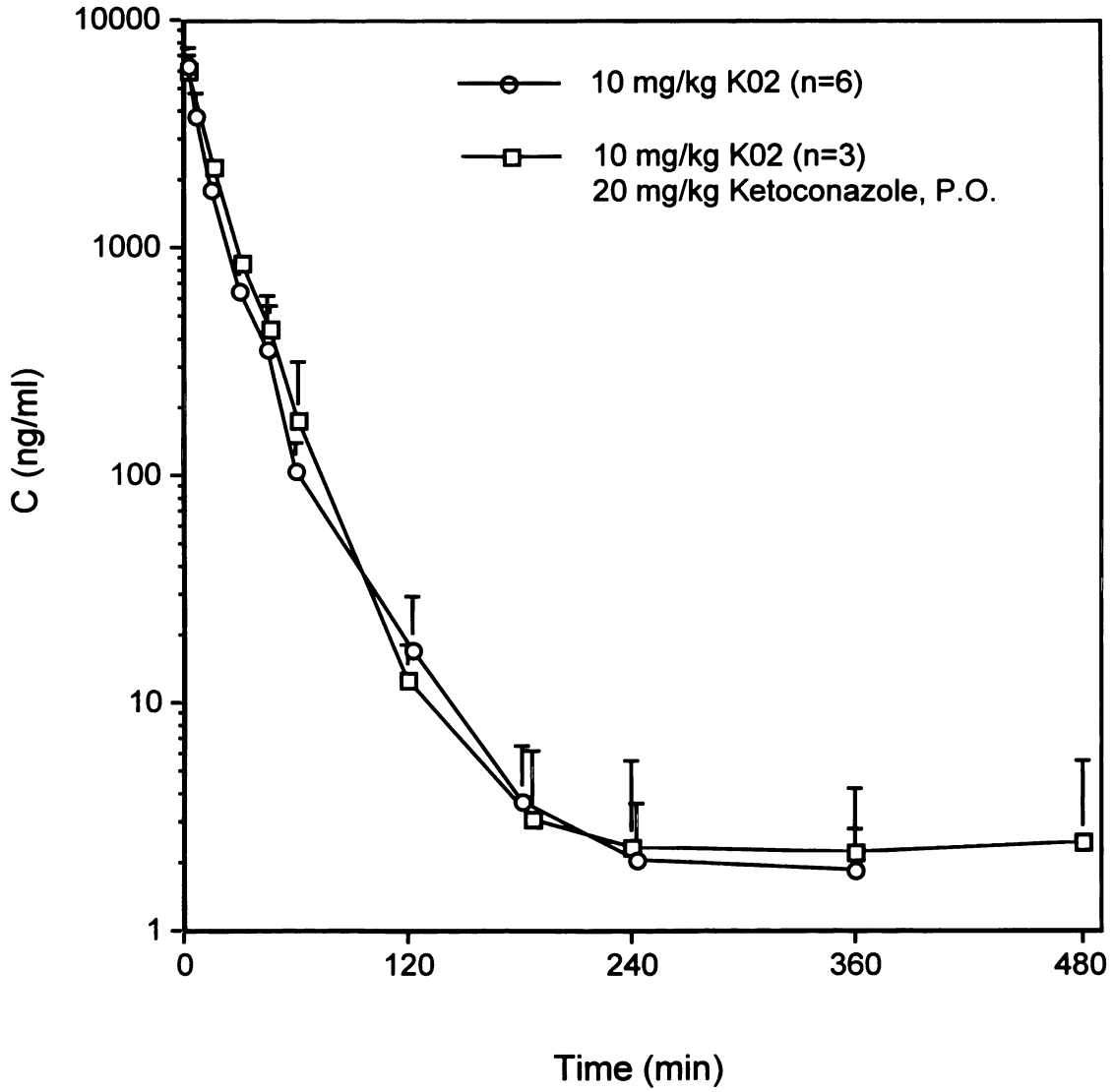

Figure 5.3.1.1 K02 plasma concentration versus time curves following IV (10 mg/kg) administration with and without a concomitant oral ketoconazole dose (20 mg/kg). Circles, without ketoconazole, n=6; squares, with ketoconazole, n=3. Values are mean ± standard deviation.

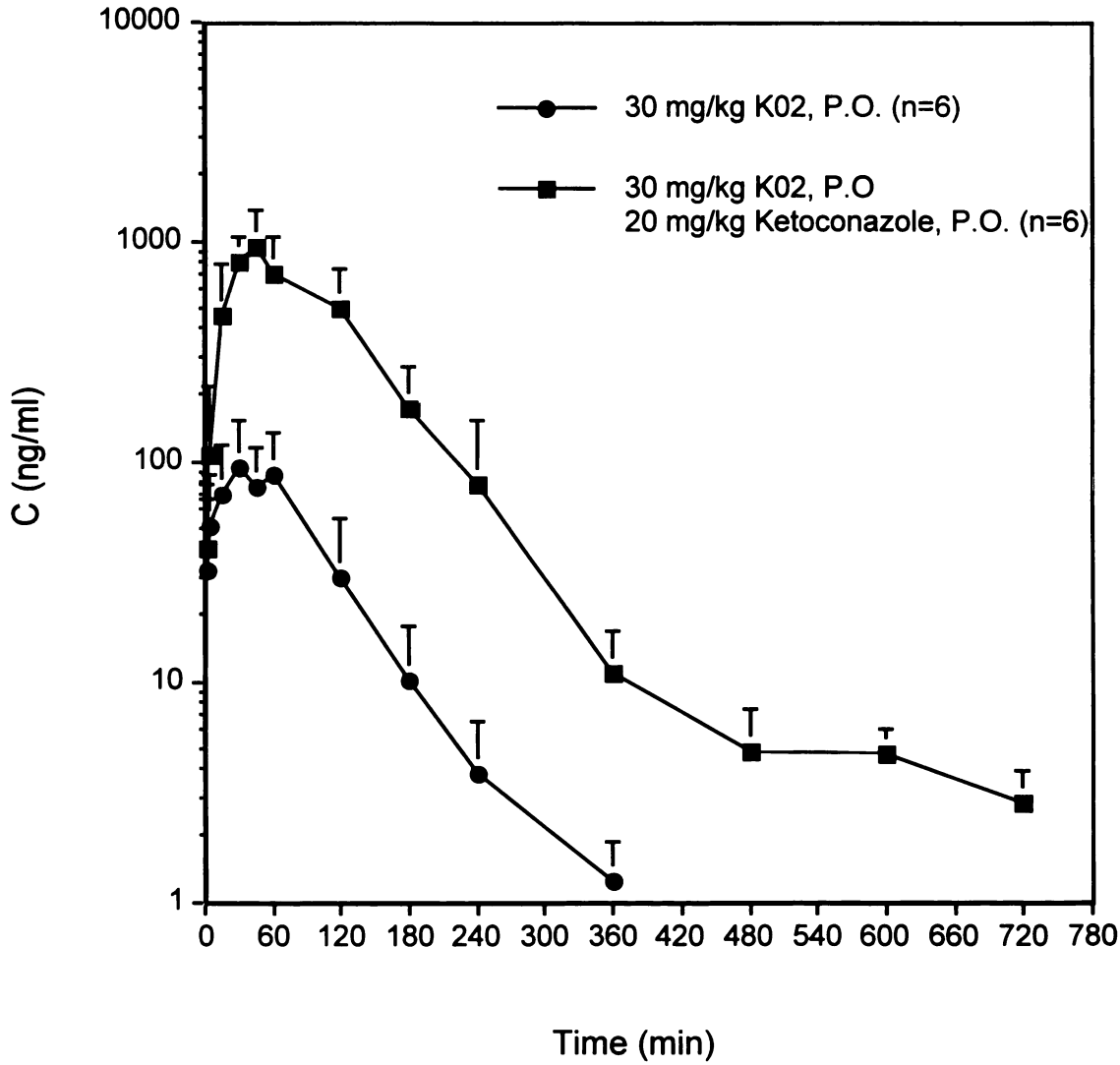

Figure 5.3.1.2 K02 plasma concentration versus time curves following PO (30 mg/kg) administration with and without a concomitant oral ketoconazole dose (20 mg/kg). Circles, without ketoconazole, n=6; squares, with ketoconazole, n=6. Values are mean ± standard deviation.

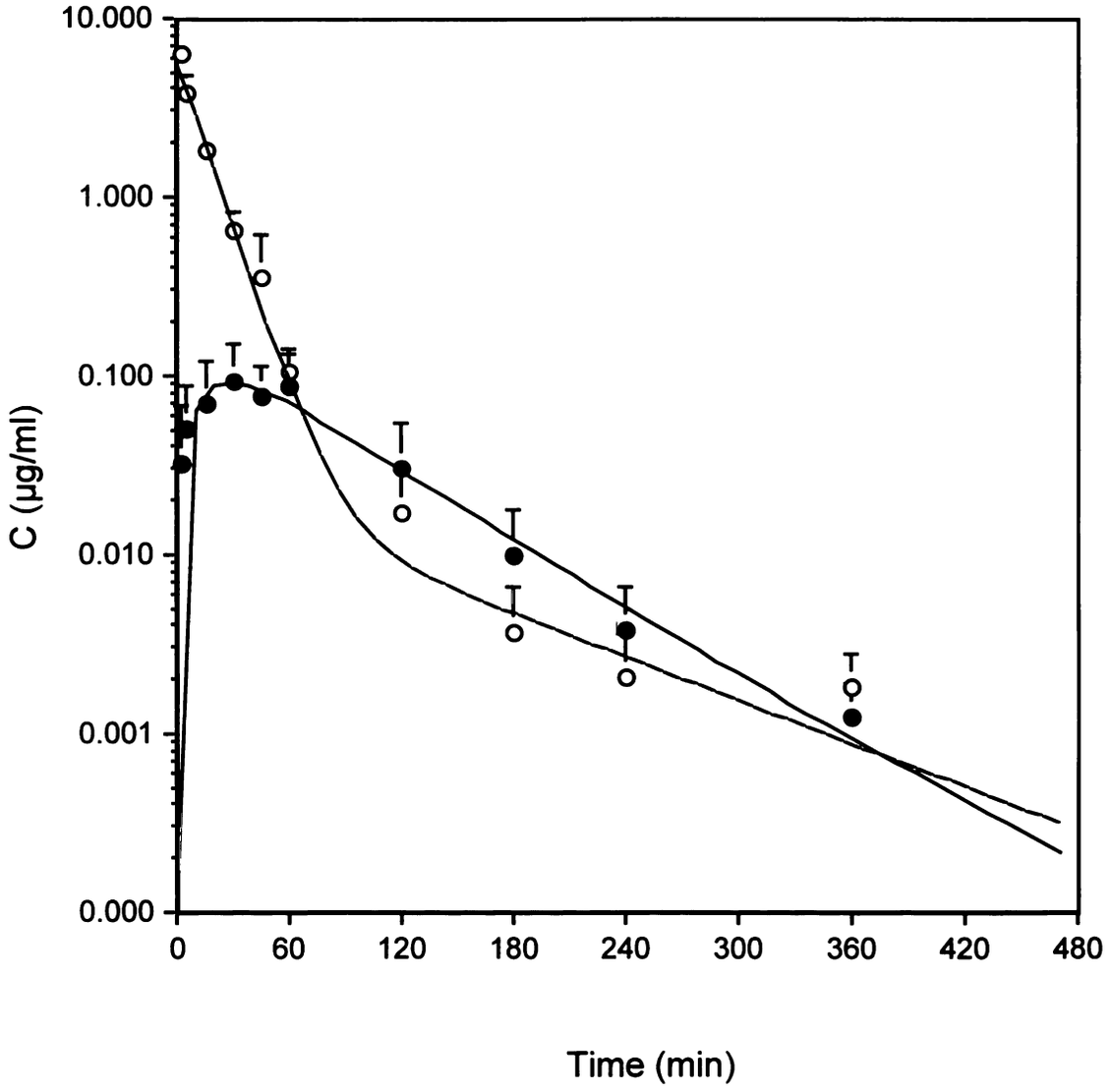

Figure 5.3.1.3 Simultaneous fitting of K02 IV and PO plasma concentration versus time data to the two-compartment model. Solid lines represent fitted parameters. Open circles and solid circles represent actual IV and PO data, respectively.

Table 5.3.1.1 K02 pharmacokinetic parameters calculated using non-compartmental methods

Study	AUC (mg•min/l)	CL (ml/min/kg)	CL/F (ml/min/kg)	F (%)	V_{ss} (l/kg)	MRT (min)	MAT (min)	T_{max} (min)
Control								
IV, 10 mg/kg	93.8±17.1	110±22	3810±1620	2.9±1.4	1.9±0.3	17.4±2.0		
PO, 30 mg/kg	9.4±4.4					82.2±12.1	64.9±14.1	40.0±18.0
Ketoconazole[a]								
IV, 10 mg/kg	107±14	95±13	306±60	31.0±7.5[d]	2.0±0.6	21.4±8.3		
PO, 30 mg/kg	102.±24					98.5±23.1	77.1±39.5	46.8±11.7
Midazolam[b]								
IV, 10 mg/kg	96.8±36.1	112±32	1970±580	5.7±2.3[e]	1.6±0.4	14.8±1.4		
PO, 30 mg/kg	16.1±3.9					76.2±19.3	61.3±20.6	23.8±7.5
TPGS[c]								
IV, 10 mg/kg	106±22	98±23	2810±600	3.5±1.1	1.5±0.4	15.1±1.1		
PO, 30 mg/kg	11.1±3.1					50.1±7.9	35.0±8.9[d]	13.5±3.7[e]

a, b, c simultaneously PO dosing of 20 mg/kg ketoconazole, 20 mg/kg midazolam and 8 IU/kg TPGS, respectively.

Significantly different [d]$P < 0.001$ and [e]$P < 0.05$ versus control.

5.3.2 Effects of Ketoconazole on the Pharmacokinetics of K02 in Male SD Rats

K02 plasma concentration versus time curves for IV (10 mg/kg) and PO (30 mg/kg) administration with a concomitant ketoconazole PO dose (20 mg/kg) are depicted in Figures 5.3.1.1 and 5.3.1.2, respectively, by squares connected by solid lines. Non-compartmental pharmacokinetic parameters are listed in Table 5.3.1.1. The fitted K02 IV data with concomitant ketoconazole dosing yielded comparable two-compartment model parameters to those obtained in the absence of ketoconazole (α, 0.0619 min^{-1}; β, 0.0041 min^{-1} and V_1, 1.6 l/kg). Simultaneous fitting of K02 IV and PO data (with the 20 mg/kg ketoconazole PO dose) to the two-compartment model was not successful, most probably due to the fact that the absorption process is not well described by first order absorption.

5.3.3 Effects of Midazolam on the Pharmacokinetics of K02 in Male SD Rats

K02 plasma concentration versus time curves for IV (10 mg/kg) and PO (30 mg/kg) administration with a concomitant midazolam PO dose (20 mg/kg) are depicted in Figures 5.3.3.1 and 5.3.3.2, respectively, by squares. Non-compartmental pharmacokinetic parameters are listed in Table 5.3.1.1. The K02 IV data with concomitant midazolam dosing fitted to a two-compartment model

yielded pharmacokinetic parameters, V_1, α and β (1.4 l/kg, 0.0963 min^{-1} and 0.0274 min^{-1}). A reasonable fit of simultaneous IV and PO data was obtained yielding an first order absorption rate constant of 0.0166 min^{-1}, a V_1, α and β (1.4 l/kg, 0.0927 min^{-1} and 0.0132 min^{-1}) close to that obtained for the IV data alone (Figure 5.3.3.3).

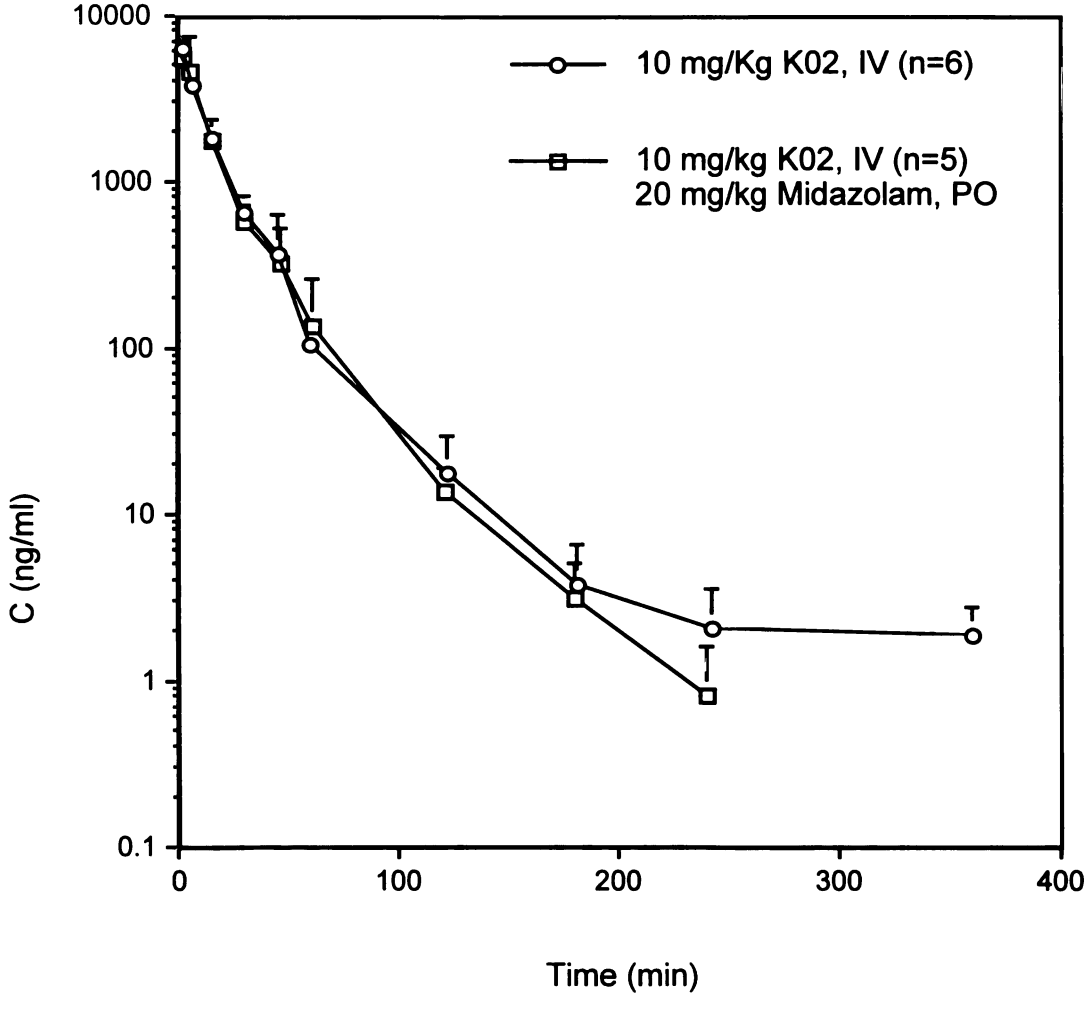

Figure 5.3.3.1 K02 plasma concentration versus time curves following IV (10 mg/kg) administration with and without a concomitant oral midazolam dose (20 mg/kg). Circles, without midazolam, n=6; squares, with midazolam, n=5. Values are mean ± standard deviation.

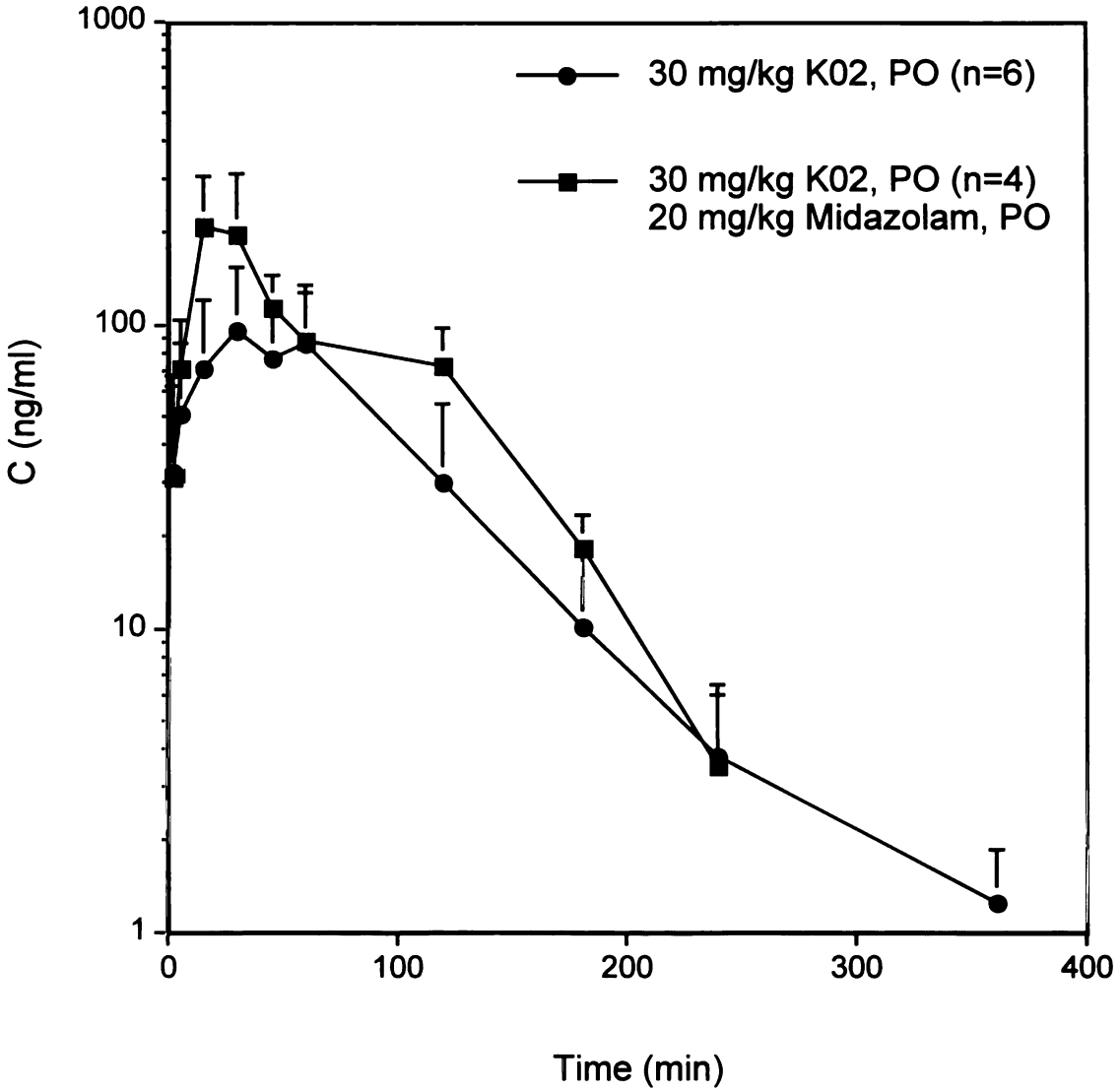

Figure 5.3.3.2 K02 plasma concentration versus time curves following PO (30 mg/kg) administration with and without a concomitant oral midazolam dose (20 mg/kg). Circles, without midazolam, n=6; squares, with midazolam, n=4. Values are mean ± standard deviation.

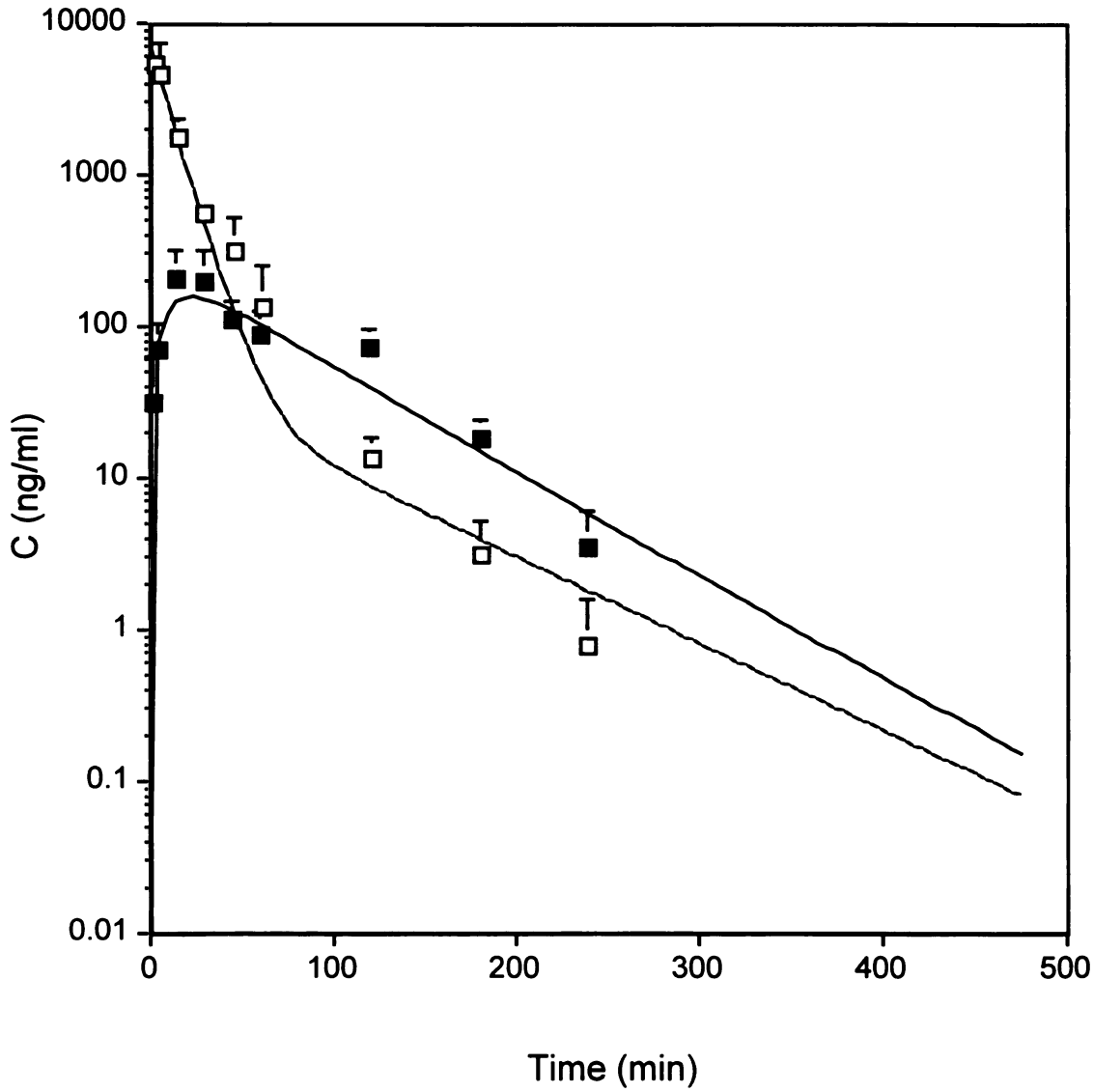

Figure 5.3.3.3 Simultaneous fitting of K02 IV and PO plasma concentration versus time data to the two-compartment model. Solid lines represent fitted parameters. Open squares and solid squares represent actual IV and PO data, respectively.

5.3.4 Effects of TPGS on the Pharmacokinetics of K02 in Male SD Rats

K02 plasma concentration versus time curves for IV (10 mg/kg) and PO (30 mg/kg) administration with a concomitant TPGS PO dose (8 IU/kg) are depicted in Figures 5.3.4.1 and 5.3.4.2, respectively, by squares. Non-compartmental pharmacokinetic parameters are listed in Table 5.3.1.1. The K02 IV data with concomitant TPGS dosing fitted to a two-compartment model yielded pharmacokinetic parameters, V_1, α and β (1.2 l/kg, 0.1306 min^{-1} and 0.0377 min^{-1}). A reasonable fit of simultaneous IV and PO data was obtained yielding an first order absorption rate constant of 0.0242 min^{-1}, a V_1, α and β (1.0/kg, 0.1388 min^{-1} and 0.0352 min^{-1}) close to that obtained for the IV data alone (Figure 5.3.4.3).

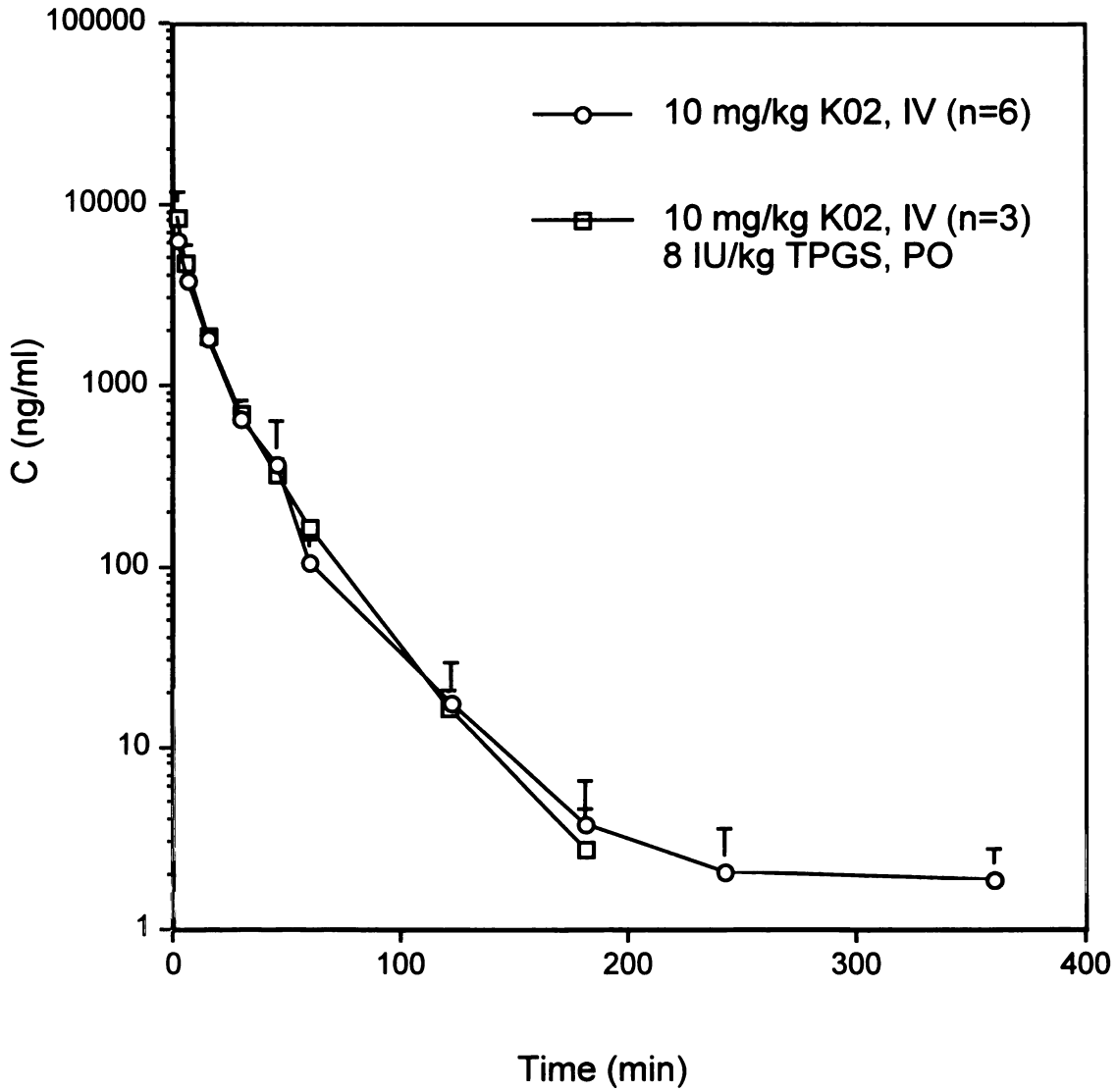

Figure 5.3.4.1 K02 plasma concentration versus time curves following IV (10 mg/kg) administration with and without a concomitant oral TPGS dose (8 IU/kg). Circles, without TPGS, n=6; squares, with TPGS, n=3. Values are mean ± standard deviation.

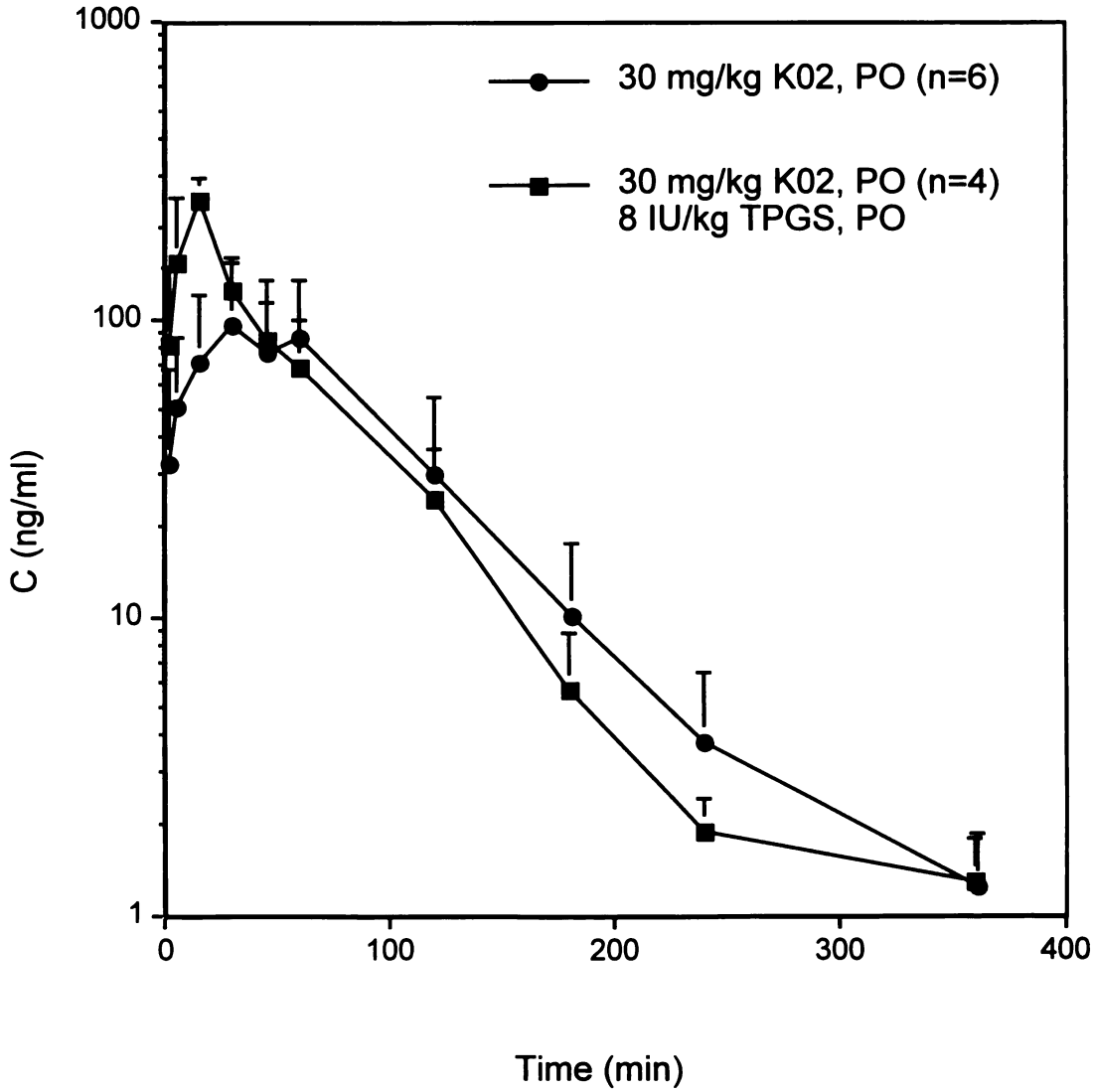

Figure 5.3.4.2 K02 plasma concentration versus time curves following PO (30 mg/kg) administration with and without a concomitant oral TPGS dose (8 IU/kg). Circles, without TPGS, n=6; squares, with TPGS, n=4. Values are mean ± standard deviation.

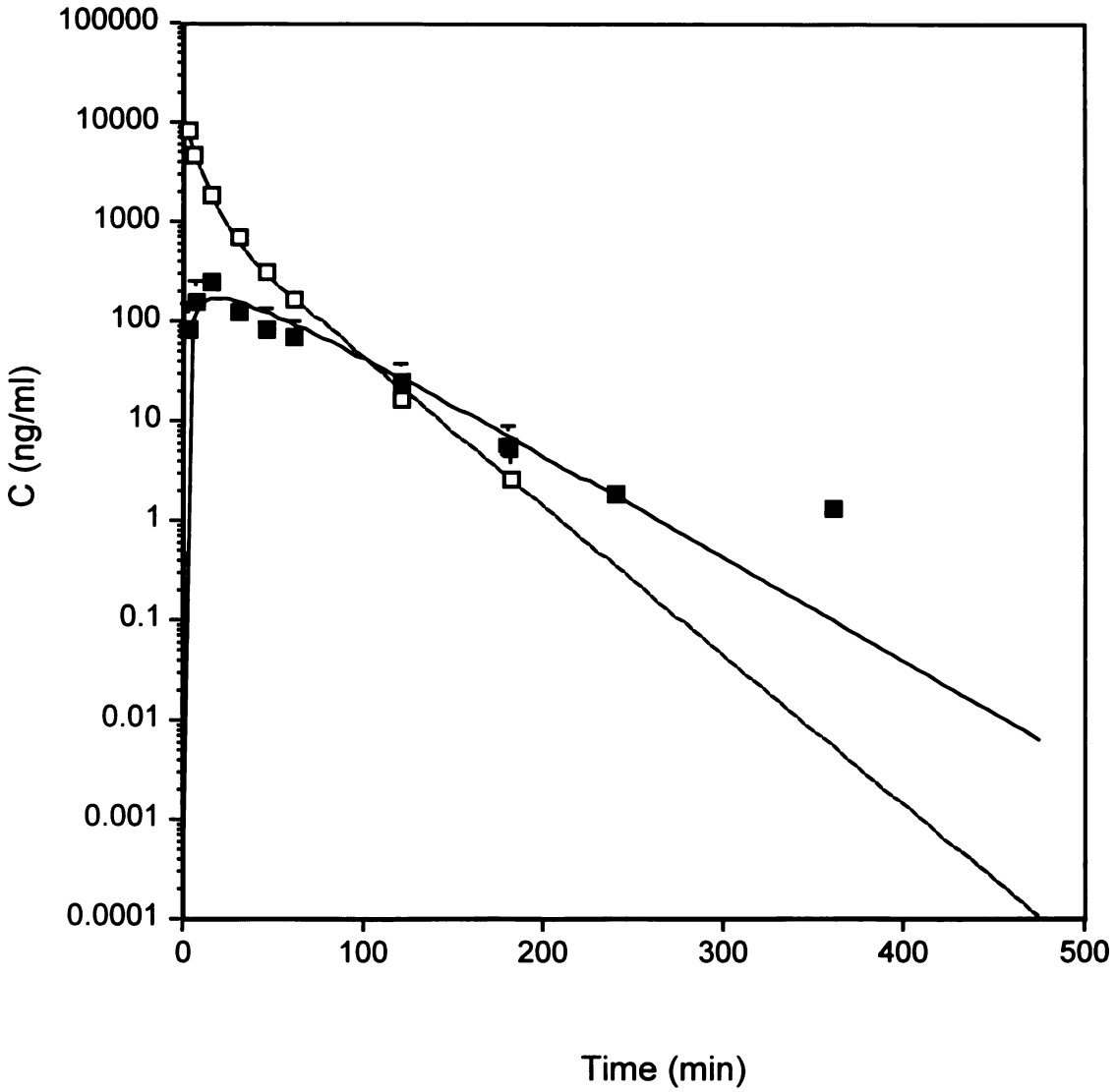

Figure 5.3.4.3 Simultaneous fitting of K02 IV and PO plasma concentration versus time data to the two-compartment model. Solid lines represent fitted parameters. Open squares and solid squares represent actual IV and PO data, respectively.

5.4 Discussion

CYP3A mediated drug metabolism and P-gp countertransport process in the intestine have been recognized to contribute to the poor oral drug bioavailability of some drugs which are CYP3A and P-gp substrates(Benet *et al.*, 1996b). Recognition of this potential for metabolism and countertransport process in the gut leads to new approaches for improving drug bioavailability, such as co-administration of CYP3A and/or P-gp inhibitors.

Here a concomitant ketoconazole oral dose (20mg/kg) raised the AUC of orally administered K02 from 9.4 ± 4.4 mg•min/l to 102 ± 24 mg•min/l and decreased K02 plasma oral clearance (CL/F) from 3810 ± 1620 to 306 ± 60 ml/min/kg. For IV administered K02 with concomitant oral ketoconazole, changes versus control for AUC (from 94 ± 17 mg•min/l to 107 ± 14 mg•min/l), CL (from 110 ± 22 to 95 ± 13 ml/min/kg), volume of distribution at steady-state (V_{ss}) (from 1.9 ± 0.3 l/kg to 2.0 ± 0.6 l/kg) and mean residence time (MRT) (from 17.4 ± 2.0 min to 21.4 ± 8.3 min) were not significant. However, the concomitant ketoconazole oral dose (20mg/kg) markedly increases K02 oral bioavailability from 2.9 ± 1.4% to 31.0 ± 7.5% (p<0.001) (Table 5.3.1.1)

Oral ketoconazole dosing had little effect on the pharmacokinetics of IV K02 as seen in Figure 5.4.1.1. It is very obvious that the primary influence of the concomitant oral dosing of ketoconazole on K02 oral data is explained by effects on the absorption process (F increases more than 10-fold) and although

ketoconazole causes minimal changes in T_{max} and MAT, we were unable to obtain a reasonable fit of the PO and IV K02 data in the presence of ketoconazole with a first order absorption model.

A concomitant midazolam oral dose (20mg/kg) raised the AUC of orally administered K02 from 9.4 ± 4.4 mg•min/l to 16.1 ± 3.9 mg•min/l and decreased K02 plasma oral clearance (CL/F) from 3810 ± 1620 to 1970± 580 ml/min/kg. For IV administered K02 with concomitant oral midazolam changes versus control for AUC (from 94 ± 17 mg•min/l to 97 ± 36 mg•min/l), CL (from 110 ± 22 to 112 ± 32 ml/min/kg), volume of distribution at steady-state (V_{ss}) (from 1.9 ± 0.3 l/kg to 1.6 ± 0.4 l/kg) and mean residence time (MRT) (from 17.4 ± 2.0 min to 14.8 ± 1.4 min) were not significant. However, the concomitant midazolam oral dose (20mg/kg) moderately increases K02 oral bioavailability from 2.9 ± 1.4% to 5.7 ± 2.3% (p<0.05) (Table 5.3.1.1). Oral midazolam dosing had little effect on the pharmacokinetics of IV K02 as seen in Figure 5.3.3.1. Similar to ketoconazole oral dosing, the primary influence of the concomitant oral dosing of midazolam on K02 oral data is explained by effects on the absorption process (F increases 2-fold). A reasonable simultaneous fit of the PO and IV K02 data in the presence of midazolam with a first order absorption model was obtained yielding an first order absorption rate constant (k_a) of 0.0166 min^{-1} and an oral bioavailability (F) of 0.056. Compared with the k_a (0.0153 min^{-1}) obtained from the fit of the simultaneous PO and IV K02 control data (in the absence of any

interacting compound), the absorption rate remains constant, although oral bioavailability increases (Table 5.3.1.1).

Ketoconazole is a potent CYP3A inhibitor (IC_{50} for K02 metabolism is approximately 5 μM, see Chapter 2) and a moderate P-gp inhibitor (IC_{50} for K02 transport is about 120 μM, see Chapter 3). Midazolam is a moderate CYP3A inhibitor (IC_{50} for K02 metabolism is about 45 μM) and we found that midazolam has no inhibitory effect on K02 transport across MDR1-MDCK cell monolayers in the Transwell system, even with midazolam concentration as high as 500 μM. Both ketoconazole (20 mg/kg) and midazolam (20 mg/kg) increase K02 oral bioavailability without significantly changing other K02 pharmacokinetic parameters. We speculate that both ketoconazole and midazolam decrease K02 gut metabolism by inhibiting intestinal CYP3A. Our observation that 10-fold and 2-fold K02 oral bioavailability increase by oral dosing of ketoconazole and midazolam, respectively, reflects the relative inhibitory potency of ketoconazole and midazolam to CYP3A.

TPGS, a water soluble form of vitamin E, has been used to improve cyclosporine absorption in pediatric transplant patients(Sokol *et al.*, 1991). TPGS has no inhibitory effect on CYP mediated drug metabolism(Chang *et al.*, 1996). We demonstrated that TPGS is a weak P-gp inhibitor for K02 transport in both MDR1-MDCK and Caco-2 cell monolayers in the Transwell system (IC_{50} is approximately 590 μM). Due to the lack of the availability of specific and potent

P-gp inhibitors, we were limited to TPGS, a weak P-gp inhibitor, in attempting to assess the role of P-gp in the intestinal CYP3A/P-gp absorption barrier.

A concomitant TPGS oral dose (8 IU/kg or 20mg/kg) had little effect on the pharmacokinetics of IV K02 as seen in Figure 5.3.4.1. Changes versus control were not significant for AUC (from 94 ± 17 mg•min/l to 106 ± 22 mg•min/l), CL (from 110 ± 22 to 98 ± 23 ml/min/kg), volume of distribution at steady-state (V_{ss}) (from 1.9 ± 0.3 l/kg to 1.5 ± 0.4 l/kg) and mean residence time (MRT) (from 17.4 ± 2.0 min to 15.1 ± 1.1 min)(Table 5.3.1.1). The changes of AUC of orally administered K02 (from 9.4 ± 4.4 to 11.1 ± 3.1 mg•min/l), K02 plasma oral clearance (CL/F) (from 3810 ± 1620 to 2810± 600 ml/min/kg) and K02 oral bioavailability (from 2.9 ± 1.4% to 3.5 ± 1.1%) were also not significant. However, the concomitant TPGS oral dose (8 IU/kg) decreased mean absorption time (MAT)(from 64.9 ± 14.1 to 35.0 ± 8.9 min, $p<0.001$) and peak time (T_{max}) (from 40.0 ± 18.0 to 13.5 ± 3.7 min, $P < 0.05$) (Table 5.3.1.1 and Figure 5.3.4.2). A first order absorption rate constant of 0.0242 min^{-1} was obtained from a fit of simultaneous IV and PO data(Figure 5.3.4.3). This k_a is approximately 50% greater than that (0.0153 min^{-1}) obtained from the fit of the simultaneous PO and IV control K02 data (in the absence of any interacting compound), and the 0.0166 min^{-1} value obtained for the simultaneous fit of the K02 data with concomitant midazolam. However, for TPGS no significant change in F was observed (Table 5.3.1.1).

We had expected to observe decreases for MAT and T_{max} by inhibiting P-gp as an efflux pump in the gut with a concomitant increase in F. With co-administration of TPGS, we observed a significant decrease of K02 MAT and Tmax, but no significant increase of F (from 2.9 ± 1.4% to 3.5 ± 1.1%). In contrast, with co-administration of ketoconazole, a more potent inhibitor of K02 P-gp transport, we saw no change in MAT or T_{max}. We thus speculate that TPGS does not effectively inhibit P-gp in the gut and the increased absorption rate of K02 (or decreased MAT and T_{max}) with co-administration of TPGS may be due to other mechanisms, such as increased membrane permeability by TPGS, or increased solubility of K02 in the presence of TPGS. Such an alternate explanation is consistent with the low critical micelle concentration (0.02% w/w, 37°C) exhibited by TPGS.

The primary goal of this study was to support the hypothesis that CYP3A-mediated intestinal metabolism and P-gp-mediated countertransport processes in the gut create a bioavailability barrier for drugs which are CYP3A and/or P-gp substrates, and to demonstrate that this CYP3A/P-gp oral bioavailability barrier can be overcome by oral coadministration of CYP3A and/or P-gp inhibitors, e.g., ketoconazole. The most important evidence in support of this hypothesis is the 10-fold and 2-fold increase of K02 oral bioavailability with coadministration of an oral dose of ketoconazole and midazolam, respectively, without significant changes in other pharmacokinetic parameters, e.g., plasma clearance (CL).

Thus, for K02 in rats, we may only conclude that inhibition of CYP3A in the intestine will increase oral bioavailability.

5.5 Summary

Here we investigated the effects of CYP3A and/or P-gp inhibitors on the oral bioavailability of K02, a CYP3A and P-gp dual substrate, in male Sprague-Dawley (SD) rats, so as to evaluate the roles of CYP3A and P-gp in K02 disposition. Male Sprague-Dawley (SD) rats (8-10 weeks old, n=3-6) were administered a single dose of K02 (10 mg/kg) intravenously (IV) or (30 mg/kg) orally with or without a concomitant oral dose of ketoconazole (20 mg/kg), a dual CYP3A and P-gp inhibitor; or midazolam (20mg/kg), a CYP3A inhibitor; or TPGS, a P-gp inhibitor. Blood samples were collected from 2 min to 8 hrs following administration through a implanted jugular vein cannula. K02 plasma concentrations were determined by LC/MS/MS analysis. Ketoconazole markedly raised the AUC of orally administered K02 from 9.4 ± 4.4 mg•min/l to 102 ± 24 mg•min/l and decreased K02 oral plasma clearance (CL/F) from 3810 ± 1620 to 306 ± 60 ml/min/kg. With concomitant ketoconazole dosing, the changes of AUC of IV administered K02 (from 94 ± 17 mg•min/l to 107 ± 14 mg•min/l), CL (from 110 ± 22 to 95 ± 13 ml/min/kg) and MAT (from 64.9 ± 14.1 to 77.1 ± 39.5 min) were not significant, while K02 oral bioavailability increased from 2.9 ± 1.4% to

31.0 ± 7.5% (p<0.001). Midazolam moderately raised the AUC of orally administered K02 from 9.4 ± 4.4 mg•min/l to 16.1 ± 3.9 mg•min/l and decreased K02 oral plasma clearance (CL/F) from 3810 ± 1620 to 1969 ± 583 ml/min/kg. With concomitant midazolam dosing, the changes of AUC of IV administered K02 (from 94 ± 17 mg•min/l to 97 ± 36 mg•min/l), CL (from 110 ± 22 to 112 ± 32 ml/min/kg) and MAT (from 64.9 ± 14.1 to 61.3 ± 20.6 min) were not significant, while K02 oral bioavailability increased from 2.9 ± 1.4% to 5.7 ± 2.3% (p<0.05). With concomitant TPGS dosing, the changes of the AUC of orally administered K02 (from 9.4 ± 4.4 mg•min/l to 11.1 ± 3.1 mg•min/l), K02 oral plasma clearance (CL/F) (from 3810 ± 1620 to 2813 ± 604 ml/min/kg), the AUC of IV administered K02 (from 94 ± 17 mg•min/l to 106 ± 22 mg•min/l), CL (from 110 ± 22 to 98 ± 23 ml/min/kg) and K02 oral bioavailability (from 2.9 ± 1.4% to 3.5 ± 1.1%) were not significant. However, TPGS decreased K02 MAT (from 64.9 ± 14.1 to 35.0 ± 8.9 min) and T_{max} (from 40.0 ± 18.0 to 13.5 ± 3.7 min) (P < 0.05). In summary, ketoconazole, a dual inhibitor of CYP3A and P-gp, can effectively increase K02 oral bioavailability by inhibiting the CYP3A/P-gp absorption barrier in the small intestine. Midazolam, a inhibitor of CYP3A (less potent than ketoconazole), can moderately increase K02 oral bioavailability by inhibiting CYP3A in the small intestine. TPGS, a weak P-gp inhibitor, can increase K02 absorption rate rather than extent.

Chapter 6 Conclusions and Perspectives

K02 is the first member of the class of vinylsulfone peptidomimetics, potent mechanism-based cysteine protease inhibitors(Palmer *et al.*, 1995), that has been subjected to *in vitro* and *in vivo* biotransformation and transport studies(Zhang *et al.*, 1998). K02 and other members of this vinylsulfone series act as potent inhibitors of cathepsins B and L, two cancer associated cysteine proteases, cathepsin K, and cathepsin S and to cruzain, the major cysteine protease present in *T. cruzi*. The studies described here demonstrate that K02 is a substrate of CYP3A and CYP3A plays a principle role in the oxidative biotransformation of K02 in human liver, rat liver and rat intestinal microsome preparations. This conclusion is based on the results of an integrated *in vitro* approach utilizing: 1) selective CYP chemical inhibitors; 2) immunoinhibition with CYP3A antibody; and 3) cDNA-expressed human CYP3A4. Both ketoconazole, a CYP3A selective inhibitor, and rabbit anti-CYP3A antibody produced potent and concentration dependent inhibitory effects on the formation of three major primary hydroxylated metabolites of K02, designated M12, M19 and M20. The IC_{50}s of ketoconazole were in the range of 1-4 μM, which are typical values for this reversible CYP3A inhibitor. Representative chemical inhibitors to other major cytochrome P450 enzymes responsible for human drug metabolism, CYP2D6 (quinidine), CYP2C9 (7,8-benzoflavone), and CYP1A2 (sulfaphenazole), at their recommended concentrations, showed no significant effects on K02 metabolite formation. Incubation of K02 with cDNA-expressed human CYP3A4 demonstrates an almost identical metabolite profile to that

obtained in human liver microsomes. K02 also competetively inhibits the formation of 1'-hydroxymidazolam, the major midazolam metabolite in human, which is catalyzed by CYP3A4. This suggests the potential for drug-drug interactions of K02 with other CYP3A substrates, if the drugs are administered concomitantly.

K02 strongly inhibits the photoaffinity labeling of P-glycoprotein with azidopine and LU-49888, a photoaffinity analogue of verapamil. Verapamil is a documented inhibitor and substrate of P-gp, which has been clinically co-administered with many cancer drugs as a P-gp inhibitor to overcome or alleviate multidrug resistance in cancer chemotherapy. This indicates that K02 is a potent P-gp inhibitor. Bidirectional transepithelial transport studies of K02 utilizing MDR1-MDCK and Caco-2 cell monolayers in the Transwell system strongly support the conclusion that K02 is a substrate of P-gp. This conclusion is based on the following results: 1) The basolateral to apical (B-A) flux of ^{14}C-K02 across both MDR1-MDCK and Caco-2 cell monolayers was markedly greater than its apical to basolateral (A-B) flux; 2) This specific B-A transport was temperature dependent, saturable and followed simple Michaelis-Menten kinetics; and 3) This B-A flux was significantly inhibited by P-gp substrates/inhibitors, e.g., cyclosporine, vinblastine, verapamil and ketoconazole. In Caco-2 cell monolayers, the B-A flux was reduced about 50% compared to that in MDR1-MDCK and the A-B flux was increased about 8-fold, which is consistent with Western blots showing that the P-gp expression level in MDR1-MDCK cells was much greater than that in Caco-2 cells. Caco-2 cells have been used as an *in*

vitro model for evaluating intestinal drug absorption, as it resembles the small intestine in many aspects. In Caco-2 cells, the K02 A-B flux (corresponding to serosa to mucosa absorption in gut wall *in vivo*) is 2.19 pmol/min/cm^2 and the corresponding apparent permeability is $3.6 \bullet 10^{-6}$ cm/s. This permeability value is very low and we predict that K02 will be a compound with poor oral bioavailability in human. Applying P-gp inhibitors, such as cyclosporine, vinblastine, verapamil and ketoconazole to the system, we can increase this K02 A-B transport. These results suggest the potential clinical importance of modulation of P-gp in the small intestine to increase the K02 oral absorption.

These data support our hypothesis that there is a substrate specificity overlap between CYP3A and P-gp for hydrophobic protease inhibitors as therapeutic agents and provides the basis to further test our working hypotheses that CYP3A and P-gp act synergistically in the small intestine as a barrier to oral drug bioavailability. We can also test our hypothesis that the poor oral bioavailability caused by CYP3A and P-gp can be overcome by co-administration of CYP3A and/or P-gp inhibitors using K02, a dual CYP3A and P-gp substrate, as a model compound.

K02 pharmacokinetic studies conducted in male Sprague-Dawley rats demonstrate that K02 exhibits relatively poor oral bioavailability. A concomitant oral dose of ketoconazole (20 mg/kg), a potent CYP3A inhibitor and a moderate P-gp inhibitor, raised K02 oral bioavailability markedly (10-fold). A concomitant oral dose of midazolam (20mg/kg), a moderate CYP3A inhibitor which has no

inhibitory effect on P-gp transport *in vitro*, increased K02 oral bioavailability by 2-fold. Neither ketoconazole nor midazolam significantly changed other pharmacokinetic parameters of K02. A concomitant oral dose of D-alpha tocopheryl polyethylene glycol 1000 succinate (TPGS, 8 IU/kg), a water soluble vitamin E and a weak P-gp inhibitor, increased K02 absorption rate (decreased mean absorption time and concentration peak time), but had no significant effect on other K02 pharmacokinetic parameters, including oral bioavailability. We thus speculate that TPGS does not effectively inhibit P-gp in the gut and the increase of absorption rate of K02 by TPGS may be due to other mechanisms, such as increased membrane permeability by TPGS.

These results strengthen our working hypothesis that CYP3A and P-gp play complementary roles in peptidomimetic disposition and that poor oral-peptidomimetic bioavailability caused by the intestinal CYP3A/P-gp barrier can be improved by approaches, such as co-administration of CYP3A and/or P-gp inhibitors. These studies also provide valuable feedback for further drug development of this new class of therapeutically important vinylsulfone peptidomimetics, e.g., in formulating strategies to increase the absorption and to decrease the elimination of K02 in terms of co-administration of CYP3A and/or P-gp inhibitors with K02, and to optimize its delivery to parasite infected host cells or cancer cells.

The studies reported in this thesis may serve as a template for *in vitro* characterization of interactions of new investigational drugs with CYP3A and P-gp in support of early drug discovery and development, as well as for *in vivo*

approaches to improve drug bioavailability by overcoming the intestinal CYP3A/P-gp absorption barrier.

References

Adibi, S. A.: The oligopeptide transporter (Pept-1) in human intestine: biology and function. Gastroenterology. **113:** 332-40, 1997.

Almquist, K. C., Loe, D. W., Hipfner, D. R., Mackie, J. E., Cole, S. P., AND Deeley, R. G.: Characterization of the M(r) 190,000 multidrug resistance protein (MRP) in drug-selected and transfected human tumor cell. Cancer Res. **55:** 102-10, 1995.

Ambudkar, S. V., Cardarelli, C. O., Pashinsky, I., AND Stein, W. D.: Relation between the turnover number for vinblastine transport and for vinblastine-stimulated ATP hydrolysis by human P-glycoprotein. J Biol Chem. **272:** 21160-6, 1997.

Bayley, H., AND Staros, J.: Photoaffinity labeling and related techniques. In Azides and nitrenes: reactivity and utility, ed. by E. F. V. Scriven, Chapter 9, pp. 433-87, Academic Press, Orlando, 1984.

Beck, W. T., Cirtain, M. C., Look, A. T., AND Ashmun, R. A.: Reversal of vinca alkaloid resistance but not multiple drug resistance in human leukemic cells by verapamil. Cancer Res. **46:** 778-84, 1986.

Benet, L. Z., Kroetz, D.L. and Sheiner, L.B.: Pharmacokinetics: The dynamics of drug absorption, distribution, and elimination. In Goodman & Gilman's The Pharmacological Basis of Therapeutics, ed. by J.H. Hardman, L.E. Limbird, P.B. Molinoff, R.W. Ruddon and A.G. Gilman, 9th Ed., Chapter 1, pp. 3-28, McGraw-Hill, New York, 1996a.

Benet, L. Z., Wu, C. Y., Hebert, M. F., AND Wacher, V. J.: Intestinal drug metabolism and antitransport procsses: A potential paradigm shift in oral drug delivery. J Controlled Release. **39:** 139-43, 1996b.

Berger, B. J., AND Fairlamb, A. H.: Cytochrome P450 in Trypanosomatids. Biochem Pharmacol. **46:** 149-57, 1993.

Bornheim, L. M., AND Correia, M. A.: Effect of cannabidiol on cytochrome P-450 isozymes. Biochem Pharmacol. **38:** 2789-94, 1989.

Calkins, C. C., AND Sloane, B. F.: Mammalian cysteine protease inhibitors: biochemical properties and possible roles in tumor progression. Biol Chem Hoppe Seyler. **376:** 71-80, 1995.

Chang, T., Benet, L. Z., AND Hebert, M. F.: The effect of water-soluble vitamin E on cyclosporine pharmacokinetics in healthy volunteers. Clin Pharmacol Ther. **59:** 297-303, 1996.

Chiba, M., Hensleigh, M., AND Lin, J. H.: Hepatic and intestinal metabolism of indinavir, an HIV protease inhibitor, in rat and human microsomes. Major role of CYP3A. Biochem Pharmacol. **53:** 1187-95, 1997.

Chrusciel, R. A., AND Romines, K. R.: Recent developments in HIV protease inhibitor research. Expert Opin Ther Patents. **7:** 111-21, 1997.

Clawson, G. A.: Protease inhibitors and carcinogenesis: A review. Cancer Investigation. **14:** 597-608, 1996.

Cordon-Cardo, C., O'Brien, J. P., Boccia, J., Casals, D., Bertino, J. R., AND Melamed, M. R.: Expression of the multidrug resistance gene product (P-

glycoprotein) in human normal and tumor tissues. J Histochem Cytochem. **38:** 1277-87, 1990.

Cornwell, M. M., Pastan, I. AND Gottesman, M. M.: Certain calcium channel blockers bind specifically to multidrug-resistant human KB carcinoma membrane vesicles and inhibit binding to P-glycoprotein. J Biol Chem. **262:** 21660-70, 1987.

Cowman, A. F., AND Foote, S. J.: Chemotherapy and drug resistance in malaria. Int J Parasitol. **20:** 503-13, 1990.

Cowman, A. F., Galatis, D., AND Thompson, J. K.: Selection for mefloquine resistance in Plasmodium falciparum is linked to amplification of the pfmdr1 gene and cross-resistance to halofantrine and quinine. Proc Natl Acad Sci U S A. **91:** 1143-7, 1994.

Dallagiovanna, B., Gamarro, F., AND Castanys, S.: Molecular characterization of a P-glycoprotein-related tcpgp2 gene in Trypanosoma cruzi. Mol Biochem Parasitol. **75:** 145-57, 1996.

Das, S., AND Mukhopadhyay, P.: Protease inhibitors in chemoprevention of cancer. An overview. Acta Oncol. **33:** 859-65, 1994.

DeClerk, Y. A., AND Imren, S.: Protease inhibitors: Role and potential therapeutic use in human cancer. Eur J Cancer. **30a:** 2170-80, 1994.

de Waziers, P. H., Cugnenc, P. H., Yang, C. S., Leroux, J. P., AND Beaune, P. H.: Cytochrome P450 isoenzymes, epoxide hydrolase and glutathione transferases in rat and human hepatic and extrahepatic tissues. J Pharmacol Exp Ther. **253:** 387-94, 1990.

Dey, S., Ramachandra, M., Pastan, I., Gottesman, M. M., AND Ambudkar, S. V.: Evidence for two nonidentical drug-interaction sites in the human P-glycoprotein. Proc Natl Acad Sci U S A. **94:** 10594-9, 1997.

Elliott, E., AND Sloane, B. F.: The cysteine protease cathepsin B in cancer. Perspectives in Drug Discovery and Design. **6:** 12-32, 1996.

Ferenczy, G. G., AND Morris, G. M.: The active site of cytochrome P-450 nifedipine oxidase: a model-building study. J Mol Graphics. **7:** 206-11, 1989.

Fitzsimmons, M. E., AND Collins, J. M.: Selective biotransformation of the human immunodeficiency virus protease inhibitor saquinavir by human small-intestinal cytochrome P4503A4: potential contribution to high first-pass metabolism. Drug Metab Dispos. **25:** 256-66, 1997.

Floren, L. C., Bekersky, I., Benet, L. Z., Mekki, Q., Dressler, D., Lee, J. W., Roberts, J. P., AND Hebert, M. F.: Tacrolimus oral bioavailability doubles with coadministration of ketoconazole. Clin Pharmacol Ther. **62:** 41-9, 1997.

Friche, E., Demant, E. J., Sehested, M., AND Nissen, N. I.: Effect of anthracycline analogs on photolabelling of p-glycoprotein by [125I]iodomycin and [3H]azidopine: relation to lipophilicity and inhibition of daunorubicin transport in multidrug resistant cells. Br J Cancer. **67:** 226-31, 1993.

Futscher, B. W., Foley, N. E., Gleason-Guzman, M. C., Meltzer, P. S., Sullivan, D. M., AND Dalton, W. S.: Verapamil suppresses the emergence of P-glycoprotein-mediated multi-drug resistance. Int J Cancer. **66:** 520-5, 1996.

Germann, U. A., Chambers, T. C., Ambudkar, S. V., Licht, T., Cardarelli, C. O., Pastan, I., AND Gottesman, M. M.: Characterization of phosphorylation-

defective mutants of human P-glycoprotein expressed in mammalian cells. J Biol Chem. **271:** 1708-16, 1996.

Gorski, J. C., Jones, D. R., Wrighton, S. A., AND Hall, S. D.: Characterization of dextromethorphan N-demethylation by human liver microsomes. Contribution of the cytochrome P450 3A (CYP3A) subfamily. Biochem Pharmacol. **48:** 173-82, 1994.

Gorski, J. C., Jones, D. R., Wrighton, S. A., AND Hall, S. D.: Contribution of human CYP3A subfamily members to the 6-hydroxylation of chlorzoxazone. Xenobiotica. **27:** 243-56, 1997.

Gottesman, M. M., AND Pastan, I.: Biochemistry of multidrug resistance mediated by the multidrug transporter. Annu Rev Biochem. **62:** 385-427, 1993.

Greenberger, L. M.: Major photoaffinity drug labeling sites for iodoaryl azidoprazosin in P-glycoprotein are within, or immediately C-terminal to, transmembrane domains 6 and 12. J Biol Chem. **268:** 11417-25, 1993.

Guengerich, F. P.: Reactions and significance of cytochrome P450 enzymes. J Biol Chem. **266:** 10019-22, 1991.

Haehner, B. D., Gorski, J. C., Vandenbranden, M., Wrighton, S. A., Janardan, S. K., Watkins, P. B., AND Hall, S. D.: Bimodal distribution of renal cytochrome P450 3A activity in humans. Mol Pharmacol. **50:** 52-9, 1996.

Halpert, J. R., Guengerich, F. P., Bend, J. R., AND Correia, M. A.: Selective inhibitors of cytochromes P450. Toxicol Appl Pharmacol. **125:** 163-75, 1994.

Harth, G., Andrews, N., Mills, A. A., Engle, J. C., Smith, R., AND McKerrow, J. H.: Peptide-fluoromethyl ketones arrest intracellular replication and intercellular transmission of Trypanosoma cruzi. Mol Biochem Parasitol. **58:** 17-24, 1993.

Hebert, M. F., Roberts, J. P., Prueksaritanont, T., AND Benet, L. Z.: Bioavailability of cyclosporine with concomitant rifampin administration is markedly less than predicted by hepatic enzyme induction. Clin Pharmacol Ther. **52:** 453-7, 1992.

Hidalgo, I. J., Raub, T. J., AND Borchardt, R. T.: Characterization of the human colon carcinoma cell line (Caco-2) as a model system for intestinal epithelial permeability. Gastroenterology. **96:** 736-49, 1989.

Higgins, C. F.: ABC transporters: from microorganisms to man. Annu Rev Cell Biol. **8:** 67-113, 1992.

Higgins, C. F., AND Gottesman, M. M.: Is the multidrug transporter a flippase? Trends Biochem Sci. **17:** 18-21, 1992.

Hu, Y. P., Chapey, C., AND Robert, J.: Relationship between the inhibition of azidopine binding to P-glycoprotein by MDR modulators and their efficiency in restoring doxorubicin intracellular accumulation. Cancer Lett. **109:** 203-9, 1996.

Hugli, T. E.: Protease inhibitors: novel therapeutic application and development. Trends in Biotechnology. **14:** 409-12, 1996.

Hunter, J., Jepson, M. A., Tsuruo, T., Simmons, N., AND Hirst, B. H.: Functional expression of P-glycoprotein in apical membranes of human intestinal

Caco-2 cells. J Biol Chem. **268:** 14991-7, 1993.

Ito, K., Suzuki, H., Hirohashi, T., Kume, K., Shimizu, T., AND Sugiyama, Y.: Molecular cloning of canalicular multispecific organic anion transporter defective in EHBR. Am J Physiol. **272:** G16-22, 1997.

Izumi, T., Enomoto, S., Hosiyama, K., Sasahara, K., Shibukawa, A., Nakagawa, T., AND Sugiyama, Y.: Prediction of the human pharmacokinetics of troglitazone, a new and extensively metabolized antidiabetic agent, after oral administration, with an animal scale-up approach. J Pharmacol Exp Ther. **277:** 1630-41, 1996.

Juliano, R. L., AND Ling, V.: A surface glycoprotein modulating drug permeability in Chinese hamster ovary cell mutants. Biochim Biophys Acta. **455:** 152-62, 1976.

Kolars, J. C., Schmiedlin-Ren, P., Dobbins, W. O. D., Schuetz, J., Wrighton, S. A., AND Watkins, P. B.: Heterogeneity of cytochrome P450IIIA expression in rat gut epithelia. Gastroenterology. **102:** 1186-98, 1992a.

Kolars, J. C., Schmiedlin-Ren, P., Schuetz, J. D., Fang, C., AND Watkins, P. B.: Identification of rifampin-inducible P450IIIA4 (CYP3A4) in human small bowel enterocytes. J Clin Invest. **90:** 1871-8, 1992b.

Kolars, J. C., Lown, K. S., Schmiedlin-Ren, P., Ghosh, M., Fang, C., Wrighton, S. A., Merion, R. M., AND Watkins, P. B.: CYP3A gene expression in human gut epithelium. Pharmacogenetics. **4:** 247-59, 1994.

Koymans, L., Vermeulen, N. P., van Acker, S. A., te Koppele, J. M., Heykants, J. J., Lavrijsen, K., Meuldermans, W., AND Donne-Op den Kelder, G. M.: A

predictive model for substrates of cytochrome P450-debrisoquine (2D6). Chem Res Toxicol. **5:** 211-9, 1992.

Kumar, G. N., Rodrigues, A. D., Buko, A. M., AND Denissen, J. F.: Cytochrome P450-mediated metabolism of the HIV-1 protease inhibitor ritonavir (ABT-538) in human liver microsomes. J Pharmacol Exp Ther. **277:** 423-31, 1996.

Li, A. P., Kaminski, D. L., AND Rasmussen, A.: Substrates of human hepatic cytochrome P450 3A4. Toxicology. **104:** 1-8, 1995.

Loo, T. W., AND Clarke, D. M.: Drug-stimulated ATPase activity of human P-glycoprotein requires movement between transmembrane segments 6 and 12. J Biol Chem. **272:** 20986-9, 1997.

Lowry, O. H., Rosebrough, N. J., Farr, A. L., AND Randall, R. J.: Protein measurement with the Folin phenol reagent. J Biol Chem. **193:** 265-75, 1951.

McGrath, M. E., Eakin, A. E., Engel, J. C., McKerrow, J. H., Craik, C. S., AND Fletterick, R. J.: The crystal structure of cruzain: A therapeutic target for Chagas' disease. J Mol Biol. **247:** 251-9, 1995.

McKerrow, J. H., McGrath, M. E., AND Engel, J. C.: The cysteine protease of Trypanosoma cruzi as a model for antiparasite drug design. parasitology today. **11:** 279-82, 1995.

McKinnon, R. A., Burgess, W. M., Hall, P. M., Roberts-Thomson, S. J., Gonzalez, F. J., AND McManus, M. E.: Characterisation of CYP3A gene subfamily expression in human gastrointestinal tissues. Gut. **36:** 259-67, 1995.

Morris, D. I., Greenberger, L. M., Bruggemann, E. P., Cardarelli, C., Gottesman, M. M., Pastan, I., AND Seamon, K. B.: Localization of the forskolin labeling sites to both halves of P-glycoprotein: similarity of the sites labeled by forskolin and prazosin. Mol Pharmacol. **46:** 329-37, 1994.

Murray, G. I., Barnes, T. S., Sewell, H. F., Ewen, S. W. B., Melvin, W. T., AND Burke, M. D.: The immunocytochemical localization and distribution of cytochrome P-450 in normal human hepatic and extrahepatic tissues with a monoclonal antibody to human cytochrome P-450. Br J Clin Pharmacol. **25:** 465-75, 1988.

Murray, G. I., Shaw, D., Weaver, R. J., McKay, J. A., Ewen, S. W., Melvin, W. T., AND Burke, M. D.: Cytochrome P450 expression in oesophageal cancer. Gut. **35:** 599-603, 1994.

Murray, G. I., Taylor, V. E., McKay, J. A., Weaver, R. J., Ewen, S. W., Melvin, W. T., AND Burke, M. D.: Expression of xenobiotic metabolizing enzymes in tumours of the urinary bladder. Int J Exp Pathol. **76:** 271-6, 1995a.

Murray, G. I., Taylor, V. E., McKay, J. A., Weaver, R. J., Ewen, S. W., Melvin, W. T., AND Burke, M. D.: The immunohistochemical localization of drug-metabolizing enzymes in prostate cancer. J Pathol. **177:** 147-52, 1995b.

Nelson, D. R., Koymans, L., Kamataki, T., Stegeman, J. J., Feyereisen, R., Waxman, D. J., Waterman, M. R., Gotoh, O., Coon, M. J., Estabrook, R. W., Gunsalus, I. C., AND Nebert, D. W.: The P450 superfamily: update on new sequences, gene mapping, accession number and nomenclature. Pharmacogenetics. **6:** 1-42, 1996.

Omura, T., AND Sato, R.: The carbon monoxide-binding pigment of liver microsomes II. Solubilization, purification, and properties. J Biol Chem. **239:** 2370-8, 1964.

Palmer, J. T., Rasnick, D., Klaus, J. L., AND Bromme, D.: Vinyl sulfones as mechanism-based cysteine protease inhibitors. J Med Chem. **38:** 3193-6, 1995.

Pastan, I., Gottesman, M. M., Ueda, K., Lovelace, E., Rutherford, A. V., AND Willingham, M. C.: A retrovirus carrying an MDR1 cDNA confers multidrug resistance and polarized expression of P-glycoprotein in MDCK cells. Proc Natl Acad Sci U S A. **85:** 4486-90, 1988.

Patel, N. H., AND Rothenberg, M. L.: Multidrug resistance in cancer chemotherapy. Invest New Drugs. **12:** 1-13, 1994.

Perry, C. M., AND Benfield, P.: Nelfinavir. Drugs. **54:** 81-7; discussion 88, 1997.

Podobnik, M., Kuhelj, R., Turk, V., AND Turk, D.: Crystal structure of the wild-type human procathepsin B at 2.5 A resolution reveals the native active site of a papain-like cysteine protease zymogen. J Mol Biol. **271:** 774-88, 1997.

Qian, X. D., AND Beck, W. T.: Binding of an optically pure photoaffinity analogue of verapamil, LU-49888, to P-glycoprotein from multidrug-resistance human leukemic cell lines. Cancer Res. **50:** 1132-37, 1990.

Rasnick, D.: Small synthetic inhibitors of cysteine proteases. Perspectives in Drug Discovery and Design. **6:** 47-63, 1996.

Riley, R. J., Hemingway, S. A., Graham, M. A., AND Workman, P.: Initial characterization of the major mouse cytochrome P450 enzymes involved in

the reductive metabolism of the hypoxic cytotoxin 3-amino-1,2,4-benzotriazine-1,4-di-N-oxide (tirapazamine, SR 4233, WIN 59075). Biochem Pharmacol. **45:** 1065-77, 1993.

Robertson, C. D., Coombs, G. H., North, M. J., AND Mottram, J. C.: Parasite cysteine proteinases. Perspectives in Drug Discovery and Design. **6:** 99-118, 1996.

Rosenberg, M. F., Callaghan, R., Ford, R. C., AND Higgins, C. F.: Structure of the multidrug resistance P-glycoprotein to 2.5 nm resolution determined by electron microscopy and image analysis. J Biol Chem. **272:** 10685-94, 1997.

Safa, A. R.: Photoaffinity labeling of the multidrug-resistance-related P-glycoprotein with photoactive analogs of verapamil. Proc Natl Acad Sci U S A. **85:** 7187-91, 1988.

Sankaran, B., Bhagat, S., AND Senior, A. E.: Photoaffinity labelling of P-glycoprotein catalytic sites. FEBS Lett. **417:** 119-22, 1997.

Schinkel, A. H., Kemp, S., Dolle, M., Rudenko, G., AND Wagenaar, E.: N-glycosylation and deletion mutants of the human MDR1 P-glycoprotein. J Biol Chem. **268:** 7474-81, 1993.

Schinkel, A. H., Smit, J. J., van Tellingen, O., Beijnen, J. H., Wagenaar, E., van Deemter, L., Mol, C. A., van der Valk, M. A., Robanus-Maandag, E. C., te Riele, H. P., Berns, A. J. M. AND Borst, P.: Disruption of the mouse mdr1a P-glycoprotein gene leads to a deficiency in the blood-brain barrier and to increased sensitivity to drugs. Cell. **77:** 491-502, 1994.

Schinkel, A. H., Mol, C. A., Wagenaar, E., van Deemter, L., Smit, J. J., AND Borst, P.: Multidrug resistance and the role of P-glycoprotein knockout mice. Eur J Cancer. **31A:** 1295-8, 1995a.

Schinkel, A. H., Wagenaar, E., van Deemter, L., Mol, C. A., AND Borst, P.: Absence of the mdr1a P-glycoprotein in mice affects tissue distribution and pharmacokinetics of dexamethasone, digoxin, and cyclosporin A. J Clin Invest. **96:** 1698-705, 1995b.

Schinkel, A. H., Mayer, U., Wagenaar, E., Mol, C. A., van Deemter, L., Smit, J. J., van der Valk, M. A., Voordouw, A. C., Spits, H., van Tellingen, O., Zijlmans, J. M., Fibbe, W. E., AND Borst, P.: Normal viability and altered pharmacokinetics in mice lacking mdr1-type (drug-transporting) P-glycoproteins. Proc Natl Acad Sci U S A. **94:** 4028-33, 1997.

Schuetz, E. G., Beck, W. T., AND Schuetz, J. D.: Modulators and substrates of P-glycoprotein and cytochrome P4503A coordinately up-regulate these proteins in human colon carcinoma cells. Mol Pharmacol. **49:** 311-8, 1996.

Schumacher, U., AND Mollgard, K.: The multidrug-resistance P-glycoprotein (Pgp, MDR1) is an early marker of blood-brain barrier development in the microvessels of the developing human brain. Histochem Cell Biol. **108:** 179-82, 1997.

Shapiro, A. B., AND Ling, V.: Positively cooperative sites for drug transport by P-glycoprotein with distinct drug specificities. Eur J Biochem. **250:** 130-7, 1997.

Shimada, T., Yamazaki, H., Mimura, M., Inui, Y., AND Guengerich, F. P.: Interindividual variations in human liver cytochrome P-450 enzymes involved in the oxidation of drugs, carcinogens and toxic chemicals: studies with liver microsomes of 30 Japanese and 30 caucasians. J Pharmacol Exp Ther. **270:** 414-23, 1994.

Shou, M., Grogan, J., Mancewicz, J. A., Krausz, K. W., Gonzalez, F. J., Gelboin, H. V., AND Korzekwa, K. R.: Activation of CYP3A4: evidence for the simultaneous binding of two substrates in a cytochrome P450 active site. Biochemistry. **33:** 6450-5, 1994.

Siegsmund, M. J., Cardarelli, C., Aksentijevich, I., Sugimoto, Y., Pastan, I., AND Gottesman, M. M.: Ketoconazole effectively reverses multidrug resistance in highly resistant KB cells. J Urol. **151:** 485-91, 1994.

Silverman, J. A., AND Schrenk, D.: Hepatic canalicular membrane 4: expression of the multidrug resistance genes in the liver. FASEB J. **11:** 308-13, 1997.

Silverman, J. A., AND Thorgeirsson, S. S.: Regulation and function of the multidrug resistance genes in liver. Prog Liver Dis. **13:** 101-23, 1995.

Sloane, B. F., Moin, K., Krepela, E., AND Rozhin, J.: Cathepsin b and its endogenous inhibitor: the role in tumor malignancy. Cancer Metastasis Rev. **9:** 333-352, 1990.

Smith, D. A., AND Jones, B. C.: Speculations on the substrate structure-activity relationship (SSAR) of cytochrome P450 enzymes. Biochem Pharmacol. **44:** 2089-98, 1992.

Sokol, R. J., Johnson, K. E., Karrer, F. M., Narkewicz, M. R., Smith, D., AND Kam, I.: Improvement of cyclosporine absorption in children after liver transplantation by means of water soluble vitamin E. Lancet. **338:** 212-4, 1991.

Sparreboom, A., van Asperen, J., Mayer, U., Schinkel, A. H., Smit, J. W., Meijer, D. K., Borst, P., Nooijen, W. J., Beijnen, J. H., AND van Tellingen, O.: Limited oral bioavailability and active epithelial excretion of paclitaxel (Taxol) caused by P-glycoprotein in the intestine. Proc Natl Acad Sci U S A. **94:** 2031-5, 1997.

Spracklin, D. K., Thummel, K. E., AND Kharasch, E. D.: Human reductive halothane metabolism in vitro is catalyzed by cytochrome P450 2A6 and 3A4. Drug Metab Dispos. **24:** 976-83, 1996.

Taguchi, Y., Kino, K., Morishima, M., Komano, T., Kane, S. E., AND Ueda, K.: Alteration of substrate specificity by mutations at the His61 position in predicted transmembrane domain 1 of human MDR1/P-glycoprotein. Biochemistry. **36:** 8883-9, 1997.

Tanigawara, Y., N, O., Hirai, M., Yasuhara, M., Ueda, K., Kioka, N., Komano, T., AND Hori, R.: Transport of digoxin by human P-glycoprotein expressed in a porcine kidney epithelial cell line (LLC-Pk1). J Pharmacol Exp Ther. **263:** 840-5, 1992.

Thiebaut, F., Tsuruo, T., Hamada, H., Gottesman, M. M., Pastan, I., AND Willingham, M. C.: Cellular localization of the multidrug-resistance gene

product P-glycoprotein in normal human tissues. Proc Natl Acad Sci U S A. **84:** 7735-8, 1987.

Thummel, K. E., O'Shea, D., Paine, M. F., Shen, D. D., Kunze, K. L., Perkins, J. D., AND Wilkinson, G. R.: Oral first-pass elimination of midazolam involves both gastrointestinal and hepatic CYP3A-mediated metabolism. Clin Pharmacol Ther. **59:** 491-502, 1996.

Turk, D., Podobnik, M., Popovic, T., Katunuma, N., Bode, W., Huber, R., AND Turk, V.: Crystal structure of cathepsin B inhibited with CA030 at 2.0-A esolution: A basis for the design of specific epoxysuccinyl inhibitors. Biochemistry. **34:** 4791-7, 1995.

Ullman, B.: Multidrug resistance and P-glycoproteins in parasitic protozoa. J Bioenerg Biomembr. **27:** 77-84, 1995.

Upton, R. A.: Simple and reliable method for serial sampling of blood from rats. J Pharm Sci. **64:** 112-4, 1975.

van Asperen, J., Schinkel, A. H., Beijnen, J. H., Nooijen, W. J., Borst, P., AND van Tellingen, O.: Altered pharmacokinetics of vinblastine in mdr1a P-glycoprotein-deficient mice. J Natl Cancer Inst. **88:** 994-9, 1996.

van Asperen, J., vanTellingen, O., Sparreboom, A., Schinkel, A. H., Borst, P., Nooijen, W. J., AND Beijnen, J. H.: Enhanced oral bioavailability of paclitaxel in mice treated with the P-glycoprotein blocker SDZ PSC 833. Br J Cancer. **76:** 1181-3, 1997.

Wacher, V. J., Wu, C. Y., AND Benet, L. Z.: Overlapping substrate specificities and tissue distribution of cytochrome P450 3A and P-glycoprotein:

implications for drug delivery and activity in cancer chemotherapy. Mol Carcinog. **13:** 129-34, 1995.

Watkins, P. B., Wrighton, S. A., Schuetz, E. G., AND Guzelian, P. S.: Identification of glucocorticoid-inducible cytochrome P-450 in the intestine mucosa of rats and human. J Clin Invest. **80:** 1029-36, 1987.

Williams, J. A., Chenery, R. J., Berkhout, T. A., AND Hawksworth, G. M.: Induction of cytochrome P4503A by the antiglucocorticoid mifepristone and a novel hypocholesterolaemic drug. Drug Metab Dispos. **25:** 757-61, 1997.

Wrighton, S. A., AND Ring, B. J.: Inhibition of human CYP3A catalyzed 1'-hydroxy midazolam formation by ketoconazole, nifedipine, erythromycin, cimetidine, and nizatidine. Pharm Res. **11:** 921-4, 1994.

Wrighton, S. A., VandenBranden, M., AND Ring, B. J.: The human drug metabolizing cytochromes P450. J Pharmacokinet Biopharm. **24:** 461-73, 1996.

Wu, C. Y., Benet, L. Z., Hebert, M. F., Gupta, S. K., Rowland, M., Gomez, D. Y., AND Wacher, V. J.: Differentiation of absorption and first-pass gut and hepatic metabolism in humans: studies with cyclosporine. Clin Pharmacol Ther. **58:** 492-7, 1995.

Zhang, L., Dresser, M. J., Gray, A. T., Yost, S. C., Terashita, S., AND Giacomini, K. M.: Cloning and functional expression of a human liver organic cation transporter. Mol Pharmacol. **51:** 913-21, 1997.

Zhang, X., Collins, K. I., AND Greenberger, L. M.: Functional evidence that transmembrane 12 and the loop between transmembrane 11 and 12 form

part of the drug-binding domain in P-glycoprotein encoded by MDR1. J Biol Chem. **270:** 5441-8, 1995.

Zhang, Y. C., Guo, X., Lin, E. T., AND Benet, L. Z.: Overlapping substrate specificity of cytochrome P450 3A and P-glycoprotein for a novel cysteine protease inhibitor. Drug Metab Dispos. **in press,** 1998.